

DIPARTIMENTO DI ASTRONOMIA
Corso di Dottorato di Ricerca in Astronomia
Ciclo XX (2005-2007)

MODELING THE COSMOLOGICAL CO-EVOLUTION OF
SUPERMASSIVE BLACK HOLES AND GALAXIES

Dottorando:
Federico Marulli

Relatori:
Ch.mo Prof. Lauro Moscardini
Ch.mo Prof. Enzo Branchini

Coordinatore:
Ch.mo Prof. Lauro Moscardini

Contents

Introduction	5
1 Black Holes and Active Galactic Nuclei	9
1.1 Observations	10
1.1.1 BH scaling relations	10
1.1.2 BH fundamental plane	17
1.1.3 BH mass function	19
1.1.4 AGN luminosity function	25
1.1.5 AGN number count	29
1.1.6 AGN clustering	31
1.2 Theory	36
1.2.1 General features	36
1.2.2 Theoretical methods	37
2 Analytic models: dark matter + black holes	43
2.1 The WL02 model	44
2.2 The WL03 model	47
2.3 Models vs. observations	48
2.3.1 AGN optical luminosity function	48
2.3.2 AGN biasing function	52
2.4 Discussion	52
3 Semi-analytic models: dark matter + black holes	55
3.1 The VHM model	56
3.2 Model vs. observations	61
3.2.1 $M_{\text{BH}} - \sigma_c$ scaling relation	61
3.2.2 AGN optical luminosity function	61
3.2.3 AGN bolometric luminosity function	64
3.2.4 AGN hard X-ray luminosity function at $z \sim 0.1$	68
3.2.5 AGN biasing function	70
3.3 Discussion	75
4 Hybrid simulations: dark matter + baryons + black holes	81
4.1 Model description	83
4.1.1 Numerical simulation	83
4.1.2 Galaxy evolution	84

4.1.3 BH mass accretion and AGN	88
4.2 Model vs. Observations	92
4.2.1 BH scaling relations	92
4.2.2 BH mass function	101
4.2.3 AGN bolometric luminosity function	102
4.3 Discussion	107
Conclusions	111
Bibliography	114
Index	127

Introduction



VER the last years, several observations demonstrated that supermassive black holes [BHs] reside at the centres of almost all spheroidal galaxies (see e.g. Kormendy & Richstone, 1995; Richstone et al., 1998). Even more interestingly, their properties appear to strongly correlate with those of their hosting galaxies (Magorrian et al., 1998; Ferrarese & Merritt, 2000; Gebhardt et al., 2000; Graham et al., 2001; Tremaine et al., 2002; McLure & Dunlop, 2002; Baes et al., 2003; Marconi & Hunt, 2003; Häring & Rix, 2004; Feoli & Mele, 2005, 2007; Graham & Driver, 2007a) and, apparently, also with the ones of the whole host dark matter [DM] haloes (Ferrarese, 2002; Baes et al., 2003; Ferrarese & Ford, 2005; Shankar et al., 2006). Although it is not yet clear which of these relations is “more fundamental” (see e.g. Novak et al., 2006; Lauer et al., 2007), they reasonably suggest a close link between the assembly history of the BHs and the cosmological evolution of galaxies. Most recently, Hopkins et al. (2007a) have shown that these relationships are not independent and could be interpreted as different projections of a BH fundamental plane, analogous to the fundamental plane for elliptical galaxies (see also Marconi & Hunt, 2003; de Francesco et al., 2006; Barway & Kembhavi, 2007; Aller & Richstone, 2007). The striking similarity between these two fundamental planes is another clue that galaxy spheroids and BHs did not form independently. The paradigm that the Active Galactic Nuclei [AGN] are powered by mass accretion onto these BHs (Salpeter, 1964; Lynden-Bell, 1969) has got very strong support from spectroscopic and photometric observations of the stellar and gas dynamics in the central regions of local spheroidal galaxies and bulges. Moreover, by estimating the total energy radiated by AGN during their whole life, it can be shown that nearly all the mass in BHs have been accumulated during periods of bright AGN activity (Soltan, 1982; Fabian & Iwasawa, 1999; Elvis et al., 2002; Hopkins et al., 2007e), implying that the common physical process which produces galaxy spheroids and BHs also must be responsible for triggering bright AGN.

Such a cosmological co-evolution of BHs, AGN and galaxies is expected in the standard framework of an expanding Universe dominated by cold dark matter and accelerated by dark energy. In fact, in this scenario structures form and evolve in a hierarchical way through mergers that can destabilize the gas at the galaxy centres and consequently trigger star formation and BH mass accretion. In order to approximate this complex scenario, several models have been developed, based on either pure analytical techniques (see, e.g., Efsthathiou & Rees, 1988; Haehnelt & Rees, 1993; Haiman & Loeb, 1998; Percival & Miller, 1999; Haiman & Menou, 2000; Martini & Weinberg, 2001; Wyithe & Loeb, 2003; Hatziminaoglou et al., 2003; Miller et al., 2006; Hopkins & Hernquist, 2006), or semi-analytical ones (see, e.g., Kauffmann & Haehnelt, 2000; Cavaliere & Vittorini, 2002; Enoki et al., 2003; Volonteri et al., 2003a; Springel et al., 2005a; Cattaneo et al., 2005; Croton et al., 2006; Malbon et al., 2007; Monaco et al., 2007). More recently, thanks to the high computational power reached in the last years, also fully numerical models have been proposed (see, e.g., Li et al., 2007; Pelupessy et al., 2007; Di Matteo et al., 2007).

As we will explicitly show in Chapter 2, simple analytic models in which AGN activity is only triggered by DM halo major mergers succeeded in quantitatively describing the observed evolution of the AGN number counts and luminosity at all but low redshifts, provided that some mechanisms are advocated to inhibit accretion within massive haloes hosting bright AGN, but they generally have serious problems in reproducing the observed AGN clustering at high redshifts (Marulli et al., 2006). Slightly more sophisticated semi-analytic models in which the baryonic physics is neglected as well, can correctly reproduce both the AGN luminosity and clustering function at $z \gtrsim 1$ (Marulli et al., 2006), but the number density of faint AGN is significantly below observations, as will be demonstrated in Chapter 3, a clear indication that DM halo mergers cannot constitute the only trigger to accretion episodes in the local BH population (Marulli et al., 2007), and that in order to properly describe the cosmological evolution of BHs and AGN the main baryonic phenomena involving the gas contents of DM halos cannot be neglected.

After all, such a complication is of the same kind of the one found in the description of galaxies, where the well-known mismatch in shape between the predicted distribution of DM halo masses and the observed distribution of galaxy luminosities forces to introduce in the models complex baryonic phenomena like, for instance, cooling inefficiencies to reduce gas condensation in massive structures, and supernova (White & Rees, 1978; White & Frenk, 1991) and stellar kinetic feedback (Fontanot et al., 2006) to remove cold gas

in low mass systems, as well as photoionisation heating to suppress the formation of dwarfs (Efstathiou, 1992). Cooling effects alone are however too weak to produce the bright end cut-off of the luminosity function [LF], and it seems to be mandatory to include additional feedback processes in massive systems (e.g. Benson et al., 2003; Fontanot et al., 2006; Croton et al., 2006). Other two important problems of the standard models of structure evolution regard i) the description of the observed properties of the gas at the centre of most galaxy clusters which do not condense and turn into stars when the cooling time is expected to be much shorter than the age of the system (see, e.g. Cowie & Binney, 1977; Fabian & Nulsen, 1977; Peterson et al., 2001; Tamura et al., 2001; Fabian et al., 2003; McNamara et al., 2005; Morandi & Ettori, 2007, and references therein), and ii) the fact that most massive galaxies, typically ellipticals in clusters, are made of the oldest stars and so finished their star formation earlier than lower mass galaxies (see, e.g. Cowie et al., 1996; Cimatti et al., 2006, and references therein).

In this Thesis, we will study the cosmological co-evolution of galaxies and their central BHs by using both analytic, semi-analytic and the so-called hybrid models, and compare their predictions to the most recent observational data available. First, in Chapter 1, we will give a brief overview of the general properties of the BH and AGN populations, from both the observational and theoretical sides. Then, we will focus on very simple analytic models where the assembly of BHs is directly related to the merger history of DM haloes. For this purpose, we will implement the two original analytic models of Wyithe & Loeb (2002) and Wyithe & Loeb (2003), compare their predictions to the AGN LF and clustering data, and discuss possible modifications to the models that improve the match to the observation. All the details will be described in Chapter 2. In Chapter 3, we will study more sophisticated semi-analytic models in which however the baryonic physics is neglected as well. Finally, in Chapter 4, we will improve the hybrid simulation of De Lucia & Blaizot (2007). Differently from the other models considered in this work, here the main baryonic phenomena of the galaxy evolution are included. Moreover, *radio mode* feedback from AGN at the centre galaxy groups and clusters is introduced to prevent significant gas accretion, thus limiting the mass of the central galaxies and preventing them from forming stars at late times when their mass and morphology can still change through mergers. Thanks to this mechanism, Croton et al. (2006) demonstrated that such a model can simultaneously explain the low observed mass drop-out rate in cooling flows, the exponential slope of the bright end tail of the galaxy LF, and the bulge-dominated morphologies and stellar ages of the most massive

galaxies in clusters. We will add new semi-analytical prescriptions to describe the BH mass accretion rate during each merger event and its conversion into radiation. Then we will compare the derived BH scaling relations, fundamental plane and mass function, and the AGN luminosity function with observations.

CHAPTER 1

Black Holes and Active Galactic Nuclei



THIS chapter aims at providing a brief overview of the general properties of the BH and AGN populations, from both the observational and theoretical sides. We will describe the most recent determinations of the BH scaling relations, fundamental plane and mass function. Then, we will discuss the available observational constraints on the AGN population, i.e. the AGN number counts, luminosity function and clustering. Finally, we will give a short summary of the most interesting analytic, semi-analytic and numerical models developed so far to describe the cosmological co-evolution of BHs, AGN and galaxies.

The AGN population is extremely heterogeneous, including very different objects like Quasars, radio galaxies, Seyfert nuclei, Blazars, LINERS and BL-Lac objects. These sources can be very different from each other, for instance due to different kinds of activity which take place in their nuclei and/or different properties of their galaxy hosts. However, from an observational point of view, there are at least three notable common properties. First, all AGN are extremely compact objects, as can be directly deduced from their flux variability; for example, in the X-ray band, variability has been observed on time scales of less than a day, and flares on time scales of minutes. The second point is that their spectral energy distribution, constant over about seven decades in frequency, is clearly non-stellar. Thirdly, since AGN remain active for more than 10^7 years with bolometric luminosities which are extremely large (often several orders of magnitude larger than the luminosities of their host galaxies), these objects must be very massive. Indeed, a very large amount of mass has to be accreted to sustain such luminosities, even assuming a very high efficiency of energy production.

From the above properties, it seems evident that the source of the nuclear activity must be the accretion of mass onto a central, supermassive compact object (Rees, 1984). Although there is no direct proof that all of them are BHs (Maoz, 1998), the evidence in favour of a BH singularity is now very strong in the Milky Way (see e.g. Schödel et al., 2002; Ghez et al., 2003). Moreover, the possibility for alternative types of engine is severely constrained in NGC 4258 and other local galaxies (see e.g. Miyoshi et al., 1995; Kormendy, 2004). In the standard picture, the accreting matter is thought to be confined in accretion disks, glowing brightly at ultraviolet and soft X-ray wavelengths. Medium and hard X-ray emission is produced by inverse Compton scattering in a corona of optically thin plasma which might surround the disk. Clouds of line-emitting gas move at high velocity around this core and are in turn surrounded by an obscuring torus or warped disk of gas and dust, with a sea of electrons permeating the volume within and above the torus. The “standard AGN paradigm” states that all the different properties which are observed among different types of AGN are not intrinsic, but are determined by external factors, like the angle at which the AGN is observed, the spin and/or mass of the BH, the mass accretion rate and the way with which the surrounding interstellar medium interacts with the emerging AGN flux.

SECTION 1.1

Observations

1.1.1 BH scaling relations

Modern BH searches have targeted almost exclusively quiescent or weakly active nearby galaxies. Indeed, at the present time, the dynamical signature imprinted by a central compact object on the motion of the surrounding gas and stars can only be observed directly in the nearest galactic centers and, unfortunately, most nearby galaxies are not powerful AGN. “Dormant” BHs are expected to be found in the nuclei of such galaxies, as the cumulative BH mass density needed to explain the energetics of high-redshift powerful AGN falls short, by at least two orders of magnitudes, to the one required to power local AGN. The unaccounted BHs must therefore reside in local, quiescent galaxies.

BH - bulge

The ever-increasing number of BHs with accurate mass measurements has revealed strong connections between these objects and their host galaxies. These correlations pose a theoretical challenge because the mass accretion onto BHs takes place on extremely small spatial scales compared to the galactic scales. Kormendy & Richstone (1995) first pointed out that the existence of a scaling relation between $M_{\text{BH}} - L_{\text{bulge}}$ (where M_{BH} is the BH mass and L_{bulge} is the host bulge luminosity) indicates that BHs and bulge formation are tightly connected or even that the presence of a bulge might be a necessary condition for BH formation. Magorrian et al. (1998), using a sample of 36 nearby galaxies with Hubble Space Telescope photometry and ground-based kinematics, found that the BHs located at the galaxy centres have masses linearly related to the masses of their hosting bulges, $M_{\text{BH}} \sim 0.006M_{\text{bulge}}$. Two years later, Ferrarese & Merritt (2000) showed, instead, that all secure BH mass estimates available since then indicated that the masses of BH correlate more strongly with the velocity dispersions of their host bulges, $M_{\text{BH}} \sim \sigma_c^\alpha$, where $\alpha = 4.8 \pm 0.5$, with a scatter no larger than expected on the basis of measurement error alone. BH masses estimated by Magorrian et al. (1998) lied systematically above the $M_{\text{BH}} - \sigma_c$ relation by Ferrarese & Merritt (2000), some by as much as two orders of magnitude. Gebhardt et al. (2000) confirmed and improved this result, finding $M_{\text{BH}} = 1.2(\pm 0.2) \times 10^8 M_\odot (\sigma_c / 200 \text{ km s}^{-1})^{3.75(\pm 0.3)}$ over almost 3 orders of magnitude in M_{BH} , for a sample of 26 galaxies, including 13 galaxies with newer determinations of BH masses from Hubble Space Telescope measurements of stellar kinematics. For this sample, the scatter found in M_{BH} at fixed σ_c is only 0.30 dex, and most of this is due to observational errors. In the following years, several authors improved the accuracy in the determination of such scaling relations. Tremaine et al. (2002) proposed that the above discrepancies arised mostly because of systematic differences in the velocity dispersions measured by the different groups for the same galaxies. In particular, they suggested that a significant component of the difference results from the Ferrarese & Merritt (2000)'s extrapolation of central velocity dispersions to $r_e/8$ (r_e is the effective radius) using an empirical formula, and from dispersion-dependent systematic errors in the measurements. Using a sample of 31 galaxies, they proposed a new determination of the fitting parameters, $\log(M_{\text{BH}}/M_\odot) = \alpha + \beta \log(\sigma_c/\sigma_0)$, where $\beta = 4.02 \pm 0.32$ and $\alpha = 8.13 \pm 0.06$ for $\sigma_c = 200 \text{ km s}^{-1}$.

In spite of the fundamental importance of such scaling relations for our understanding of the co-evolution of BHs and galaxies, it is not yet clear

which of them is “more fundamental” (see e.g. Novak et al., 2006; Lauer et al., 2007). For instance, Graham et al. (2001) found a strong correlation between the concentration of bulges, C_r , defined as the luminosity ratio between the flux enclosed by some inner radii and the outermost radii, and the mass of their central BHs of the form $\log(M_{\text{BH}}/M_{\odot}) = 6.81(\pm 0.95)C_r(1/3) + (5.03 \pm 0.41)$, with comparable or even less scatter with respect to the $M_{\text{BH}} - \sigma_c$ relation (0.31 dex in $\log M_{\text{BH}}$, which decreases to 0.19 dex for galaxies whose BH radii of influence are resolved). Using a combined 90-object sample of Seyfert galaxies with BH mass estimates obtained from both reverberation mapping and stellar velocity dispersions, plus a sample of 18 nearby inactive elliptical galaxies with dynamical BH mass measurements, McLure & Dunlop (2002) found that the scatter around the $M_{\text{BH}} - L_{\text{bulge}}$ relation is comparable to that of the $M_{\text{BH}} - \sigma_c$ relation. Later on, Marconi & Hunt (2003) confirmed this result for a sample of 27 galaxies with a secure BH mass measurement, finding that the spread of $M_{\text{BH}} - L_{\text{bulge}}$ ($\simeq 0.3$ dex in $\log M_{\text{BH}}$) is similar to the one of $M_{\text{BH}} - \sigma_c$. Confirming and refining this result for a sample of 30 galaxies, Häring & Rix (2004) found $M_{\text{BH}} \sim M_{\text{bulge}}^{1.12 \pm 0.06}$ with an observed scatter of $\lesssim 0.30$ dex, a significant fraction of which can be attributed to measurement errors, and therefore comparable to the scatter in the $M_{\text{BH}} - \sigma_c$ relation.

In Figure 1.1, we show the most recent observational data and best fits available for the observed scaling relations between BHs and bulges. Starting from the upper left panel down to the lower right one, we plot the $M_{\text{BH}} - M_K$ and $M_{\text{BH}} - M_B$ relations by Marconi & Hunt (2003) as revised by Graham & Driver (2007a) and the $M_{\text{BH}} - M_B$ one by McLure & Dunlop (2002) (where M_K and M_B are the bulge magnitude as measured in K- and B- band), the $M_{\text{BH}} - \sigma_c$ relation by Ferrarese & Ford (2005) and by Hu (2008) and the $M_{\text{BH}} - M_{\text{bulge}}$ relation by Häring & Rix (2004). The magenta lines in the lower two panels show the fits obtained by Wyithe (2006), who demonstrated that a log-linear relation does not provide an adequate description of the Tremaine et al. (2002) and Häring & Rix (2004) data, and instead proposed a log-quadratic relation of the form $\log(M_{\text{BH}}) = \alpha + \beta_1 \log(M_{\text{bulge}}/10^{11}M_{\odot}) + \beta_2 [\log(M_{\text{bulge}}/10^{11}M_{\odot})]^2$, with $\beta_1 = 1.15 \pm 0.18$, $\beta_2 = 0.12 \pm 0.14$.

Very recently, Hu (2008) investigated the $M_{\text{BH}} - \sigma_c$ relation in two types of host galaxies: the classical bulges (or elliptical galaxies), and pseudobulges, identified as “bulges” which contain a nuclear bar, nuclear spiral, and/or nuclear ring. Using a sample of 41 classical bulges plus 12 pseudobulges, the larger catalogue of spatially well-resolved M_{BH} measurement to date, he found that the $M_{\text{BH}} - \sigma_c$ relation for pseudobulges is different from the relation in the classical bulges at a significance level $> 3\sigma$. If this result is confirmed,

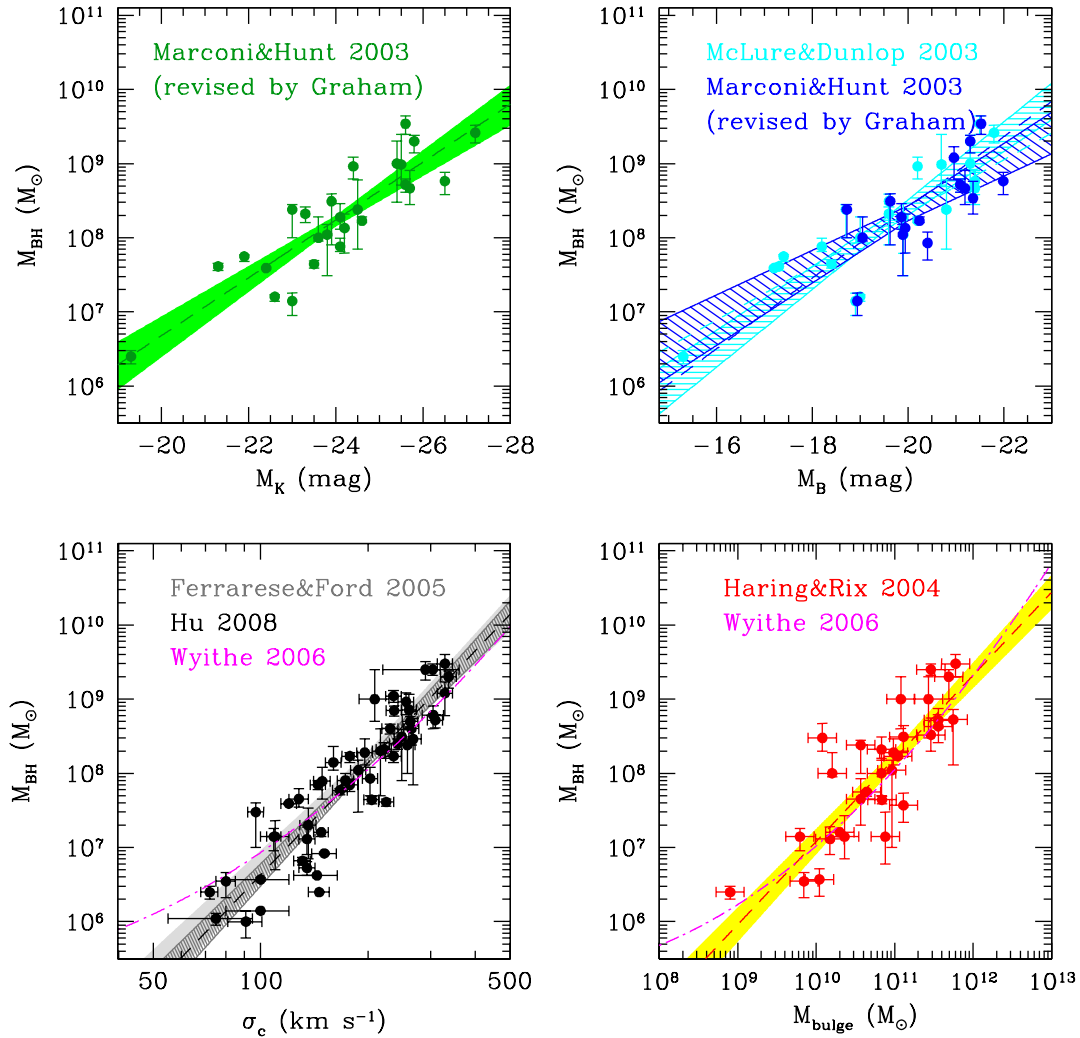


Figure 1.1: The most recent observational data and fits available for the observed scaling relation between BHs and bulges. Starting from the upper left panel down to the lower right panel one: $M_{\text{BH}} - M_K$ and $M_{\text{BH}} - M_B$ relations by Marconi & Hunt (2003) as revised by Graham & Driver (2007a) and the $M_{\text{BH}} - M_B$ one by McLure & Dunlop (2002) (where M_K and M_B are the bulge magnitude as measured in K- and B- band); $M_{\text{BH}} - \sigma_c$ relation by Ferrarese & Ford (2005) and by Hu (2008); $M_{\text{BH}} - M_{\text{bulge}}$ relation by Häring & Rix (2004). The magenta lines in the lower two panels show the log-quadratic fits obtained by Wyithe (2006).

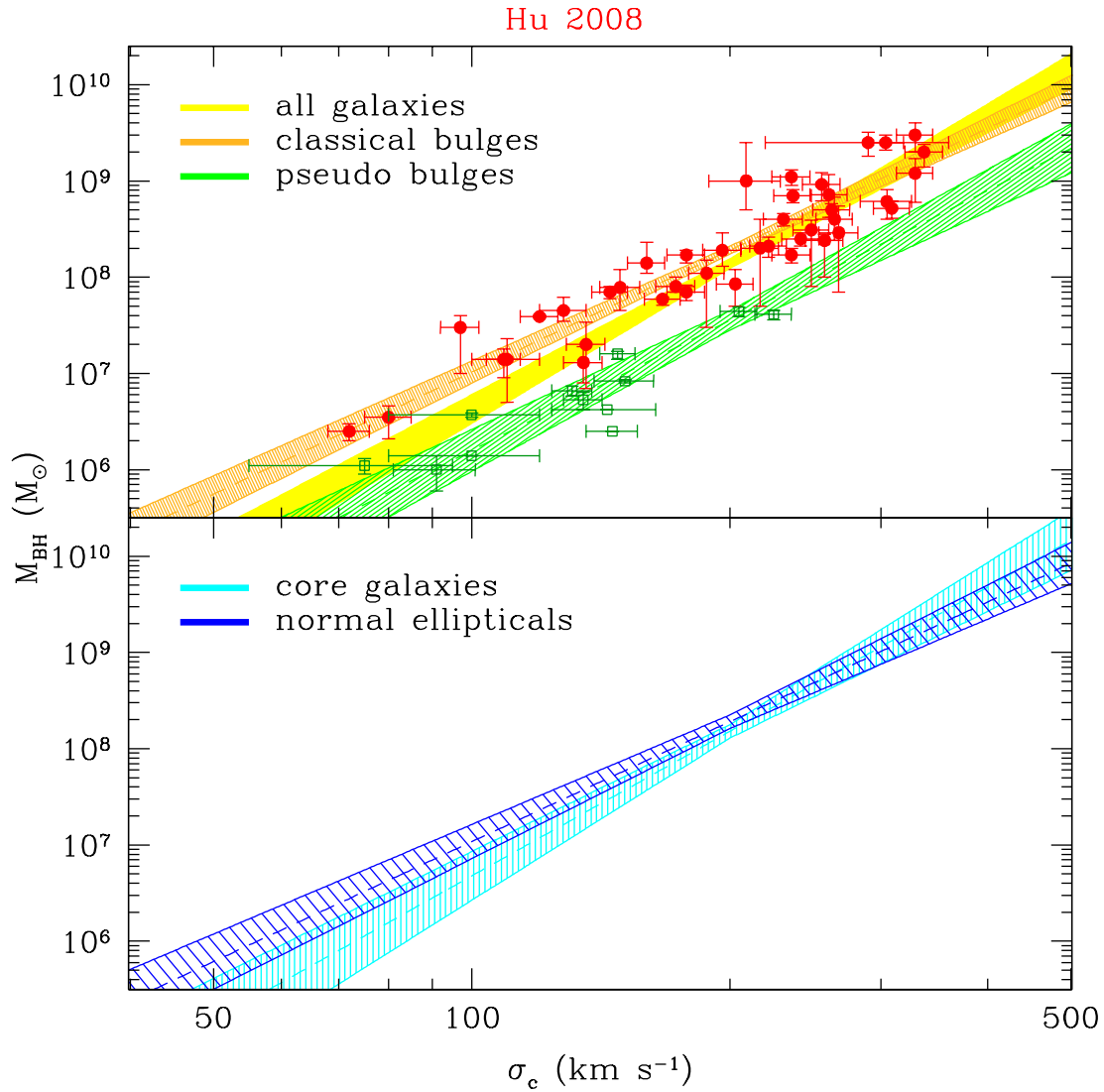


Figure 1.2: $M_{\text{BH}} - \sigma_c$ relation by Hu (2008); upper panel: BHs hosted in classical bulges (red) and pseudobulges (green); lower panel: BHs in core galaxies (cyan) and normal ellipticals (blue).

it would indicate that the formation and growth histories of BHs depend on their host type, in particular the pseudobulges seem to be relatively low efficient to fuel the central BHs. Moreover, he found that the slope for the 13 “core” elliptical galaxies in the high mass range of the relation appears slightly steeper, which may be the imprint of the fact that they originate from dissipationless mergers, in agreement with what previously found by Lauer et al. (2007). Figure 1.2 shows Hu (2008)’s data and fit for BHs hosted in classical bulges (red) and pseudobulges (green) in the upper panel, and for BHs in core galaxies (cyan) and normal ellipticals (blue) in the lower one.

BH - DM halo

Some observational data support a strong correlation between the masses of BHs and the total gravitational mass of their host galaxy, or the mass of the DM halo in which they presumably formed. Using a sample of 16 spiral and 20 elliptical galaxies, Ferrarese (2002) demonstrated that the bulge velocity dispersion correlates tightly with the galaxy circular velocity, v_c , the latter measured at distances from the galactic centre at which the rotation curve is flat, $R \sim 20 - 80$ kpc. The derived $M_{\text{BH}} - M_{\text{DM}}$ relation was found to be nonlinear, with the ratio $M_{\text{BH}}/M_{\text{DM}}$ decreasing from 2×10^{-4} for $M_{\text{DM}} \sim 10^{14} M_{\odot}$ to 10^{-5} for $M_{\text{DM}} \sim 10^{12} M_{\odot}$. Over the last years, this result has been also confirmed by Baes et al. (2003), Ferrarese & Ford (2005) and Shankar et al. (2006). The most recent data and fits for the $V_c - \sigma_c$, $M_{\text{BH}} - V_c$ and $M_{\text{BH}} - M_{\text{DM}}$ relations are shown in Figure 1.3. The blue, black and green lines in the lower right panel correspond to Eqs. (4), (6) and (7) of Ferrarese (2002), who derived them using different assumptions for the for the $M_{\text{DM}} - V_c$ relation. The red and orange lines show the $M_{\text{BH}} - M_{\text{DM}}$ relation derived by Baes et al. (2003) and Shankar et al. (2006), respectively. All other symbols are explicitly described in the labels.

The $M_{\text{BH}} - M_{\text{DM}}$ relation represents the observational evidence for an intimate link between DM haloes and BHs, and it is used, though often implicitly, as starting point in almost all analytic and semi-analytic models for the cosmological co-evolution of BHs and AGN, as we will describe in the next chapters. However, although there is no doubt that such a relation implies that the formation of BHs is controlled, perhaps indirectly, by the properties of the DM haloes in which they reside, it is still unclear if it is “genuine” or simply reflects the fact that massive haloes preferentially host massive spheroids (Wyithe & Loeb, 2005a).

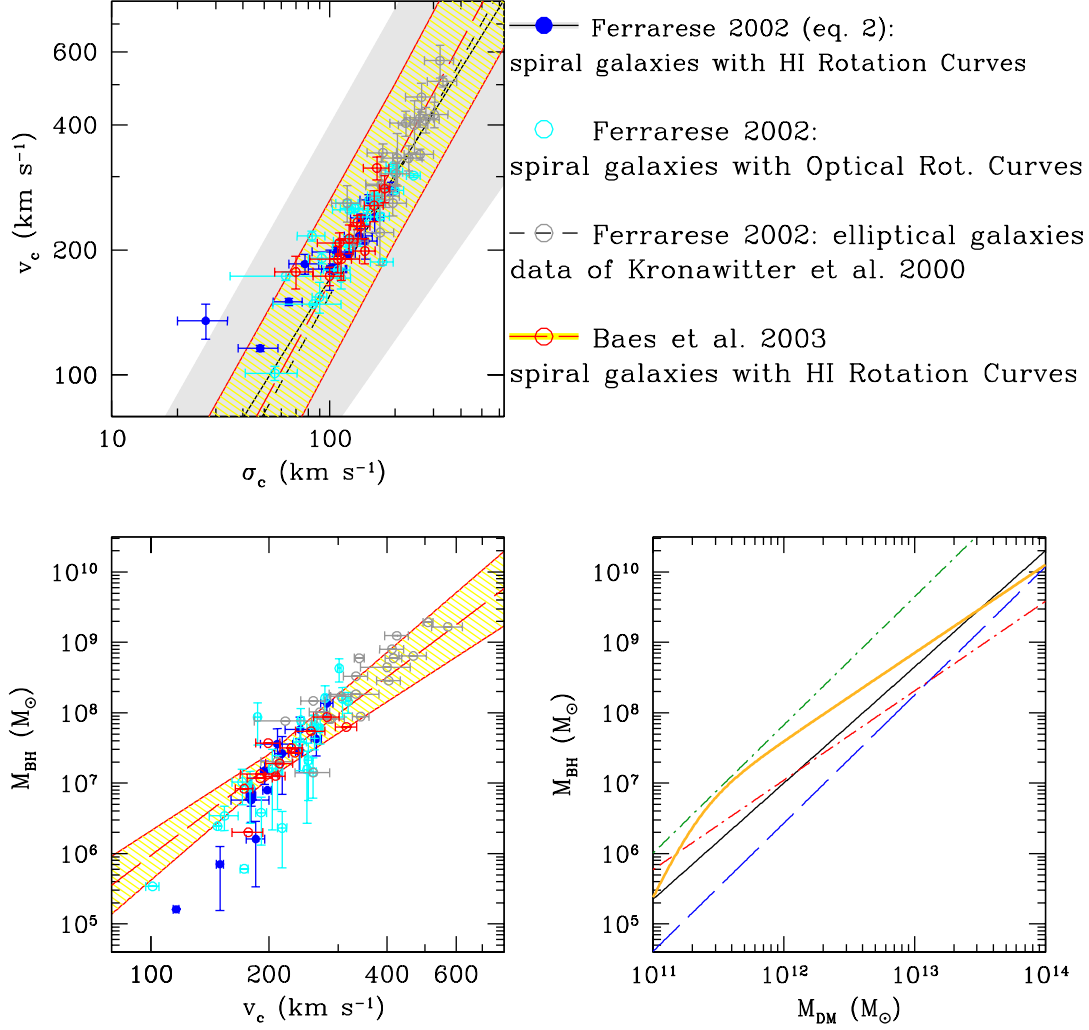


Figure 1.3: The most recent data and fits for the $V_c - \sigma_c$, $M_{\text{BH}} - V_c$ and $M_{\text{BH}} - M_{\text{DM}}$ relations. In the lower right panel, the blue, black and green lines correspond to Eqs. (4), (6) and (7) of Ferrarese (2002), who derived them using different assumptions for the $M_{\text{DM}} - V_c$ relation. The red and orange lines show the $M_{\text{BH}} - M_{\text{DM}}$ relation derived by Baes et al. (2003) and Shankar et al. (2006), respectively. All other symbols are explicitly described in the labels.

Scaling relations at higher redshift

All of the scaling relations described above concern the population of BHs hosted in the nuclei of local galaxies. Unfortunately, the situation at $z > 0$ is still very unclear since is limited by the small number of observable hosts. Indeed, different groups have reached seemingly contradictory conclusions. Velocity dispersion measurements have favored both the case of no evolution (Shields et al., 2003, from O III velocity dispersions) and that of substantial evolution (Shields et al., 2006; Woo et al., 2006, from CO dispersions and spectral template fitting). AGN clustering (Adelberger & Steidel, 2005; Wyithe & Loeb, 2005a; Hopkins et al., 2007d; Lidz et al., 2006) suggests moderate evolution in the ratio of BH to host halo mass at redshifts $z \sim 1 - 3$. Direct host R-band luminosity measurements (Peng et al., 2006) and indirect comparison of quasar luminosity and stellar mass densities (Merloni et al., 2004b) or BH and stellar mass functions (Hopkins et al., 2006b) similarly favor moderate evolution in the ratio of BH to host spheroid stellar mass occurring at $z \gtrsim 1$, and dynamical masses from CO measurements suggest that this evolution may extend to $z \sim 6$ (Walter et al., 2004).

1.1.2 BH fundamental plane

Using a sample of local BHs for which masses have been reliably determined via either kinematic or maser measurements (the local 38 systems compiled by Marconi & Hunt (2003) and Häring & Rix (2004)), Hopkins et al. (2007a) showed that all the BH scaling relations described in the previous section could be interpreted as 2D-projections of the same *fundamental plane* [FP], of the form $M_{\text{BH}} \propto \sigma_{\text{c}}^{3.0 \pm 0.3} R_e^{0.43 \pm 0.19}$ or $M_{\text{BH}} \propto M_*^{0.54 \pm 0.17} \sigma_{\text{c}}^{2.2 \pm 0.5}$, where M_* is the galaxy stellar mass. This relation is analogous to the well-established FP of elliptical galaxies. In order to define such a plane, Hopkins et al. (2007a) looked for correlations between the residuals of the various projections. Specifically, the residual with respect to the $M_{\text{BH}} - \sigma_{\text{c}}$ relation has been determined by fitting $M_{\text{BH}}(\sigma_{\text{c}})$ to an arbitrary log-polynomial

$$\langle \log(M_{\text{BH}}) \rangle = \Sigma [a_n \log(\sigma_{\text{c}})^n],$$

allowing as many terms as the data favor (i.e. until $\Delta\chi^2$ with respect to the fitted relation is < 1), and then computing the residual,

$$\Delta \log(M_{\text{BH}} | \sigma_{\text{c}}) \equiv \log(M_{\text{BH}}) - \langle \log(M_{\text{BH}}) \rangle(\sigma_{\text{c}}).$$

The residual $\Delta \log(R_e | \sigma_{\text{c}})$ and $\Delta \log(M_* | \sigma_{\text{c}})$ were computed in the same way. The analysis showed that the BH FP is preferred over a simple relation

between M_{BH} and any of the host galaxy properties alone at $> 3\sigma$ (99.9%) significance, and its existence can account for the presence of several outliers in both the $M_{\text{BH}} - \sigma_c$ and $M_{\text{BH}} - M_*$ relations. This result puts strong constraints on theoretical models of BH growth and evolution: BH mass does not simply scale with the star formation (stellar mass) or virial velocity of the host galaxy.

With a large set of numerical simulations of major galaxy mergers, Hopkins et al. (2007b) demonstrated also that a feedback-driven model of BH growth and self-regulation is in perfect agreement with this BH FP. Moreover, while various changes in the properties of the simulated mergers (including the redshift) biased the various projections of the BH FP to different values, they simply move remnants *along* the BH FP relation. Given the empirical tendency toward more compact spheroids with smaller R_e at a given stellar mass M_* at high redshift, the BH FP predicts that BHs should be more massive at high redshifts than at low ones, at fixed M_* . This evolution is in agreement with the theoretical expectation that the progenitor disks in typical mergers should be more gas-rich at higher redshifts, and mergers more dissipational, yielding more concentrated remnants and driving the evolution in M_{BH}/M_* along the BH FP. Figure 1.4 shows the masses of BHs in the simulations of Hopkins et al. (2007b) and from local measurements, compared to the expectations from the best-fit BH FP relations in σ_c , R_e and M_* , σ_c . The two agree well at all masses, without any evidence for curvature in the relations. The intrinsic scatter in M_{BH} at fixed σ_c , R_e or M_* , σ_c is estimated from the simulations to be ~ 0.20 dex, which is consistent with the scatter in the observed points (given their measurement errors).

In substantial agreement with this result, Feoli & Mele (2005) and Feoli & Mele (2007) proposed a relationship between the mass of a BH and the kinetic energy of random motions in the host galaxy (irrespective of its morphology). They found $M_{\text{BH}} \propto (M_G \sigma_c^2 / c^2)^\beta$ with $0.8 \leq \beta \leq 1$ depending on the different fitting methods and samples used, with an internal scatter smaller than the one found from the $M_{\text{BH}} - \sigma_c$ relation derived from the same catalogue. Their results are shown in Figure 1.5. Similar results have also been obtained by Marconi & Hunt (2003); de Francesco et al. (2006); Barway & Kembhavi (2007); Aller & Richstone (2007).

However, given the small number of BHs with secure mass measurements, it may be premature to conclusively believe in the existence of a FP for BHs. For instance, Graham (2008) have recently suggested that the presence of disk (especially barred) galaxies appears responsible for much of the alleged evidence for requiring a FP. Indeed, the galaxies which deviate

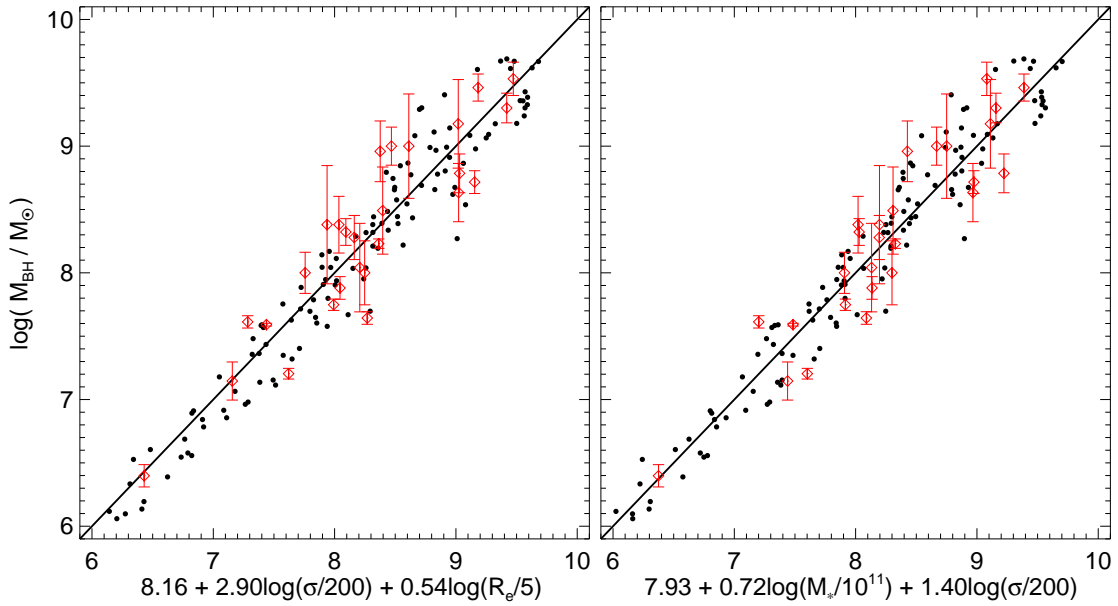


Figure 1.4: Masses of BHs in the simulations of Hopkins et al. (2007b) and from local measurements, compared to the expectation from the best-fit BHFP relations in σ_c , R_e and M_* , σ_c (from Hopkins et al. (2007b)).

from the $M_{\text{BH}} - \sigma_c$ relation, giving rise to the FP relations with less scatter than the $M_{\text{BH}} - \sigma_c$ relation, are predominantly barred galaxies. A “barless $M_{\text{BH}} - \sigma_c$ ” relation and an elliptical-only $M_{\text{BH}} - \sigma_c$ relation are both found to apparently eliminates the need for a BH FP.

1.1.3 BH mass function

The BH mass function [MF] is defined as the differential comoving number density of BHs as a function of their mass. Due the small number of accurately measured BH masses, at the present time the BH MF can only be derived by coupling the statistical information on local LF of galaxies with relationships among luminosity (or related quantities such as stellar mass and velocity dispersion) and the central BH mass:

$$\Phi_M(M_{\text{BH}}, z) = \frac{dn_{\text{BH}}}{d\log(M_{\text{BH}})} = \frac{dn_{\text{BH}}}{dn_{\text{galaxy}}} \frac{dn_{\text{galaxy}}}{d\log(L_{\text{galaxy}})} \frac{d\log(L_{\text{galaxy}})}{d\log(M_{\text{BH}})}. \quad (1.1)$$

Because the BH mass correlates with the luminosity and velocity dispersion of the bulge stellar population, it is necessary to separate LFs for different morphological types (which have different bulge to total luminosity ratios), and it is convenient to use galaxy LFs derived in red and infrared bands, which are more directly linked to the mass in old stars.

Based on both kinematic and photometric data, Shankar et al. (2004)

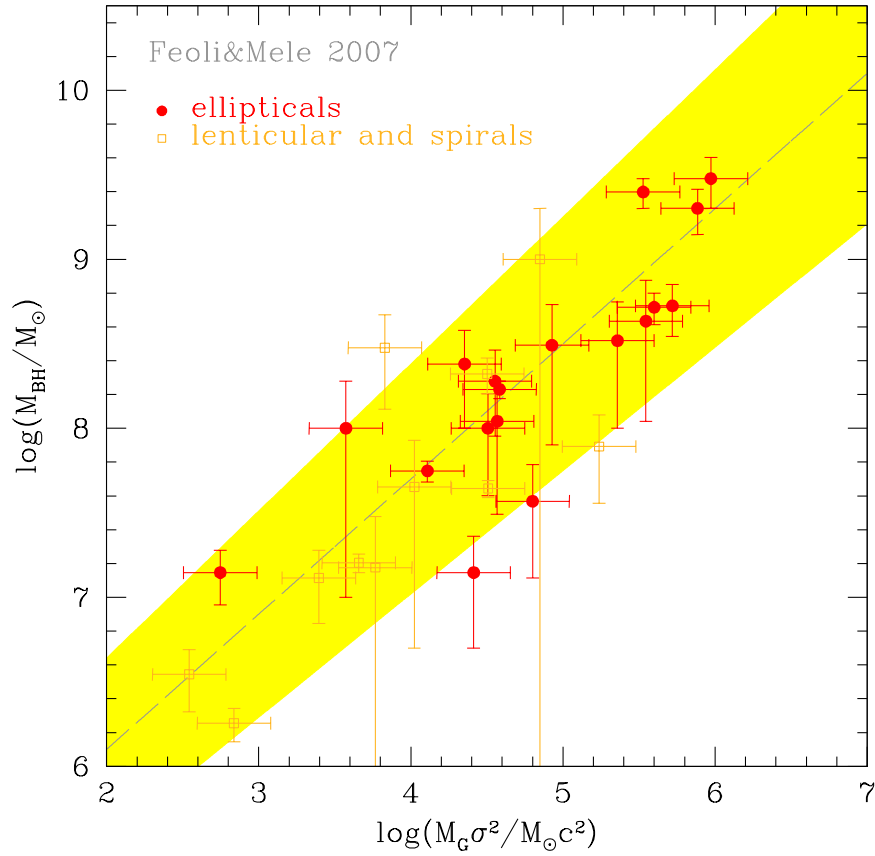


Figure 1.5: The relationship between the BH mass and the kinetic energy of random motions in the host galaxy found by Feoli & Mele (2007).

derived an analytical fit to the local BH MF in the range $10^6 \leq M_{\text{BH}}/M_{\odot} \leq 5 \times 10^9$:

$$\Phi_M(M_{\text{BH}}, z=0) = \Phi_* \left(\frac{M_{\text{BH}}}{M_*} \right)^{\alpha+1} \exp \left[- \left(\frac{M_{\text{BH}}}{M_*} \right)^{\beta} \right], \quad (1.2)$$

with $\Phi_* = 7.7(\pm 0.3) \cdot 10^{-3} \text{Mpc}^{-3}$, $M_* = 6.4(\pm 1.1) \cdot 10^7 M_{\odot}$, $\alpha = -1.11(\pm 0.02)$ and $\beta = 0.49(\pm 0.02)$ ($H_0 = 70 \text{km s}^{-1} \text{Mpc}^{-1}$).

Eq.(1.2) implies a total BH mass density of $(4.2 \pm 1.1) \times 10^5 M_{\odot} \text{Mpc}^{-3}$, about 25 per cent of which is contributed by BHs residing in bulges of late-type galaxies. If most of the accretion occurs at constant $\dot{M}_{\text{BH}}/M_{\text{BH}}$, as in the case of Eddington-limited accretion, this MF is fully accounted for by mass accreted by X-ray selected AGN, for reliably bolometric corrections and with an *accretion efficiency*, $\varepsilon := L_{\text{bol}}/(M_{\text{accr}}c^2) \sim 0.1$. An unlikely fine tuning of the parameters would be required to account for the local BH MF accommodating a dominant contribution from “dark” BH growth (due, for example, to BH coalescence). Moreover, this work supports the scenario in which the most massive BHs accreted their mass faster and at higher redshifts (typically at $z > 1.5$), while the lower-mass ones, responsible for most of the hard X-ray background, have mostly grown at $z < 1.5$. The visibility time, during which AGN are luminous enough to be detected by the currently available X-ray surveys, ranges from ~ 0.1 Gyr for present-day BH masses $M_{\text{BH}} \simeq 10^6 M_{\odot}$ to ~ 0.3 Gyr for $M_{\text{BH}} \simeq 10^9 M_{\odot}$. More precisely, the match between the MF of the mass accreted during the nuclear activity (derivable from the AGN LFs) and the local BH MF (Eq. (1.2)) implies a redshift-dependent *Eddington factor*, $f_{\text{Edd}} := L_{\text{bol}}(t)/L_{\text{Edd}}(t)$, of the form:

$$f_{\text{Edd}}(z) = \begin{cases} f_{\text{Edd},0} & z \geq 3 \\ f_{\text{Edd},0} \cdot [(1+z)/4]^{1.4} & z < 3 \end{cases} \quad (1.3)$$

with $f_{\text{Edd},0} = 0.3$.

The BH MF described by Eq. (1.2) is very close to the one found by Marconi et al. (2004), who used a similar methodology. However, different authors reached somewhat discrepant conclusions (see e.g. Aller & Richstone, 2002; Yu & Tremaine, 2002; McLure & Dunlop, 2002). Recently, Graham et al. (2007b) provided a new estimate of the local BH MF, using the relation between BH mass and the Sérsic index of the host spheroidal stellar system and the measured (spheroid) Sérsic indices drawn from the galaxies in the Millennium Galaxy Catalogue (both early- and late-type galaxies). Considering spheroidal stellar systems brighter than $M_B = -18$ mag, and integrating down to BH masses of $10^6 M_{\odot}$, they derived the local mass density of BHs in early-type galaxies $\rho_{\text{BH,early-type}} = (3.5 \pm 1.2) \times 10^5 h_{70}^3 M_{\odot} \text{Mpc}^{-3}$, and

in late-type galaxies $\rho_{\text{BH,late-type}} = (1.0 \pm 0.5) \times 10^5 h_{70}^3 M_{\odot} \text{Mpc}^{-3}$. The combined, cosmological, BH mass density is thus $\rho_{\text{BH,total}} = (3.2 \pm 1.2) \times 10^6 h_{70}^3 M_{\odot} \text{Mpc}^{-3}$.

Figure 1.6 shows the local MFs for the whole population of BHs (higher panel), and for BHs hosted in early- and late-type galaxies separately, observed by Shankar et al. (2004) (yellow area), by Shankar (private communication) (red area) and by Graham et al. (2007b) (blue area). Shankar et al. (2004) derived the BH masses from the observed $M_{\text{BH}} - L_{\text{bulge}}$ relation, while Shankar (private communication) used the $M_{\text{BH}} - \sigma_c$ relation of Tundo et al. (2007). While the predictions relative to the population of BHs in early-type galaxies are quite similar, the MF of Graham et al. (2007b) differs significantly from the Shankar one for BHs in late-type galaxies, and consequently for the overall BH population, especially at $M_{\text{BH}} \lesssim 10^8 M_{\odot}$. At the present time, the question is still open.

Thus far, we have described the present knowledge about the MF of quiescent BHs in the local Universe. However, in order to better constrain the theoretical model of BH and AGN evolution, it would be of crucial importance to observationally derive the MF of both active and quiescent BHs as a function of redshift and host morphology. Considerable efforts on these aspects are expected in the near future. Meanwhile, Heckman et al. (2004) and Greene & Ho (2006) presented the first measurement of the BH MF for, respectively, narrow- and broad-line active galaxies in the local Universe. Heckman et al. (2004) used 23000 narrow-emission-line (“type 2”) AGN and the complete sample of 123000 galaxies in the Sloan Digital Sky Survey [SDSS] (York et al., 2000) from which they were drawn. With the stellar velocity dispersions of the early-type galaxies and AGN hosts and the AGN [O III] $\lambda 5007$ emission line luminosities, they could estimate their BH masses and accretion rates. They found that most present-day accretion occurs onto BHs with masses less than $10^8 M_{\odot}$ that reside in moderately massive galaxies ($M_* \sim 10^{10} - 10^{11.5} M_{\odot}$) with high stellar surface mass densities and young stellar populations. Around half this growth takes place in AGN that are radiating within a factor of 5 of the Eddington luminosity. The rest of the growth occurs in lower luminosity AGN.

Using a sample of about 8500 broad-line AGN from the SDSS, Greene & Ho (2006) converted the observed broad-line luminosities and widths into BH masses and derived the MF of BHs in broad-line AGN. A MF constructed in this way has the unique capability to probe the mass region $< 10^6 M_{\odot}$, which may place important constraints on the mass distribution of seed BHs in the early Universe. The characteristic local active BH resulted to have a mass of $\sim 10^7 M_{\odot}$ and radiates with $f_{\text{Edd}} \sim 0.1$. The active fraction is a strong function

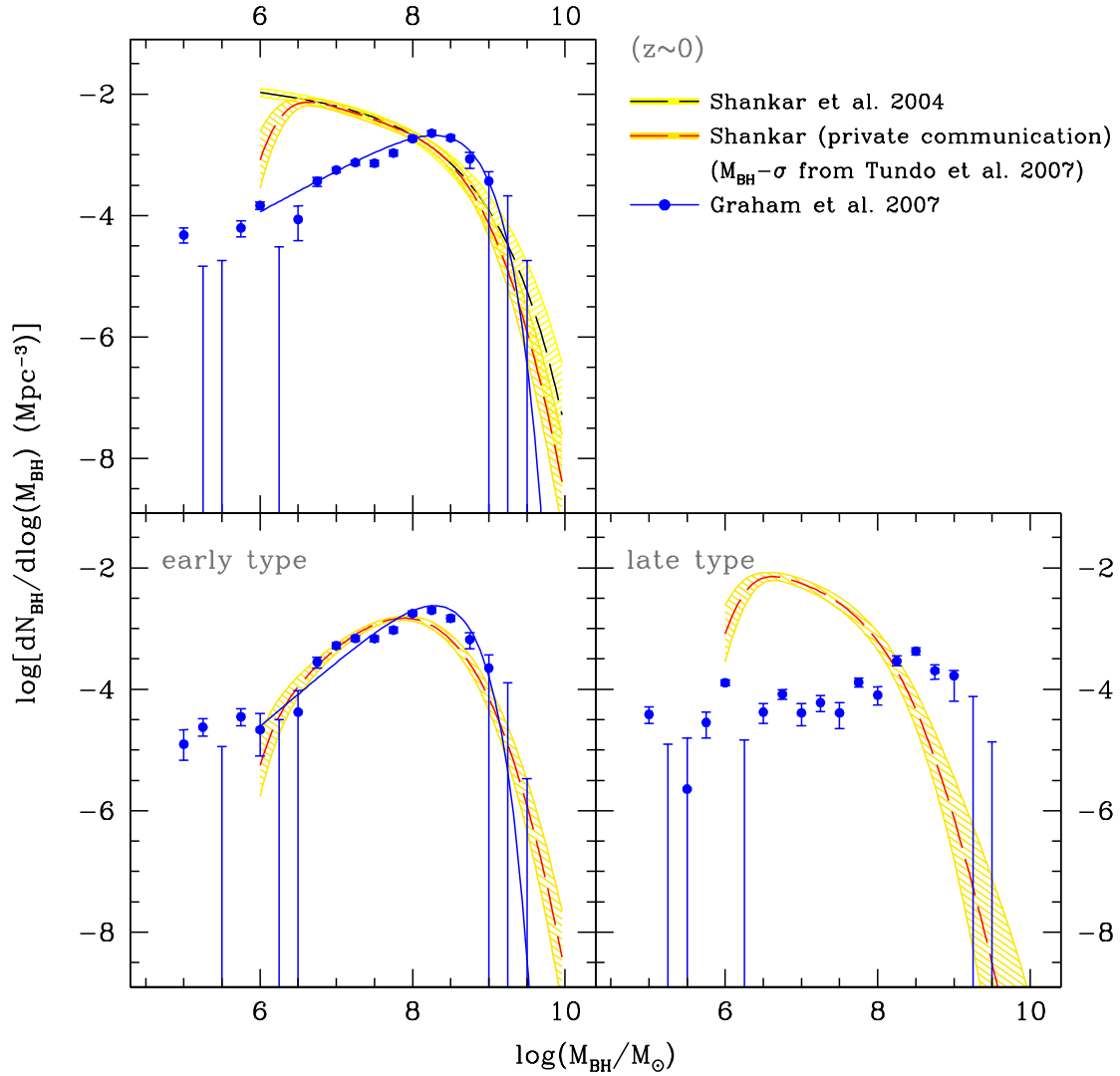


Figure 1.6: The BH MF derived by Shankar et al. (2004) (yellow area), by Shankar (private communication) (red area) and by Graham et al. (2007b) (blue are) for the whole population of BHs (higher panel), and for the BHs hosted in early- and late-type galaxies separately.

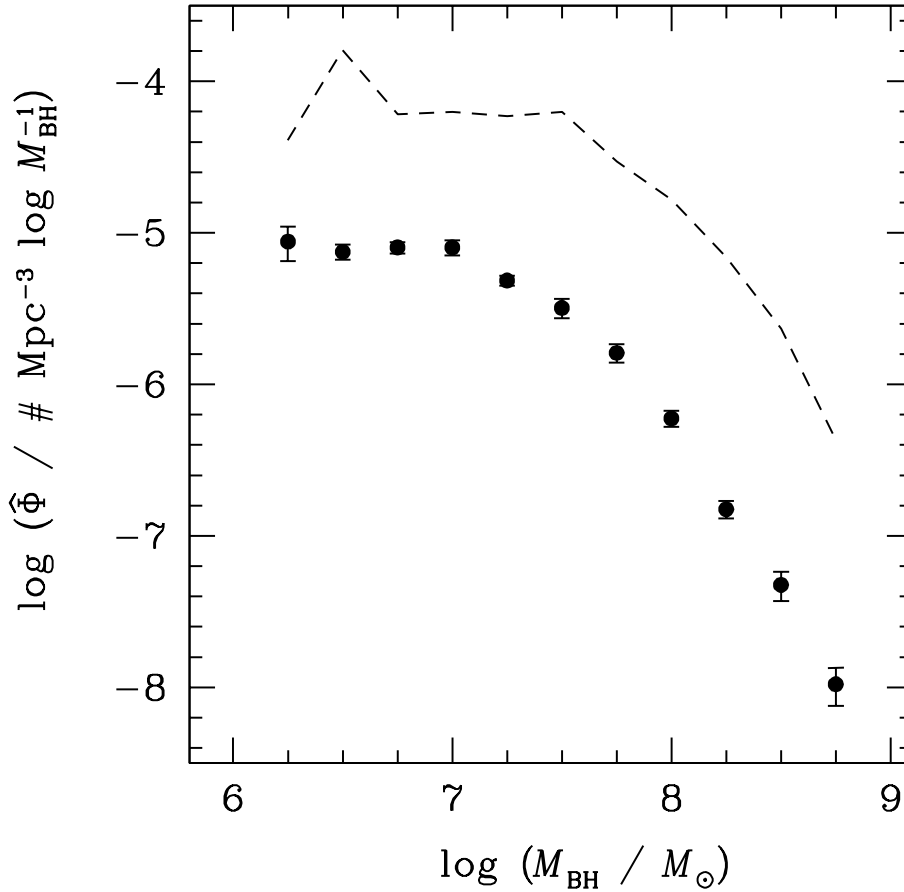


Figure 1.7: The comparison between the BH MF of broad-line (filled symbols; Greene & Ho (2006), truncated at $10^6 M_{\odot}$ for consistency with the narrow-line AGN sample) and narrow-line (dashed line; Heckman et al. (2004)) AGN (from Greene & Ho (2006)).

of BH mass; at both higher and lower masses the active mass function falls more steeply than one would infer from the distribution of bulge luminosity. The dearth of active massive BHs is a well-known result: massive BHs are mostly quiescent in the local Universe. The decreasing space density at low BH mass presumably reflects the fact that bulge fraction and BH occupation fraction both decrease in dwarf galaxies.

Figure 1.7 shows the comparison between the BH mass function of broad-line (filled symbols; Greene & Ho (2006), truncated at $10^6 M_{\odot}$ for consistency with the narrow-line AGN sample) and narrow-line (dashed line; Heckman et al. (2004)) AGN. The space density of narrow-line AGN in the Heckman et al. (2004) sample is higher than that of the broad-line sample by an order of magnitude. However, the selection effects for the two samples are very different (e.g. narrow emission lines may be detected to significantly lower luminosities than broad lines), and a really direct comparison is not possible at the present time.

1.1.4 AGN luminosity function

The LF of AGN, defined as the derivative of their comoving number density with respect to luminosity,

$$\Phi_L(L_{\text{AGN}}, z) = \frac{dn_{\text{AGN}}}{d \log L_{\text{AGN}}}, \quad (1.4)$$

represents one of the most important tools to infer the formation history of BHs and AGN, as well as the buildup of cosmic X-ray and infrared backgrounds and the contribution of quasars to reionization. The first determinations of the AGN LF started long ago (see e.g. Schmidt & Green, 1983; Koo & Kron, 1988; Boyle et al., 1988; Hewett et al., 1993; Hartwick & Schade, 1990; Warren et al., 1994; Schmidt et al., 1995; Kennefick et al., 1995; Pei, 1995), but only recently, surveys such as the Two Degree Field QSO Redshift Survey [2QZ] (Boyle et al., 2000) and the already mentioned SDSS have provided large and homogeneous AGN samples over a big redshift range ($z = 0 - 6$) (see e.g. Kennefick et al., 1995; Schmidt et al., 1995; Koehler et al., 1997; Grazian et al., 2000; Fan et al., 2001b; Wolf et al., 2003; Hunt et al., 2004; Cristiani et al., 2004; Croom et al., 2005; Richards et al., 2005, 2006; Siana et al., 2007; Fontanot et al., 2007; Shankar & Mathur, 2007; Bongiorno et al., 2007). Moreover, a great deal of information on the X-ray and infrared properties of AGN has become available, and surveys with e.g. *ROSAT*, *XMM*, *Chandra* and *Spitzer* have enabled studies of the AGN LF across many frequencies (see e.g. Brown et al., 2006; Matute et al., 2006; Babbedge et al., 2006; Barger et al., 2003a; Ueda et al., 2003; Barger et al., 2003b; Nandra et al., 2005; Sazonov & Revnivtsev, 2004; Silverman et al., 2005a; La Franca et al., 2005; Shinozaki et al., 2006; Beckmann et al., 2006; Hao et al., 2005; Nagar et al., 2005).

Many interesting trends have emerged from these studies. For instance, several authors found that the space density of low luminosity AGN peaks at redshifts lower than that of bright ones, following a similar pattern of the so-called “cosmic downsizing”, recently observed in galaxy spheroidal populations (see, e.g. Cowie et al., 1996; Cimatti et al., 2006, and references therein). However, inferences drawn from the observed trends suffer from complications arising from various biases, so that a correction is required to account for possible incompleteness effects, which includes the possible existence of a population of obscured AGN whose fraction may depend on the wavelength band and redshift (Elvis et al., 1994; Marconi et al., 2004; La Franca et al., 2005; Lamastra et al., 2006). Indeed, although optical surveys provide the largest AGN samples so far, they include almost exclusively

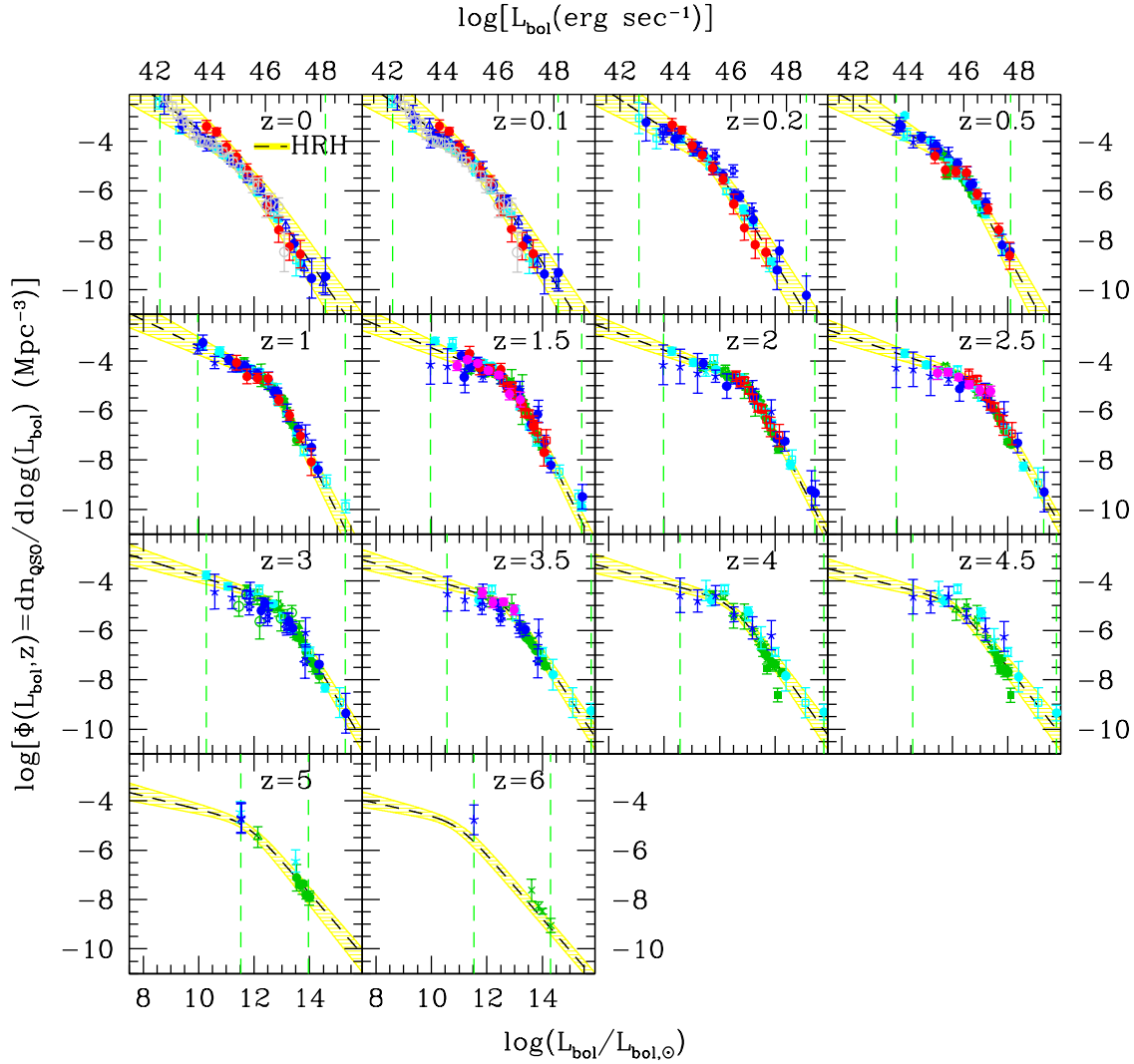


Figure 1.8: The bolometric LF by H07 (yellow areas), compared with several observed binned LFs: Ueda et al. (2003) (filled blue circles), Silverman et al. (2005a) (blue stars), Barger et al. (2003a,b) (skeletal blue pentagons), Nandra et al. (2005) (open blue circles), Sazonov & Revnivtsev (2004) (open blue triangles), Hao et al. (2005) (open grey circles), Hasinger et al. (2005) (filled cyan circles), Silverman et al. (2005b) (skeletal cyan pentagons), Bongiorno et al. (2007) (filled magenta circles), Richards et al. (2005) (open green squares), Richards et al. (2006) (filled green circles), Wolf et al. (2003) (green stars), Hunt et al. (2004) (open green circles), Cristiani et al. (2004) (open green triangles), Kennefick et al. (1995) (filled green squares), Schmidt et al. (1995) (skeletal green pentagons), Fan et al. (2001b,a, 2003, 2004) (skeletal green squares), Matute et al. (2006) (filled red circles), Brown et al. (2006) (open red squares), Miyaji et al. (2000, 2001) (open cyan squares), Siana et al. (2007) (filled green triangles). The green vertical lines mark the luminosity range covered by the data.

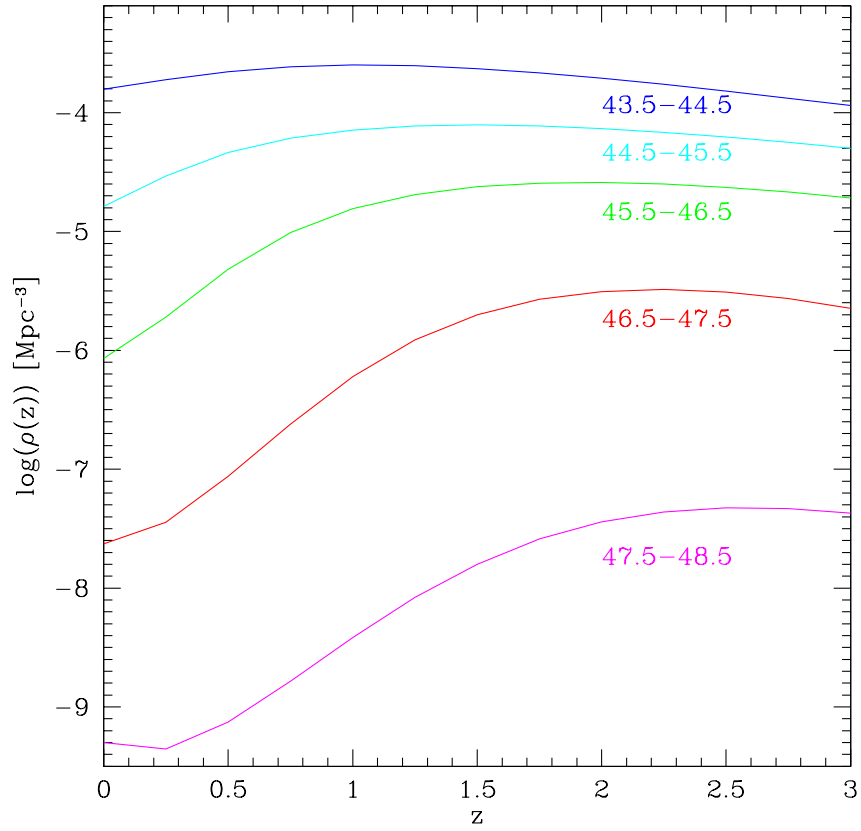


Figure 1.9: Total number density of AGN in various luminosity intervals [in $\log(L_{\text{bol}}/(\text{ergs}^{-1}))$ as labeled] as a function of redshift, from the best-fit evolving double power-law model by H07.

unobscured-type 1 objects. Obscured-type 2 AGN may instead be efficiently selected using X-ray observations, especially in the hard band, where the nuclear radiation is less affected by absorption. Moreover, a very efficient way to sample the obscured AGN population is through mid- and far-infrared surveys, since the nuclear UV radiation absorbed by the obscuring medium is expected to be re-emitted at longer wavelengths. Based on the synthesis models for the X-ray background (see e.g. Comastri et al., 1995; Gilli et al., 2001; Ueda et al., 2003), obscured AGN are believed to be a factor of $\gtrsim 4$ more abundant than unobscured ones and should therefore dominate the whole AGN population. Furthermore, theoretical models generally predict the total (bolometric) luminosity of an AGN catalogue, and to compare model LFs with observations it is necessary to specify a bolometric correction, i.e. how to convert the luminosities observed in a particular band into bolometric ones (Elvis et al., 1994; Marconi et al., 2004; Hopkins et al., 2007e).

Hopkins et al. (2007e) [H07] combined several measurements of the AGN LF in many wavelengths from the mid-IR through hard X-rays, to determine the observed bolometric AGN LF in the redshift interval $z = 1 - 6$ and for bolometric luminosities in the range $\sim 10^{41} - 10^{49} \text{ erg s}^{-1}$. In order to fit the data at a fixed redshift, H07 used a double power law parametrization:

$$\Phi(L) = \frac{\Phi_*}{(L/L_*)^{\gamma_1} + (L/L_*)^{\gamma_2}}, \quad (1.5)$$

with normalization Φ_* , break luminosity L_* , faint-end slope γ_1 , and bright-end slope γ_2 . To characterize the AGN LF as a function of redshift, a “modified” pure luminosity evolution model was adopted, where L_* evolves as a cubic polynomial in redshift,

$$\log L_* = (\log L_*)_0 + k_{L,1} \xi + k_{L,2} \xi^2 + k_{L,3} \xi^3, \quad (1.6)$$

with

$$\begin{aligned} \xi &= \log \left(\frac{1+z}{1+z_{\text{ref}}} \right), \\ \gamma_1 &= (\gamma_1)_0 \cdot 10^{k_{\gamma_1} \xi}, \\ \gamma_2 &= (\gamma_2)_0 \cdot 2 \left(10^{k_{\gamma_2,1} \xi} + 10^{k_{\gamma_2,2} \xi} \right)^{-1}. \end{aligned} \quad (1.7)$$

The best-fit parameters in the above equation are: $\log \Phi_* = -4.825 \pm 0.060$, $(\log \Phi_*)_0 = 13.036 \pm 0.043$, $k_{L,1} = 0.632 \pm 0.077$, $k_{L,2} = -11.76 \pm 0.38$, $k_{L,3} = -14.25 \pm 0.80$, $(\gamma_1)_0 = 0.417 \pm 0.055$, $k_{\gamma_1} = -0.623 \pm 0.132$, $(\gamma_2)_0 = 2.174 \pm 0.055$, $k_{\gamma_2,1} = 1.460 \pm 0.096$ and $k_{\gamma_2,2} = -0.793 \pm 0.057$. This bolometric LF is plotted in Figure 1.8 with yellow areas, compared with several observed binned LFs: Ueda

et al. (2003) (filled blue circles), Silverman et al. (2005a) (blue stars), Barger et al. (2003a,b) (skeletal blue pentagons), Nandra et al. (2005) (open blue circles), Sazonov & Revnivtsev (2004) (open blue triangles), Hao et al. (2005) (open grey circles), Hasinger et al. (2005) (filled cyan circles), Silverman et al. (2005b) (skeletal cyan pentagons), Bongiorno et al. (2007) (filled magenta circles), Richards et al. (2005) (open green squares), Richards et al. (2006) (filled green circles), Wolf et al. (2003) (green stars), Hunt et al. (2004) (open green circles), Cristiani et al. (2004) (open green triangles), Kennefick et al. (1995) (filled green squares), Schmidt et al. (1995) (skeletal green pentagons), Fan et al. (2001b,a, 2003, 2004) (skeletal green squares), Matute et al. (2006) (filled red circles), Brown et al. (2006) (open red squares), Miyaji et al. (2000, 2001) (open cyan squares), Siana et al. (2007) (filled green triangles). The total number density of AGN in various luminosity intervals as a function of redshift (i.e. the integral of the AGN LF) for the same model is shown in Figure 1.9. The trend that the density of lower-luminosity AGN peaks at lower redshift is manifest.

1.1.5 AGN number count

The AGN number count, $N_{\text{AGN}}(> S)$, is defined as the comoving number density of AGN above a minimum flux S :

$$N_{\text{AGN}}(> S) = \int_{z_{\min}}^{z_{\max}} dz \int_{L_{\text{bol},\min}(z,S)}^{L_{\text{bol},\max}} d \log L_{\text{bol}} \phi(L_{\text{bol}}, z) \frac{d^2 V}{dz d\Omega}, \quad (1.8)$$

where L_{bol} is the AGN bolometric luminosity, $\phi(L_{\text{bol}}, z)$ is the AGN LF and $d^2 V / (dz d\Omega)$ is the comoving volume in solid angle Ω and redshift interval dz . The AGN number count is a very useful testbed to constrain the AGN evolution at redshifts larger and luminosities fainter than those directly probed by the observations. AGN surveys can be either wide-field, covering a large area but reaching relatively bright limiting fluxes, or pencil-beam over very small areas but reaching the faintest possible flux limits, like the ones performed by Chandra, namely the 2 Ms Chandra Deep Field North [CDFN] and the 1 Ms Chandra Deep Field South [CDFS]. As an example of the latter case, Bauer et al. (2004) investigated the X-ray number counts in the two Chandra Deep Fields, separating the X-ray sources into AGN, star-forming galaxies, and Galactic stars. They found that AGN dominate the number counts in the 0.5-2.0 keV and 2-8 keV bands, while the number counts of star-forming galaxies climb steeply such they will likely overtake the number of AGN below $\sim 1 \times 10^{-17} \text{ erg cm}^{-2} \text{ s}^{-1}$ (0.5-2.0 keV) and dominate the overall number counts at fainter fluxes. AGN as a whole contribute $\sim 83\%$ and $\sim 95\%$

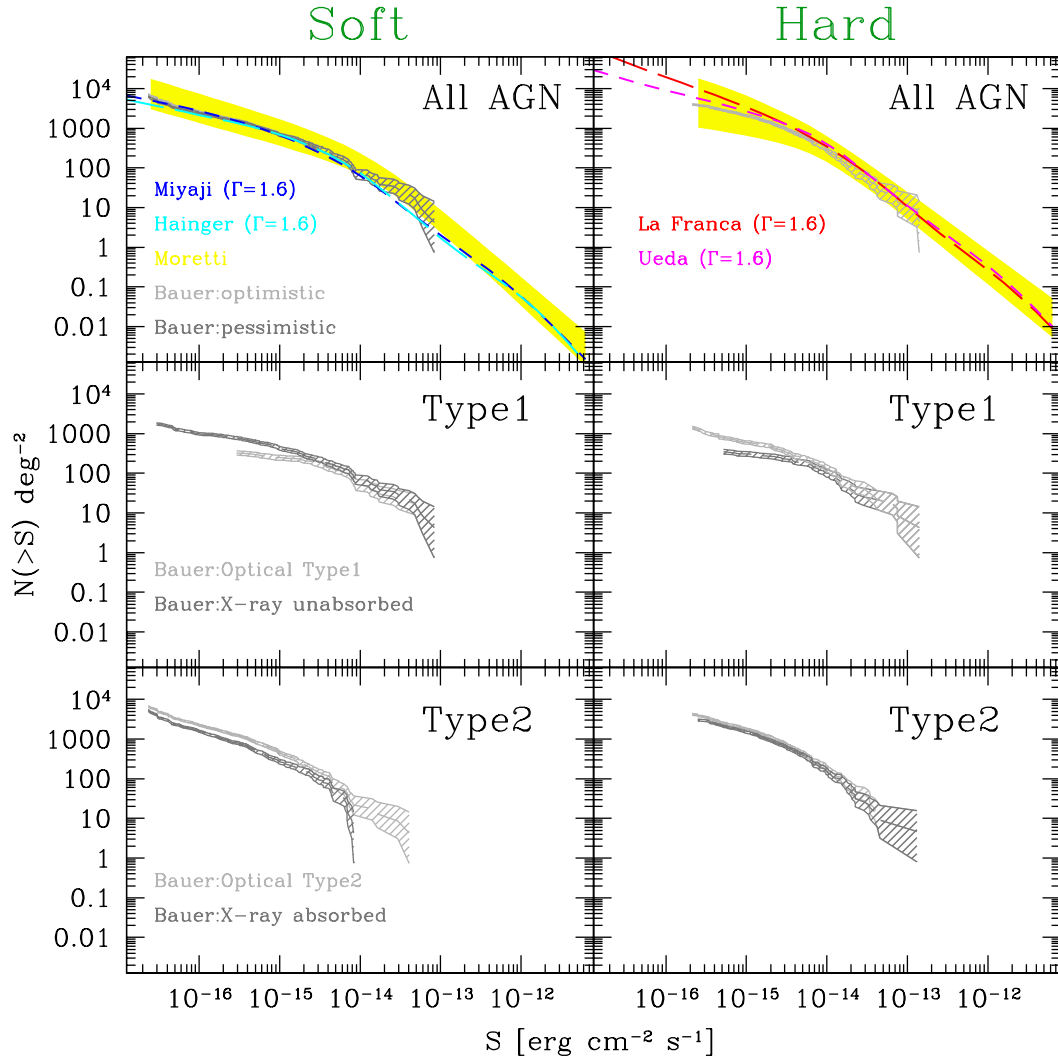


Figure 1.10: The AGN number count derived by Moretti et al. (2003) (yellow shaded areas), Bauer et al. (2004) (grey shaded areas) and by integrating the AGN LFs of Miyaji et al. (2001) (blue), Hasinger et al. (2005) (cyan), Ueda et al. (2003) (magenta) and La Franca et al. (2005) (red), through Eq. (1.8). The left (right) three panels show the AGN number count in the soft (hard) X-ray band.

to the the resolved X-Ray background fractions in the soft and hard X-ray band, while star-forming galaxies comprise only $\sim 3\%$ and $\sim 2\%$, respectively, and Galactic stars comprise the remainder.

Undoubtedly, it is very useful, when possible, to combine together data from different surveys, both wide-field and pencil-beam ones. Moretti et al. (2003) compiled a large source catalogue of this kind, including six surveys performed with three different satellites (ROSAT, Chandra and XMM-Newton). Such a big sample covers the largest possible flux range so far: $[2.4 \times 10^{-17} - 10^{-11}] \text{ergs}^{-1} \text{cm}^{-2}$ in the soft band and $[2.1 \times 10^{-16} - 8 \times 10^{-12}] \text{ergs}^{-1} \text{cm}^{-2}$ in the hard band. The measured X-ray source number counts in two energy bands (0.5-2 and 2-10 keV) revealed that the $94.3^{+7.0}_{-6.7}\%$ and $88.8^{+7.8}_{-6.6}\%$ of the soft and hard cosmic X-Ray background can be ascribed to discrete source emission. More recently, the constraints on the number counts have been extended to lower sensitivities by fluctuation analyses of the unresolved 0.5-8 keV cosmic X-ray background by Hickox & Markevitch (2006), who analyzed observations in Chandra Deep Fields North and South. The AGN number count by Moretti et al. (2003) is shown in the two upper panel of Figure 1.10 as yellow shaded areas, for the soft and hard band, respectively (left and right panels). In the same Figure, the grey areas are the pessimistic and optimistic AGN number counts obtained by Bauer et al. (2004) with two different selection criteria, which basically mark the region of uncertainty. Finally, the dashed lines in the upper panels show the AGN number count derived integrating the AGN LFs of Miyaji et al. (2001) (blue), Hasinger et al. (2005) (cyan), Ueda et al. (2003) (magenta) and La Franca et al. (2005) (red), through the Eq. (1.8).

1.1.6 AGN clustering

Given a generic ensemble of objects, the two-point correlation function, $\xi(r)$, is defined as the excess probability of finding a pair with one object in the volume dV_1 and the other in the volume dV_2 , separated by a distance r (see e.g. Peebles, 1980):

$$dP = n^2 [1 + \xi(r)] dV_1 dV_2. \quad (1.9)$$

This function represents one of the most simple and widely used statistics to measure the clustering properties of observed AGN samples. Alternatively, the AGN spatial clustering can also be quantified by means of the angular correlation function or by the AGN biasing function, the latter is defined in several different ways. Here we take the biasing function b as the ratio between the spatial two-point correlation function of AGN and DM:

$b^2 := \xi_{AGN}/\xi_{DM}$. The AGN clustering measurements are of fundamental importance, since they can be used to constrain the range of AGN lifetimes. In fact, if AGN are long-lived sources, then they are rare phenomena that are highly biased with respect to the underlying DM, while if they are short-lived they have to reside in more typical haloes that are less strongly clustered.

From an observational point of view, to quantify the AGN clustering it is convenient to start by computing the two-point correlation function in the redshift space, $\xi(r_{\perp}, \pi)$, which measures the excess probability over random to find an AGN pair separated by π along the line of sight and by r_{\perp} in the plane of the sky. First, it is necessary to build a catalogue of unclustered points with the same angular and radial selection function of the data. Then the AGN correlation function can be estimated by comparing the probability distribution of AGN and random pairs on a two-dimensional grid of separations (r_{\perp}, π) . Between the several estimators proposed to derive this quantity, the most widely used and statistically accurate are the ones by Landy & Szalay (1993):

$$\xi_{LS} = \frac{DD - 2DR + RR}{RR}, \quad (1.10)$$

and by Hamilton (1993):

$$\xi_H = \frac{DD \cdot RR}{(DR)^2} - 1, \quad (1.11)$$

where DD , DR and RR are the suitably normalised numbers of weighted data-data, data-random and random-random pairs in each radial bin, respectively.

The separations (r_{\perp}, π) are generally derived from the redshift and the angular position of each source, so that the inferred π includes a contribution from peculiar velocities. Consequently, the reconstructed clustering pattern in comoving space comes out to be a distorted representation of the real one and $\xi^{\text{obs}}(r_{\perp}, \pi)$ is found to be anisotropic. To correct for the redshift space distortions, it is convenient to determine the clustering amplitude in real space. This can be done through the computation of the *projected correlation function*, which is obtained by integrating $\xi(r_{\perp}, \pi)$ in the π direction:

$$\frac{\Xi(r_{\perp})}{r_{\perp}} = \frac{2}{r_{\perp}} \int_0^{\infty} \xi(r_{\perp}, \pi) d\pi. \quad (1.12)$$

Generally, it is assumed that the AGN two-point correlation function scales as

$$\xi(r) = \left(\frac{r_0}{r}\right)^{\gamma}, \quad (1.13)$$

where r denotes the comoving separation between AGN pairs. The corresponding projected correlation function (Eq. 1.12) is related to $\xi(r)$

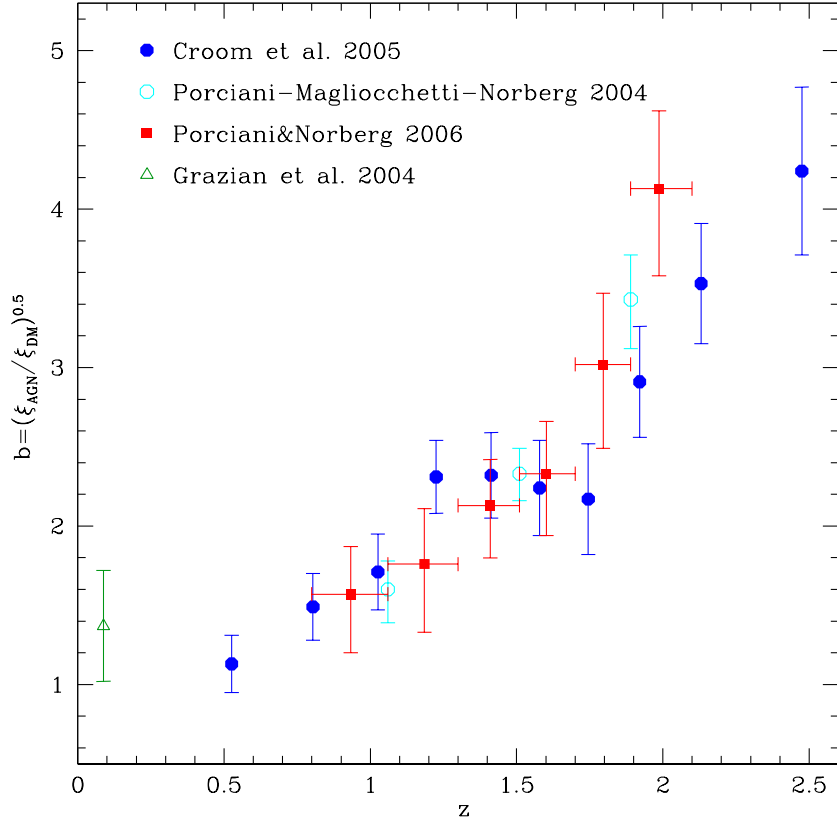


Figure 1.11: AGN biasing function for optically selected AGN samples, as indicated by the label.

through the following integral relation:

$$\Xi(r_{\perp}) = 2 \int_{r_{\perp}}^{\infty} \frac{r \xi(r)}{(r^2 - r_{\perp}^2)^{1/2}} dr, \quad (1.14)$$

which, in the power-law case, reduces to:

$$\frac{\Xi(r_{\perp})}{r_{\perp}} = \frac{\Gamma(1/2)\Gamma[(\gamma-1)/2]}{\Gamma(\gamma/2)} \left(\frac{r_0}{r_{\perp}}\right)^{\gamma} \quad (1.15)$$

with $\Gamma(x)$ representing the Euler's Gamma function.

In recent years, wide-field surveys such as the 2QZ and the SDSS, already mentioned in the previous sections, have enabled tight measurements of the AGN clustering up to redshift $z \sim 3$. For instance, Porciani et al. (2004) presented clustering measurements from the 2QZ in the redshift range $0.8 < z < 2.1$. Using a flux-limited sample of ~ 14000 AGN with effective redshift $z_{\text{eff}} = 1.47$, they found that the two-point correlation function in real space is well approximated by a power law with slope $\gamma = 1.5 \pm 0.2$ and

comoving correlation length $r_0 = 4.8_{-1.5}^{+0.9} h^{-1} \text{Mpc}$. They also found evidence for an increase of the clustering amplitude with look-back time. The ratio between the AGN correlation function and the mass autocorrelation function (derived adopting the concordance cosmological model) was found to be scale-independent, consistent with a constant biasing function. The derived bias parameter as a function of redshift is shown in Figure 1.11 with open cyan dots. These data imply that the characteristic mass of the 2QZ AGN host haloes is of the order of $10^{13} M_{\odot}$, and that the characteristic AGN lifetime is $t_Q \sim \text{a few} \times 10^7 \text{ yr}$ at $z \sim 1$ and approaches 10^8 yr at higher redshifts. In the same Figure, the red squares show the AGN biasing function obtained by Porciani & Norberg (2006) from an improved analysis of the same AGN catalogue. The blue dots show the biasing function derived by Croom et al. (2005) using over 20000 AGN from the final catalogue of the 2QZ, in the redshift range $0.3 < z < 2.2$. Finally, the green triangle is the result of Grazian et al. (2004) who used spectroscopic data for 392 AGN in the Asiago-ESO/RASS QSO Survey to infer the AGN bias at $0.02 < z < 0.22$.

Observational studies on the spatial clustering of X-ray selected AGN has been limited by the lack of sizeable samples of optically identified X-ray sources. To derive this function, Gilli et al. (2005) used the two deepest X-ray fields to date, i.e. the CDFN and the CDFS. The amplitude of the correlation was found to be significantly different in the two fields, the correlation length r_0 being $8.6 \pm 1.2 h^{-1} \text{Mpc}$ in the CDFS and $4.2 \pm 0.4 h^{-1} \text{Mpc}$ in the CDFN, while the correlation slope γ was found to be flat in both fields: $\gamma = 1.33 \pm 0.11$ in the CDFS and $\gamma = 1.42 \pm 0.07$ in the CDFN. The observed difference does not seem to be produced by any observational bias, and is therefore likely due to cosmic variance. The correlation function has also been measured separately for sources classified as type 1 AGN, type 2 AGN and galaxies. The results are shown in Figure 1.12.

The luminosity dependence of the AGN clustering would provide a direct probe to discriminate between different theoretical models of the BH growth. However, the data uncertainties are still too large to achieve a coherent picture of how AGN biasing depends on luminosity and different authors have found discrepant results. For example, Porciani & Norberg (2006) found that models with luminosity-dependent clustering are statistically favoured at the 95 per cent confidence level for $z > 1.3$, that might be expected if more luminous AGN inhabited more massive haloes. Instead, Adelberger & Steidel (2005) measured the galaxy-quasar cross correlation function, finding no evidence for luminosity-dependent clustering, in analogy with the outcomes of Croom et al. (2005). On the theoretical side, Lidz et al. (2006) demonstrated

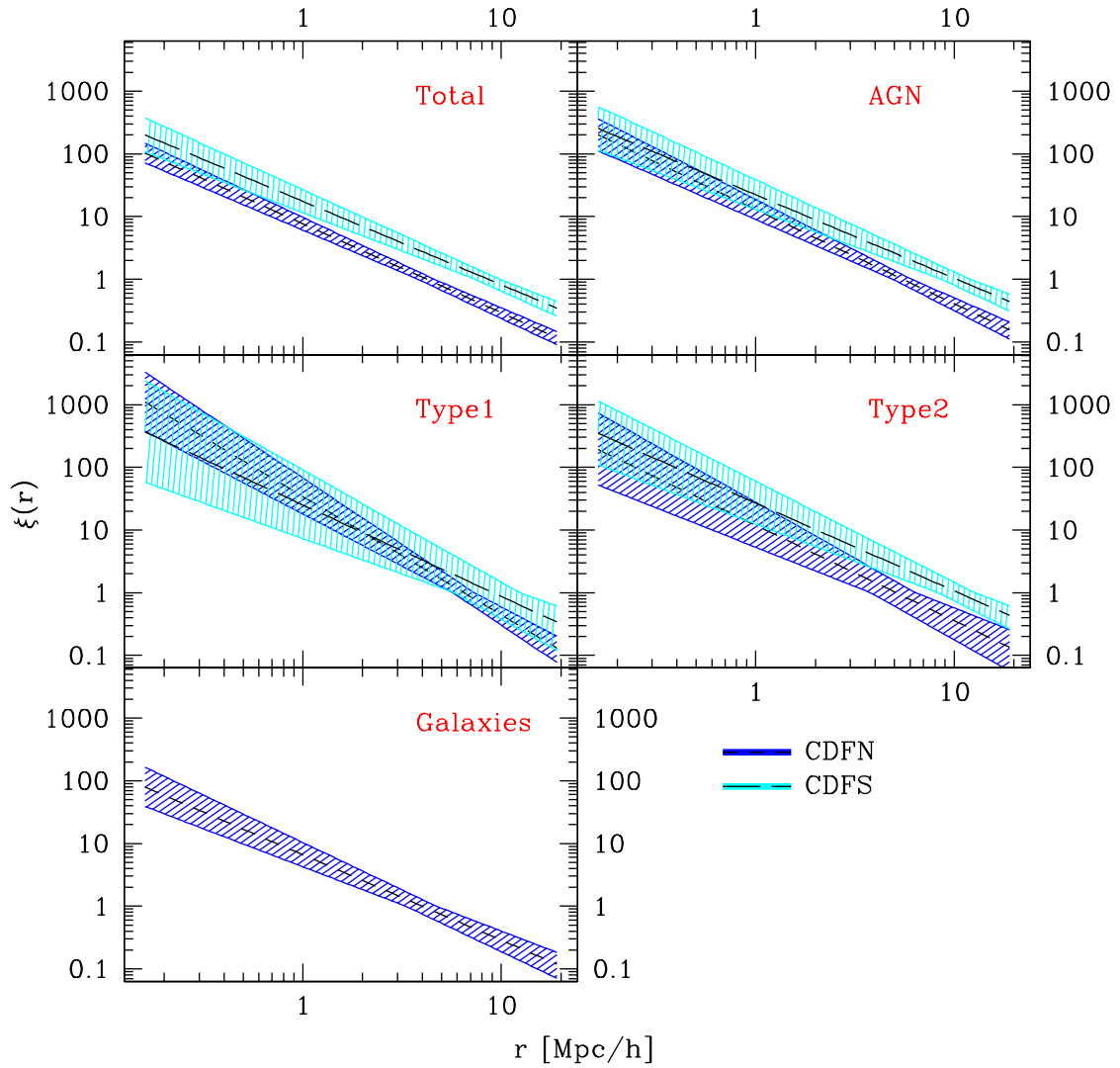


Figure 1.12: The best fitting relations corresponding to the AGN spatial two-point correlation function in real space derived by Gilli et al. (2005) in the two X-ray fields CDFN and CDFS.

that AGN light-curve and life-time models like those of Hopkins et al. (2006a) predict a relatively flat AGN bias as a function of luminosity.

SECTION 1.2

Theory

1.2.1

 General features

The Concordance Cosmological Model, generally called Λ CDM model (where Λ represents the cosmological constant, and CDM is the acronym for Cold Dark Matter) , has become so popular thanks to its ability in simultaneously matching a large number of observational data, like the microwave background fluctuations (Spergel et al., 2003, 2007), the power spectrum of the low-redshift galaxy distribution (Percival et al., 2002; Tegmark et al., 2004), the non-linear mass distribution at low redshifts as characterized by cosmic shear (Van Waerbeke et al., 2002), the structure seen in the Ly α forest (Mandelbaum et al., 2003), the present acceleration of the cosmic expansion derived from supernova observations (Perlmutter et al., 1999; Riess et al., 1998), the mass budget inferred for the present Universe from the dynamics of large-scale structure (Peacock et al., 2001), the baryon fraction in rich clusters (White et al., 1993) and the theory of the Big Bang nucleosynthesis (Olive et al., 2000). Such an extraordinary success is, however, not enough to assure that this model describes the correct picture of our Universe, since we do not have yet any direct evidence of both the dark matter and the dark energy, which are key ingredients to the Λ CDM model. Yet, among the many proposed alternative models, the Λ CDM is currently preferred because of its simplicity and widely used to describe the formation and evolution of galaxies, that in such a framework grow hierarchically through multiple episodes of accretion and mergers. Although not yet in agreement with all the observations available, theoretical models developed within the Λ CDM model can describe very well the overall properties of the galaxy population observed in the local Universe and at high redshifts. Since BHs and AGN evolve strongly in time, in a similar way as their hosting galaxies and DM haloes, it is of great interest to investigate whether the properties of these objects can be described within the Λ CDM framework. Alternatively, we can wonder what kind of assumptions we have to adopt if we want to account for the BH and AGN observations within the Λ CDM paradigm.

Mergers of galaxies are very common phenomena in the Λ CDM scenario, especially at high redshifts, and provide a natural mechanism for powering AGN. Indeed mergers between gas-rich galaxies can drive nuclear inflows of gas, triggering starbursts and fueling the growth of the BHs located at the galaxy centres (see e.g. Toomre & Toomre, 1972; Toomre, 1977; Mihos & Hernquist, 1994; Hernquist & Mihos, 1995; Cox, 2004; Hopkins et al., 2005). The BH growth is mainly driven by the gas supply and is quenched as gas is expelled by the AGN feedback. Such a self-regulated growth mechanism triggered by mergers can explain the observed BH scaling relations, described in Section 1.1.1 (Di Matteo et al., 2005), as well as the colour distribution of ellipticals (Springel et al., 2005d). Indeed, it is believed that during most of the BH mass accretion history, AGN activity is highly obscured, but once a BH dominates the energetics of the central region, feedback expels gas and dust, making the BH visible briefly as a bright AGN. Eventually, as the gas is further heated and expelled, AGN activity can no longer be maintained and the merger remnant relaxes to a normal galaxy. The remnant will then evolve passively and would be available as a seed to repeat the above cycle. As the Universe evolves and more gas is consumed, the mergers involving gas-rich galaxies will shift towards lower masses, which would explain the decline of the brightest quasars population from $z \sim 2$ to the present. The remnants that are gas-poor will redden quickly owing to the termination of star formation by BH feedback, so that they resemble elliptical galaxies surrounded by hot X-ray emitting haloes (see e.g. Cox et al., 2006). Several observations seem to support the above scenario, at least at high redshifts and high AGN luminosities. We will come back to this point in detail in Section 3.3, when we will discuss the predictions of our semi-analytic models of AGN evolution.

1.2.2 Theoretical methods

In order to describe the cosmological co-evolution of BHs, AGN and galaxies in the Λ CDM scenario, several models have been developed based on analytic, semi-analytical or hybrid techniques. All the models of the first kind developed so far are based on two simplifying hypotheses: i) the formation and evolution of DM haloes hosting galaxies and BHs can be described within the Press-Schechter model and its extensions [EPS] (Press & Schechter, 1974; Bond et al., 1991; Lacey & Cole, 1993); and ii) the BH growth is directly linked to the evolution of their host DM haloes, either via their formation rate or their merging rate. Their predictive power is limited since they cannot be used to investigate the connection between the evolution of galaxies and the accretion

history of BHs. The semi-analytic (hybrid) methods consist in coupling Monte Carlo techniques (N-body simulations) to derive the DM halo evolution together with analytic equations that describe the evolution of the baryonic matter. Present computational capabilities allow to use reliable numerical simulations to study the evolution of both DM and baryons, at least on the scales which determine the global properties of galaxies. However, once gas cools and is driven into halo cores, both its structure and the rates at which it turns into stars and possibly accretes onto the central BH are determined by physical processes occurring on scale below numerical resolution. These are so treated through semi-analytic recipes, i.e. parameteric equations which encapsulate the “subgrid” physics. Since the gas properties on larger scale are strongly affected by such small scale phenomena, every modification of a semi-analytic prescription requires the simulation to be repeated. A less time-consuming alternative is to describe the behaviour of the diffuse gas also by semi-analytic recipes. Since the DM couples to baryons only through gravity, its distribution on the scale of galactic haloes and beyond is only weakly affected by the details of galaxy formation. As a consequence, the evolution can be simulated only once via numerical techniques, and the evolution of the baryonic component of the DM component can be included in post-processing by applying semi-analytic models to the recorded histories of all DM objects (Kauffmann et al., 1999). This second step is computationally cheap, so that the available resources can be used to carry out the best possible numerical simulation of the DM component, and then several parameter studies or tests of alternative models can be carried out in post-processing.

In the following, we will briefly summarize the main aspects and results of the most interesting and powerful models developed so far, while the models by Wyithe & Loeb (2002), Wyithe & Loeb (2002), Volonteri et al. (2003a) and Croton et al. (2006), that have been extensively applied in this Thesis, will be described in details in the next chapters.

Efstathiou & Rees (1988) developed a simple analytic method to investigate the relationship between high-redshift quasars and the epoch of galaxy formation in the Λ CDM model. They assumed that luminous quasars could only form after galactic-sized systems had collapsed and that these sources are short-lived, radiating at about the Eddington limit. According to their model, the comoving density of luminous quasars is almost constant in the redshift range $z = 2 - 4$, but declines exponentially at higher redshifts.

Similarly, Haehnelt & Rees (1993) proposed a model in which quasars are assumed to be short-lived objects, constituting the first phase of the formation of a galaxy in the potential well of a DM halo. The timelag between halo

virialization and the birth of the quasar was assumed to be short compared to the cosmological time-scale, even at high redshifts. Simple assumptions were made to relate the luminosity of a quasar to the mass of its central BH and to the mass of its corresponding host halo.

Both these models could reproduce the optical AGN LF determinations available at that time. In the following years, Haiman & Loeb (1998) and Haiman & Menou (2000) derived the evolution of the quasar LF at fainter luminosities and higher redshifts based the assumptions that the ratio of central BH mass to halo mass is the same for all haloes, and that the light curve of quasars, in Eddington units, is universal. By extrapolating the evolution of their LF to high redshifts, they found that the associated early population of low-luminosity quasars could reionize the Universe at a redshift $z \sim 12$. In the local Universe, the accretion rate drops to substantially sub-Eddington values at which advection-dominated accretion flows (ADAFs) can be supposedly be sustained. This could explain both the absence of bright quasars in the local Universe and the faintness of accreting BHs at the centres of nearby galaxies.

Percival & Miller (1999) calculated the merger rate of the DM haloes using the Press-Schechter theory and showed that a simple merging-halo model can account for the bulk of the observed evolution of the comoving quasar space density.

Using the Mo & White (1996) model for the clustering of DM haloes to relate halo properties to the quasar lifetime, Martini & Weinberg (2001) calculated the minimum host halo mass by matching the observed space density of quasars, and derived a quasar lifetime of $t_Q = 4 \cdot 10^7$ yr.

With the aim of improving the previous models, Hatziminaoglou et al. (2003) proposed a new analytic model based on the assumption that the parallel growth of BHs and host galaxies is triggered by major mergers of haloes. The BH evolution was predicted by integrating a set of differential equations derived from few assumptions used to describe the accretion regime, ranging from Eddington-limited to supply-limited. The typical quasar light curves were obtained under the assumption that the fall of matter onto the BH occurs in a self-regulated stationary way. The predicted optical quasar LF is in good agreement with the observed one, but only for $z \gtrsim 1$.

To solve the problems encountered at low redshifts and faint luminosities, Hopkins & Hernquist (2006) developed an analytic model for the fueling of Seyferts (low-luminosity AGN), using a simple description of feedback from BH growth, with which they could derive a solution for the time evolution of accretion rates in presence of a feedback-driven blast wave. This model

provides a quantitative and physically motivated distinction between local, low-luminosity quiescent AGN activity and violent, merger-driven bright quasars. Its predictions agree very well with several observations in the local Universe, like the Seyfert LF, the duty cycles and AGN lifetimes, and the distribution of the galaxy host morphologies.

As a final example of the analytic method, we mention the recent work of Miller et al. (2006), who tested the simple hypothesis that the BH growth tracks directly the DM halo growth, by using a new theoretical determination of the halo merging rate. They demonstrated that both the absolute value of the integrated AGN bolometric luminosity density and its cosmological evolution derived from hard X-ray surveys are well-reproduced by this assumption. Excellent agreement is found at $z \gtrsim 0.5$, although the observed luminosity density drops by a factor 2 compared with the model by $z = 0$: the BH growth appears to decouple from halo growth at low redshifts.

Moving on to the description of the semi-analytic approach, Kauffmann & Haehnelt (2000) incorporated a simple scheme for the BH growth into semi-analytic models that follow the formation and evolution of galaxies. The most important assumption of their model is that the BHs are formed and fuelled during major galaxy mergers. In this way, they could not only fit many aspects of the observed evolution of galaxies, but also the observed scaling relation between bulge luminosity and BH mass in nearby galaxies, the strong evolution of the quasar population with redshift, and the relation between the luminosities of nearby quasars and those of their host galaxies. In this scenario, the strong decline in the number density of AGN from $z \sim 2$ to $z = 0$ is due to a combination of three different effects: (i) the decrease in the galaxy merging rate; (ii) the decrease in the amount of cold gas available to fuel BHs, and (iii) the increase in the time-scale for gas accretion (see also Springel et al., 2005a).

With a similar approach and analogous assumptions, Enoki et al. (2003) showed that the spatial distribution of galaxies is different from that of quasars, and that at $0.2 \lesssim z \lesssim 0.5$ most quasars are likely to reside in galaxy groups. On the other hand, at $1 \lesssim z \lesssim 2$ most quasars seem to reside in environments ranging from small groups of galaxies to clusters of galaxies.

Granato et al. (2004) demonstrated that the more massive protogalaxies virializing at earlier times are the sites of the faster star formation. The correspondingly higher radiation drag accelerates the angular momentum loss of the gas, resulting in a larger accretion rate onto the central BHs. However, the kinetic energy carried away by AGN-driven outflows driven by the AGN can unbind the residual gas, thus halting both the star formation

and the BH growth.

Cattaneo et al. (2005) assumed that the BH growth is linked to the starburst activity in galaxies and demonstrated that, if the BH accretion rate and the star formation rate in the starburst component are proportional to each other, the cosmic evolution of the quasar population is not reproduced. Instead, if $\dot{M}_\bullet \propto \rho_{\text{burst}}^\zeta \dot{M}_{*\text{burst}}$, where ρ_{burst} is the density of the gas in the starburst and $\zeta \simeq 0.5$, the evolution of the quasar LF in B-band and X-rays can be well described. In this scenario, for a given bulge mass, the most massive BHs are in the bulges with the oldest stars.

Malbon et al. (2007) showed that, while the direct accretion of cold gas during starbursts is an important growth mechanism for lower mass BHs and at high redshifts, the re-assembly of pre-existing BH mass into larger units via BH merging dominates the growth of more massive BHs at low redshift, a prediction which could be tested by future gravitational wave experiments. As redshift decreases, they predicted that progressively less massive BHs have the highest fractional growth rates, in line with recent claims of downsizing in quasar activity.

Also Fontanot et al. (2006) found that it is possible to reproduce the downsizing of AGN within the Λ CDM model. In particular, they proposed that one of the most relevant causes of this downsizing is the stellar kinetic feedback that arises in star-forming bulges as a consequence of the high level of turbulence.

Very recently, thanks to the high computational power reached in the last years, also fully numerical cosmological models have become possible. Li et al. (2007) demonstrated the ability of the Λ CDM model in matching the recent discovery of luminous quasars at redshift $z \sim 6$, which indicates the presence of BHs of mass $\sim 10^9 M_\odot$ when the Universe was less than 1 billion years old. They used a new multiscale technique that, together with a self-regulated model for the BH growth, produced a luminous quasar at $z \sim 6.5$, after several major mergers of galaxies. The gas is accreted below the Eddington limit in a self-regulated manner owing to feedback, and the merger remnant obeys a similar $M_{\text{BH}} - M_{\text{bulge}}$ scaling relation as observed locally. However, in their work it was assumed that BHs would undergo growth at the Eddington rate, preceding the time of major mergers at $z \sim 7 - 12$. This isolated critical growth phase implies masses $\sim 10^5 M_\odot$ at the beginning of the major merger phase. Furthermore, they used fully assembled galaxy models as their initial conditions, thus not following the assembly of galaxies and their BHs self-consistently.

Different results have been found by Pelupessy et al. (2007), who did not

impose a critical Eddington growth phase, but instead attempted to assess the detailed BH accretion history using a smooth-particle hydrodynamic simulations with a self-consistent treatment of star formation, BH accretion, and associated feedback processes. They found that BH seeds in haloes with masses $\lesssim 10^{11}M_{\odot}$ never reach the conditions for critical Eddington growth. The growth reaches the Eddington rate at late times only for haloes of $M_{\text{halo}} \gtrsim 10^{11}M_{\odot}$. Due the limited time spent in an Eddington growth phase, it seems difficult to explain in this scenario the occurrence of the $z \sim 6$ SDSS quasars.

With hydrodynamic simulations of cosmological structure formation, Di Matteo et al. (2007) self-consistently followed the DM dynamics, radiative gas cooling, star formation, BH growth and associated feedback processes, starting directly from initial conditions appropriate for the Λ CDM cosmology. Their predictions agree very well with the local BH mass density, and BH scaling relations (with a weak evolution with redshift in the normalization and the slope). The BH accretion rate density peaks at lower redshift and evolves more strongly at high redshift than the star formation rate density, but the ratio of BH to stellar mass densities shows only a moderate evolution at low redshifts. Interestingly, this simulation also produce massive BHs at high redshift, due to extended periods of exponential growth in regions that collapse early and exhibit strong gas inflows.

CHAPTER 2

Analytic models: dark matter + black holes



In this chapter, we investigate the ability of hierarchical analytic models for AGN formation and evolution to match the observed luminosity, number counts and spatial clustering of AGN at redshift $z < 2$. We find that models based on simple analytic approximations successfully reproduce the observed B-band AGN luminosity function at all redshifts, provided that some mechanism is advocated to quench mass accretion within haloes larger than $\sim 10^{13} M_{\odot}$. These models also match the observed strength of AGN clustering at $z \sim 0.8$, while at larger redshifts they significantly underpredict it. The chapter is mainly based on “Modelling the quasi-stellar object luminosity and spatial clustering at low redshifts”, Marulli et al. (2006).

We start our study by implementing and improving the two analytic models proposed by Wyithe & Loeb (2002) [WL02] and Wyithe & Loeb (2003) [WL03], which can be considered as representative examples of the large set of analytic models of the cosmological evolution of BHs and AGN developed so far. Our aim is to complement these previous works by investigating the ability of such models to match the observed luminosity, number counts and spatial clustering of AGN at redshift $z < 2$.

Both the models assume the following hypotheses: i) the evolution history of DM halo fully determines the overall properties of the BH and AGN populations, i.e. we do not need to know any detail about the cosmological evolution of the baryonic matter to predict the properties of the BHs hosted in their centres, ii) the AGN emission is triggered only by DM halo mergers, iii) all AGN shine at their Eddington luminosity, and iv) the mass of central BHs correlates with the host DM halo mass at all redshifts. As we will demonstrate in the next sections of this Thesis, the first three assumptions are satisfactory only at $z \gtrsim 2$ (i.e. in the redshift range of interest of the original WL02 and

WL03 models), while there is not yet any observational evidence to justify the hypothesis iv), as the observed scaling relations between BHs and DM haloes have been derived only in the local Universe.

Regardless these considerations, as we will describe in detail in the following sections, we found that such models successfully reproduce the observed B -band AGN LF at $z < 2$, provided that some mechanisms is advocated to quench mass accretion within haloes larger than $\sim 10^{13}M_{\odot}$. These models also match the observed strength of AGN clustering at $z \sim 0.8$. At larger redshifts, however, they strongly underpredict it, a problem not solvable inside this simple framework, if with the same set of parameters we want to match the observed AGN LF as well.

This chapter is organized as follows. In Sections 2.1 and 2.2, we will briefly summarize the main aspects of the original WL02 and WL03 models. In section 2.3, we will compare the model predictions with observations and introduce some modification to the original models to better match the observed LF. Finally, in section 2.4 we will discuss our results and draw our first conclusions.

Throughout this chapter and the next one, we will assume a flat Λ CDM cosmological model with Hubble constant $h \equiv H_0/100 \text{ km s}^{-1} \text{ Mpc}^{-1} = 0.7$, a dominant contribution to the density parameter from the cosmological constant, $\Omega_{\Lambda} = 0.7$, and a CDM density power spectrum with primordial spectral index $n = 1$ and normalized by assuming $\sigma_8 = 0.9$.

SECTION 2.1

The WL02 model

The WL02 model describes the AGN evolution within the standard framework of hierarchical structure formation. It is a fully analytic model and only the evolution of DM is followed.

Unlike the original idea of Haiman & Loeb (1998) to associate the AGN activity directly to the formation of DM haloes, the WL02 model assumes that the AGN phenomenon is triggered by halo-halo mergers. As mentioned in Section 1.2.1, both hydrodynamical simulations of galaxy mergers and the recent observations of interacting galaxies strongly support the view that mergers between gas-rich galaxies of similar masses are the main triggering mechanisms for the mass accretion onto the BHs in the galaxy centres. Actually, considering galaxy rather than halo mergers (and neglecting the

difference between gas-rich and gas-free mergers) could lead to different predictions, as it is not always true that a merger of two DM haloes will result in a merger of their galaxies, and viceversa (see, e.g. Wang & Kauffmann, 2008). However, a galaxy-merger-driven scenario can only be self-consistently implemented within the framework of a full semi-analytic or numerical model of galaxy formation and evolution. This is beyond the scope of this section in which, instead, the main target is to minimise the number of free parameters, focusing only on the fundamental aspects of the problem. Moreover, fully analytic methods cannot self-consistently follow the formation and evolution of DM substructures. For these reasons, the WL02 model can only be used to describe BHs and AGN hosted inside DM haloes with masses low enough that it is unlikely to find galaxy-side substructures within (i.e. before galaxies assemble into groups and clusters) and where the assumed one-to-one relation between halo and galaxy mergers is reasonably justified.

Another crucial assumption of the model is that the mass of the BH powering the AGN, M_{BH} , is a fraction, \mathcal{F} , of the host halo mass, M_{halo} , at all redshifts. However, at the present time there is not yet any strong observational evidence to support this idea, since almost all the observational data available concern BH hosted in local galaxies (see e.g. Ferrarese, 2002; Baes et al., 2003; Ferrarese & Ford, 2005; Shankar et al., 2006), and the situation at $z > 0$ is still very unclear, as discussed in Section 1.1.1.

Finally, it is assumed that, after a merging event, the AGN shines at the Eddington luminosity, $L_{\text{Edd}} = M_{\text{BH}}(t)c^2/t_{\text{Edd}}$ (where $t_{\text{Edd}} = \sigma_T c / (4\pi m_p G) \sim 0.45 \text{ Gyr}$) with a universal light curve, $f(t)$. Actually, this assumption is justified only at high redshifts (see e.g. Shankar et al., 2004), as several observations revealed that on average f_{Edd} (defined in Section sec:BHMF) seems to be smaller than unity for low redshift AGN (see e.g. McLure & Dunlop, 2002; Merloni et al., 2003; Merloni, 2004a, and reference therein).

With the above assumptions, the B -band AGN luminosity can be related to M_{BH} and M_{halo} through $f(t)$:

$$L_B(t) = M_{\text{BH}}f(t) = \mathcal{F}M_{\text{halo}}f(t) \quad \text{for} \quad M_{\text{halo}} > M_{\text{min}}, \quad (2.1)$$

where $M_{\text{min}} \sim 10^8 [(1+z)/10]^{-3/2} M_{\odot}$, the minimum halo mass inside which a BH can form, corresponds to the virial temperature below which atomic cooling is not effective in allowing the gas to sink to the centre (Barkana & Loeb, 2001). The AGN number density can be obtained by multiplying the number of haloes with mass between ΔM_{halo} and $\Delta M_{\text{halo}} + d\Delta M_{\text{halo}}$ that accrete onto a halo of mass $M_{\text{halo}} - \Delta M_{\text{halo}}$ per unit time by the number density of haloes in

the same mass range:

$$I(M_{\text{halo}}, \Delta M_{\text{halo}}) \equiv \left. \frac{dN(M, z)}{dM} \right|_{M=M_{\text{halo}}-\Delta M_{\text{halo}}} \times \left. \frac{d^2 N_{\text{merge}}}{d\Delta M_{\text{halo}} dt} \right|_{M=M_{\text{halo}}-\Delta M_{\text{halo}}}. \quad (2.2)$$

The quantities $d^2 N_{\text{merge}}/d\Delta M_{\text{halo}} dt$ and $dN(M, z)/dM$ represent the DM halo merging rate and mass function, respectively. To derive them we use the EPS formalism (Lacey & Cole, 1993; Sheth & Tormen, 1999), as in the original WL02 model.

Assuming that the scaling relation between the BH mass and the circular velocity of the host DM halo, v_c , observed by Ferrarese (2002) in the local Universe is valid at all redshifts, we can write:

$$M_{\text{BH}} \propto v_c^\gamma = (159.4)^\gamma \left(\frac{M_{\text{halo}}}{10^{12} h^{-1} M_\odot} \right)^{\gamma/3} \left(\frac{\Omega_m(0)}{\Omega_m(z)} \frac{\Delta_c}{18\pi^2} \right)^{\gamma/6} (1+z)^{\gamma/2}, \quad (2.3)$$

where the second equality follows from the relation between v_c and M_{halo} (Barkana & Loeb, 2001) in which $\Delta_c(z) = 18\pi^2 + 82d - 39d^2$, $d \equiv \Omega_m(z) - 1$ and $\Omega_m(z)$ represents the matter density parameter at a given redshift z . From eqs.(2.1) and (2.3):

$$\mathcal{F} = \mathcal{F}_0 \left(\frac{M_{\text{halo}}}{10^{12} M_\odot} \right)^{\gamma/3-1} \left(\frac{\Omega_m(0)}{\Omega_m(z)} \frac{\Delta_c}{18\pi^2} \right)^{\gamma/6} h^{\gamma/3} (1+z)^{\gamma/2}. \quad (2.4)$$

Finally, we assume that the AGN luminosity curve is given by a simple step function

$$f(t) = \frac{L_{\text{Edd},B}}{M_{\text{BH}}} \theta \left(\frac{\Delta M_{\text{halo}}}{M_{\text{halo}}} t_{dc,0} - t \right), \quad (2.5)$$

where $t_{dc,0} \ll H^{-1}(z)$ is the time of AGN duty cycle at $z=0$.

Eqs.(2.3), (2.4) and (2.5) allow us to compute the AGN LF:

$$\begin{aligned} \Phi(L_B, z) = & \int_{\mathcal{F}_{\text{min}}}^{\infty} dM_{\text{BH}} \int_0^{0.5\mathcal{F}M_{\text{halo}}} d\Delta M_{\text{BH}} \int_z^{\infty} dz' \left. \frac{dN_{\text{bh}}}{dM} \right|_{M=M_{\text{BH}}-\Delta M_{\text{BH}}} \\ & \times \left. \frac{d^2 N_{\text{merge}}}{d\Delta M_{\text{BH}} dt} \right|_{M=M_{\text{BH}}-\Delta M_{\text{BH}}} \frac{dt'}{dz'} \delta[L_B - M_{\text{BH}} f(t_z - t')], \quad (2.6) \end{aligned}$$

that, once integrated over M_{BH} , has an analytic expression that depends on the three free parameters $t_{dc,0}$, \mathcal{F}_0 and γ :

$$\Phi(L_B, z) = \int_0^{0.5M_{\text{halo}}} d\Delta M_{\text{halo}} \frac{3}{\gamma \mathcal{F}} \frac{t_{dc,0}}{5.7 \times 10^3} \frac{\Delta M_{\text{halo}}}{M_{\text{halo}}} I(M_{\text{halo}}, \Delta M_{\text{halo}}), \quad (2.7)$$

where $M_{\text{halo}} = L_{\text{Edd},B}/(5.7 \times 10^3 \mathcal{F} L_{\odot,B}) M_\odot$.

The connection between AGN luminosity and halo mass in our model, $L_B(M_{\text{halo}})$, and the existence of analytic models that describe the spatial clustering of DM haloes (see, e.g. Mo & White, 1996; Sheth & Tormen, 1999)

allow us to investigate also the spatial correlation properties for AGN. In particular, we can compute the AGN-to-mass luminosity-weighted biasing parameter, $b(z)$:

$$b(z) = \frac{\int_{L_{B,\min}}^{\infty} b(L_B(M_{\text{halo}}), z) \Phi(L_B, z) dL_B}{\int_{L_{\min,B}}^{\infty} \Phi(L_B, z) dL_B}, \quad (2.8)$$

where $\Phi(L_B, z)$ is the AGN LF in Eq.(2.7) and $L_{B,\min}$ is the luminosity of the faintest object in the sample. The quantity $b(L_B(M_{\text{halo}}), z)$ represents the biasing parameter of a halo with mass M_{halo} hosting an AGN of luminosity L_B at the redshift z , that has been computed by Sheth & Tormen (1999):

$$b(L_B(M_{\text{halo}}), z) = 1 + \frac{1}{\delta_c(0)} \left[\frac{a\delta_c^2(z)}{\sigma_M^2} - 1 \right] + \frac{2p}{\delta_c(0)} \left(\frac{1}{1 + [\sqrt{a}\delta_c(z)/\sigma_M]^{2p}} \right), \quad (2.9)$$

in the previous relation $a = 0.707$, $p = 0.3$, $\delta_c(z)$ is the critical threshold on the linear overdensity for spherical collapse at redshift z and σ_M^2 is the rms linear density variance smoothed with a ‘top-hat’ filter corresponding to the mass M . Eq.(2.8) provides us with an analytic expression for $b(z)$. It assumes a univocal relation between AGN luminosity and halo mass, or, in other words, that the probability of finding an AGN of a given luminosity L_B in a halo of mass M_{halo} depends on M_{halo} only.

SECTION 2.2

The WL03 model

WL03 extended the WL02 model to include feedback-limited BH growth. A self-regulated accretion mechanism is the natural outcome of the production of powerful gas winds that interrupt the infall of gas on the BH after halo mergers. Self-regulation takes place when the energy in the outflow equals the gravitational binding energy in a dynamical time (Silk & Rees, 1998). WL03 assumed that, after a merger event, a BH shines at a fraction f_{Edd} of its Eddington luminosity (previously defined in Section 1.1.3), returning a fraction F_q of this energy to the galactic gas. The self-regulation condition can be written as:

$$\begin{aligned} f_{\text{Edd}} L_{\text{Edd},\odot} M_{\text{BH}} F_q &= \frac{\varepsilon \delta M_{\text{BH}} c^2}{t_{\text{dyn}}} F_q \\ &= \frac{\frac{1}{2} \frac{\Omega_b}{\Omega_m} M_{\text{halo}} v_c^2}{t_{\text{dyn}}}, \end{aligned} \quad (2.10)$$

where δM_{BH} is the mass accreted, $L_{\text{Edd},\odot}$ is the Eddington luminosity per unit mass (M_{\odot}) and ε is the mean radiative efficiency of the accreting material. As appropriate only at high redshifts, Eq.(2.10) assumes that all gas within a galactic halo cools on a time much shorter than the Hubble time, and it implies $M_{\text{BH}} \propto v_c^5$, irrespective of the redshift.

Assuming that the gas is located in a disk with characteristic radius $\sim 0.035 r_{\text{vir}}$, it can be demonstrated that the dynamical time t_{dyn} is given by

$$t_{\text{dyn}} = 0.035 \frac{r_{\text{vir}}}{v_c} = \frac{3.64 \times 10^7}{h} \left(\frac{\Omega_m(0)}{\Omega_m(z)} \frac{\Delta_c}{18\pi^2} \right)^{-1/2} \times (1+z)^{-3/2} \text{yr}, \quad (2.11)$$

and represents the AGN duty cycle: $t_{dc} = t_{\text{dyn}}$. The major merger condition has been introduced to guarantee that the dynamical friction time-scale (Binney & Tremaine, 1987) for the satellite is shorter than a Hubble time. For this reason WL03 only considered mergers between haloes with a mass ratio $P \equiv \Delta M_{\text{halo}}/M_{\text{halo}} > 0.25$. As a consequence, the model LF can be expressed as

$$\Phi(L_B, z) = \int_{0.25M_{\text{halo}}}^{0.5M_{\text{halo}}} d\Delta M_{\text{halo}} \frac{3}{\gamma \mathcal{F}} \frac{t_{\text{dyn}}}{5.7 \times 10^3} I(M_{\text{halo}}, \Delta M_{\text{halo}}). \quad (2.12)$$

Differently from the WL02 model, now the AGN LF depends on only two free parameters: \mathcal{F}_0 and γ . The model biasing function can be computed as for the WL02 model, using the Eq.(2.8).

SECTION 2.3

Models vs. observations

2.3.1 AGN optical luminosity function

WL02 demonstrated that their model fits the AGN LF at $z \sim 2 - 3$, it reproduces the normalization and logarithmic slope at $z \sim 4$ and it explains the space density of bright SDSS quasars at $z \sim 6$. WL03 found similar results for their newer model, demonstrating that it matches the observed evolution in the number density of optically bright or X-ray faint quasars with $2 \lesssim z \lesssim 6$, across 3 orders of magnitude in bolometric luminosity and 3 orders of magnitude in comoving density per logarithm of luminosity. Here we aim at complementing their work by comparing the predictions of both the WL02 and WL03 models to the observed optical AGN LF at $z < 2$ and, in the next section, to the AGN biasing function in the redshift range $z \sim 1 - 2$.

We compare the model predictions to the observed AGN LF computed by Croom et al. (2004) [C04] by merging the 2QZ catalogue, containing objects with an apparent b_j magnitude $18.25 < b_j < 20.85$, with the 6dF QSO Redshift Survey [6QZ] of bright ($16 < b_j < 18.25$) quasars. The full sample includes 23660 quasars in a wide redshift range ($0.3 < z < 2.9$) and spread over 721.6 deg^2 on the sky. The 2QZ/6QZ catalogue is affected by various types of incompleteness described in details by C04 that need to be accounted for in order to minimize systematic effects. The optical AGN LF has been computed from a subsample of 15830 AGN brighter than $M_{b_j} = 22.5$ in the redshift range $0.4 < z < 2.1$. The cut in absolute magnitude guarantees a minimum spectroscopic sector completeness of at least 70 per cent, while redshift constraints ensure a photometric completeness of 85 per cent. The LF has been evaluated into $\delta M_{b_j} = 0.5$ bins in absolute magnitude using the $1/V$ estimator of Page & Carrera (2000) into six equally spaced, independent redshift bins. The filled black dots in the six panels of Fig. 2.1 show this AGN LF in the different redshift intervals indicated in each plot (see Section 1.1.4 for more details about the observational estimates of the AGN LF).

Given the background cosmology, the WL02 model predictions are fully specified by the set of three parameters: $(\gamma, \mathcal{F}_0, t_{dc,0})$. Here we explore two separate cases. The first one, which is slightly different from the one considered in the original WL02 paper (and labeled WL02A in Figs. 2.1 and 2.2), uses the parameters $(\gamma = 4.71, \mathcal{F}_0 = 10^{-5.1}, t_{dc,0} = 10^{6.3} \text{ yr})$. The first two chosen values represent the best fit to the observations of Ferrarese (2002), while the latter, which corresponds to a value of $t_{dc}(z = 3) = 10^{6.9} \text{ yr}$ at $z \sim 3$, is fully consistent with the lifetime of bright AGN, $t_{dc}(z \simeq 3) = 10^7 \text{ yr}$, inferred from the sample of Lyman-break galaxies of Steidel et al. (2002). The predicted AGN LF, plotted as short-dashed magenta lines in Fig. 2.1, fails to match the observed LF both in the bright and the faint ends. This result is similar to the one originally obtained by WL02 using the set of parameters $(\gamma = 5.0, \mathcal{F}_0 = 10^{-5.4}, t_{dc,0} = 10^{6.3} \text{ yr})$, that constitutes their best fit to the data they considered. Since the overall amplitude of the model LF (Eq. 2.7) linearly depends on γ^{-1} , \mathcal{F}_0^{-1} and $t_{dc,0}$, it is quite straightforward to boost up the model LF to match the number density of the observed AGN. For example, fixing the values of $\gamma = 4.71$, $\mathcal{F}_0 = 10^{-5.1}$, and leaving $t_{dc,0}$ as a free parameter, we find a best fit for $t_{dc,0} = 10^{7.2} \text{ yr}$. The resulting model, labeled WL02B, is shown in Fig. 2.1 as dot-dashed red lines. This duty-cycle is very large and some *ad hoc* modifications to the WL02 model would be required to satisfy the high-redshift constraints of Steidel et al. (2002). The WL02B LF matches the observed one at low luminosities, but it overpredicts the number density

of bright AGN, especially at low redshifts.

Let us now compare the WL03 model predictions to the observations. The first model we have explored is the one by WL03 corresponding to the choice of parameters ($\gamma = 5.0$, $\mathcal{F}_0 = 10^{-5.7}$), still consistent with the observational data of Ferrarese (2002). The model LF (labeled WL03 and plotted with solid green lines in Fig. 2.1) is very similar to that of WL02B, but has the advantage of having a physically, well motivated AGN duty-cycle. The discrepancy the observed LF can be accounted for by modifying the WL03 model. One possibility is to allow for a major merger threshold P that depends on M_{halo} . As we have checked, it is indeed possible to find some suitable function $P(M_{\text{halo}})$ monotonically increasing with M_{halo} that allows to match both the faint and bright ends of the observed AGN LF. While this is somewhat an *ad hoc* solution, a more physically plausible modification has been proposed by WL03 themselves and consists of assuming that accretion onto BH is hampered by the high temperature of the gas within group/cluster-size haloes. WL03 proposed that accretion onto the central BH should be prevented within haloes of masses larger than $10^{13.5}M_{\odot}$, corresponding to a $L \sim 2 \times 10^{13}L_{\odot,B}$ at $z \simeq 1$. We have made a similar assumption and proposed that the accretion efficiency decreases above a given critical halo mass resulting in a modified relation between L_{AGN} and M_{halo} :

$$L_{\text{AGN}} = \tilde{L}(1 - \exp(-(L^*/\tilde{L})^k)) . \quad (2.13)$$

In the previous equation $\tilde{L} = 5.7 \times 10^3 \mathcal{F}(M_{\text{halo}}/M_{\odot})$ is the B -band Eddington luminosity of the original WL03 model and L^* is the Eddington luminosity of a halo with critical mass M_{halo}^* . Both k and M_{halo}^* can be treated as free parameters. The long-dashed blue lines in Fig. 2.1 show the effect of keeping $k = 0.77$ while leaving M_{halo}^* as a free parameter, whose value is indicated in the plots. The LF predicted by the model (labeled WL03k) provides a good match to the observed one at all redshifts, except for very bright objects at low redshifts. The resulting values of M_{halo}^* range between $10^{12.9}$ and $10^{13.4}M_{\odot}$ which constitute plausible values, close to those proposed by WL03. Leaving also k as a free parameter does not improve significantly the agreement with the observational data and a best fit value close to $k = 0.77$ is found at all redshifts. We have also tried to use the model WL03 without the restriction to major mergers, but it has resulted inconsistent with the data by several orders of magnitude and we have decided not to show it.

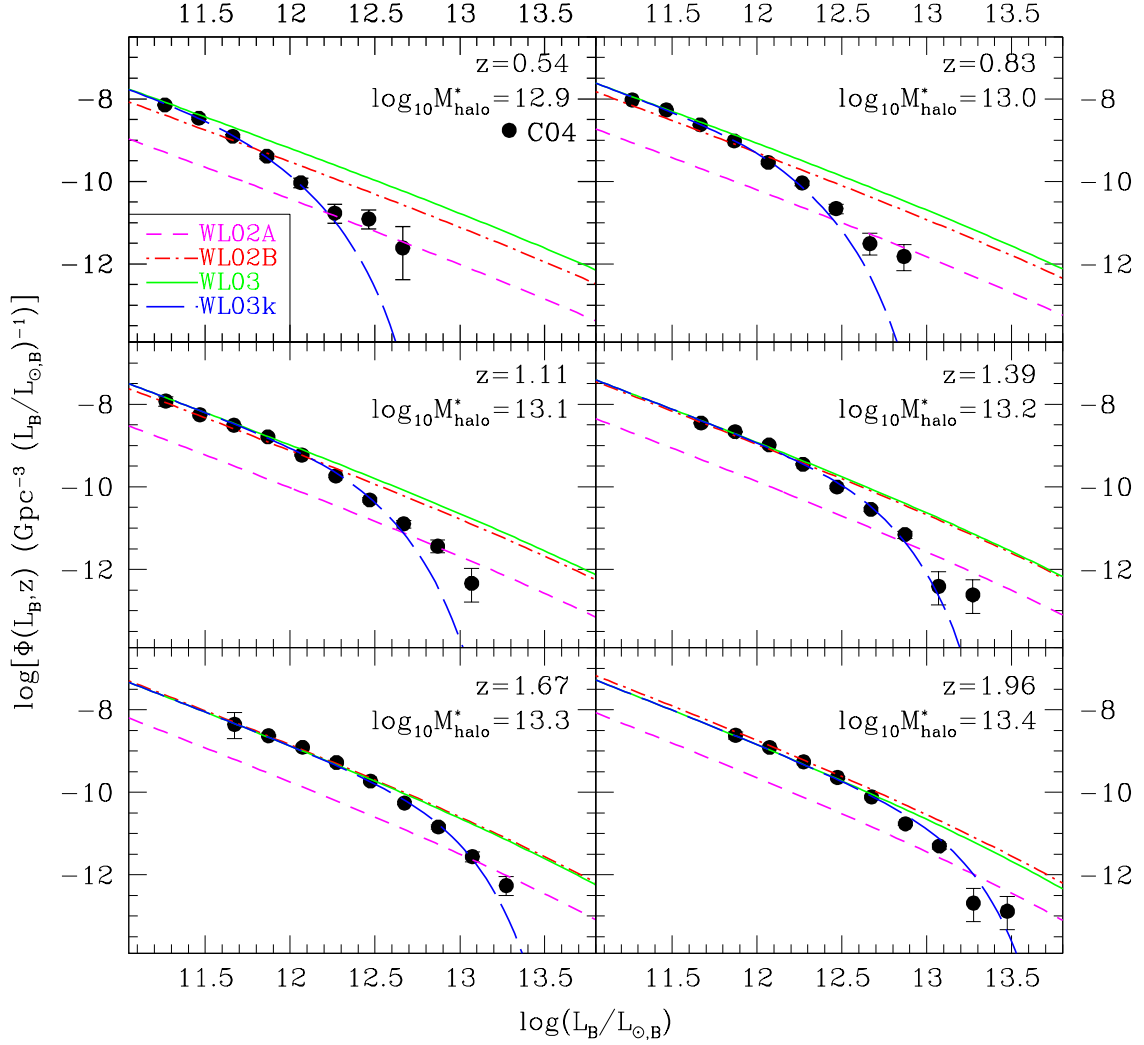


Figure 2.1: The AGN LF in B -band at six different redshifts: models vs. observations. The filled black circles show the 2dF/6dF AGN LF measured by C04 together with their 1σ error bars. The short-dashed (magenta) and dot-dashed (red) lines show the WL02 model predictions obtained by setting $(\gamma = 4.71, \mathcal{F}_0 = 10^{-5.1}, t_{dc,0} = 10^{6.3}\text{yr})$ (label: WL02A) and $(\gamma = 4.71, \mathcal{F}_0 = 10^{-5.1}, t_{dc,0} = 10^{7.2}\text{yr})$ (label: WL02B), respectively. The solid green line shows the WL03 model predictions obtained for $(\gamma = 5.0, \mathcal{F}_0 = 10^{-5.7})$, while the long-dashed blue line (label: WL03k) represents the same model with an exponential cut in the luminosity-mass relation as in Eq.(2.13), with $k = 0.77$ and M_{halo}^* indicated in the plots.

2.3.2 AGN biasing function

The biasing functions predicted by the WL02 and WL03 models are shown in Fig. 2.2 and compared to the data by Porciani et al. (2004) [PMN]. PMN have estimated the AGN two-point spatial correlation function of ~ 14000 2QZ/6QZ AGN with redshift $0.8 < z < 2.1$ in three different redshift intervals $[0.8, 1.3]$, $[1.3, 1.7]$ and $[1.7, 2.1]$. The three subsamples with median redshifts $z_{\text{eff}} = 1.06, 1.51, 1.89$ contain ~ 4300 , ~ 4700 and ~ 4900 objects, respectively. The more conservative cut in redshift and the use of these three redshift intervals guarantee (i) a photometric completeness larger than 90 per cent, (ii) a similar number of AGN in each redshift bin and (iii) that each subsample covers a similar interval of cosmic time. PMN have found that the AGN biasing function is almost independent of the projected separation between AGN and thus it is possible to characterize the AGN spatial correlation properties at z_{eff} using a single ‘bias’ parameter $b(z_{\text{eff}})$. The results of the PMN analysis are presented in Fig. 2.2, where the filled dots show the value of $b(z_{\text{eff}})$ for the 2dF/6dF AGN at three different redshifts, together with their 1σ uncertainty. The AGN-to-mass bias parameter $b(z_{\text{eff}})$ increases with redshift, in quantitative agreement with the results of several similar analyses (see Sect. 1.1.6 for more details).

The line-styles for our models are the same as in Fig. 2.1. All the models predict the same amount and evolution of AGN biasing: at $z = 1.06$, AGN are mildly biased with respect to the underlying mass, marginally consistent with observations, while their clustering at $z = 1.89$ is significantly less than observed.

SECTION 2.4

Discussion

In this chapter we have demonstrated that only minor, physically-motivated modifications to the original WL02 and WL03 models are required to match the observed AGN LF at redshifts as small as ~ 0.5 . More profound modifications seem to be required for a successful modeling of the very local AGN LF.

Previous studies have shown that analytic and semi-analytic models well reproduce the observed AGN LF at high redshifts. At low redshifts, however, these methods systematically overpredict the number density of bright objects; a mismatch that becomes increasingly large when decreasing

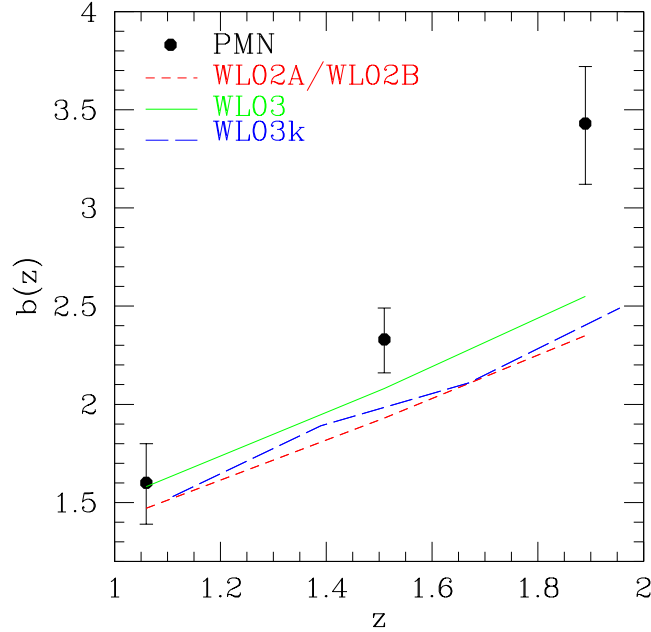


Figure 2.2: The mean AGN-to-mass biasing parameter, $b(z_{\text{eff}})$ estimated at three effective redshifts $z = 1.06$, $z = 1.51$ and $z = 1.89$: models vs. observations. The filled circles show the mean biasing of 2dF/6dF AGN measured by PMN with the associated 1σ uncertainties. Line styles are as in Fig. 2.1.

the redshift. Since the gas accretion is expected to be inefficient within large haloes due to the high temperature of the baryons, we have proposed a simple modification to the original WL03 models, namely that the accretion efficiency decreases above a given critical halo mass. Such a prescription significantly improves the fit to the bright end of the AGN LF, though some discrepancies still remain, especially at very low redshifts.

We have also shown that all the models considered here predict a moderate degree of AGN clustering at low redshift, consistent with the observations. However, at higher redshifts ($z \sim 2$) the AGN biasing appears to be significantly smaller than that of 2QZ/6QZ AGN. The only way for reproducing the observed degree of clustering would be to increase the normalization constant \mathcal{F} in the $M_{\text{BH}} - v_c^\gamma$ relation (Wyithe & Loeb, 2005a), which, however, would overpredict the AGN number density in the local Universe.

In summary, we have shown that simple models in which the AGN activity is triggered by DM halo mergers within the framework of hierarchical build-up of cosmic structures can quantitatively describe the observed evolution of the AGN number counts and luminosity at all but very low

redshifts, provided that some mechanisms are advocated to inhibit accretion within massive haloes hosting bright AGN. However, these models cannot reproduce the observed redshift evolution of the AGN bias. It is worth stressing that the hierarchical models for AGN evolution and the possible modifications discussed so far rely on two important assumptions which have recently been cast into doubt. First of all, the models considered in this work assume a simple relation between AGN activity and the mass of its hosting halo. However, Wyithe & Loeb (2005b) pointed out that the tight relation between the BH mass and the velocity dispersion of the spheroid implies that it is the spheroid rather than the halo which determines the growth of the BHs and the subsequent AGN activity. As a consequence, the observed correlation between the halo and BH masses should not be regarded as fundamental as it merely reflects the fact that massive haloes preferentially host bulges with large velocity dispersions. This would imply that AGN activity, closely related to the evolution of bulges, should be studied using the more sophisticated models for galaxy formation and evolution. The second and more important issue is related to the results of the recent Millennium Simulation (Springel et al., 2005a). The analyses performed by Gao et al. (2005) and by Harker et al. (2006) have shown that the spatial correlation properties and the formation epochs of the haloes depend on the local overdensity. This effect, which is particularly evident for galaxy-sized haloes, contradicts one of the basic assumption of the EPS theory. It is not clear, however, how serious the implications are for galaxy/AGN formation models and for halo models of clustering. In case they are and in absence of a generalized EPS theory capable of accounting for environmental effects (see, however, Abbas & Sheth, 2005; Shen et al., 2005), then the only way out would be that of resorting to halo merger histories extracted from numerical experiments that implicitly account for environmental dependencies (see, e.g. Lemson & Kauffmann, 1999). We will pursue this strategy in Chapter 4.

CHAPTER 3

Semi-analytic models: dark matter + black holes

E consider simple semi-analytic models that relate the AGN evolution to the merging history of their host DM haloes and quantify their ability of matching the AGN luminosity function and its spatial clustering at low and intermediate redshifts. While we find an acceptable agreement between the model bolometric luminosity function and the data at $1 \lesssim z \leq 2$ and for luminosities larger than $10^{10} L_{\text{bol},\odot}$, no semi-analytic model is capable of reproducing the number density of faint X-ray sources in the local Universe. Some improvement can be obtained by advocating energy feedback that we model through a time-dependent Eddington ratio. Even in this case, however, the number density of faint AGN is significantly below observations. This failure indicates that major mergers cannot constitute the only trigger to accretion episodes in the local AGN population. The chapter is mainly based on two published works: “Modelling the quasi-stellar object luminosity and spatial clustering at low redshifts”, by Marulli *et al.* (2006), and “Modeling active galactic nuclei: ongoing problems for the faint-end of the luminosity function”, by Marulli *et al.* (2007).

Similarly to the analytic models discussed in the previous chapter, semi-analytic approaches to the evolution of AGN in a hierarchical scenario generally assume some relation between AGN and DM haloes properties. However, they differ from analytic modeling since the evolution of DM haloes and of the BHs within them are treated separately. The merging history of DM haloes is described by the EPS formalism. Phenomenological relations are used to model the physical processes leading to the AGN evolution. It is therefore possible to adopt a more detailed description of the physics involving the baryonic component of cosmic structures, including BHs. A second advantage of the semi-analytic approach is the flexibility of the scheme, so that different astrophysical prescriptions can be tested within the same framework of cosmic evolution of DM haloes.

The outline of this chapter is as follows. In first section we will present the semi-analytic models considered in this work and summarize the main assumptions used therein. In Section 3.2 we will compare model predictions to the observed AGN luminosity and biasing function. Finally, in the last section we will discuss our results and draw our main conclusions.

SECTION 3.1

The VHM model

In this chapter we focus on the semi-analytic model developed by Volonteri, Haardt & Madau (2003) [VHM] that describes the hierarchical assembly, evolution and dynamics of the BHs powering AGN (see also Volonteri et al., 2003b; Madau et al., 2004; Volonteri & Rees, 2005). Like WL02 and WL03, VHM also assume that: (i) the observed correlation between BH masses and circular velocity (Ferrarese, 2002) justifies the assumption of a link between AGN activity and haloes' properties and constitutes a constraint to the semi-analytic model at $z = 0$, and that (ii) the cosmological evolution of DM haloes is well described by the EPS theory. Moreover, like in the WL03 case, they further assume that (iii) the AGN activity is triggered only by DM halo major mergers.

The numerical implementation of the semi-analytic model consists of a two-step procedure. The first step is aimed at constructing a set of halo merging histories using the EPS theory. In the EPS formalism, when one takes a small step δz back in time, the number of progenitors a parent halo of mass M_0 at $z = z_0$ fragments into is (Lacey & Cole, 1993):

$$\frac{dN}{dM}(z = z_0) = \frac{1}{\sqrt{2\pi}} \frac{M_0}{M} \frac{1}{S^{3/2}} \frac{d\delta_c}{dz} \frac{d\sigma_M^2}{dM} \delta z, \quad (3.1)$$

where $S \equiv \sigma_M^2(z) - \sigma_{M_0}^2(z_0)$, $\sigma_M^2(z)$ and $\sigma_{M_0}^2(z_0)$ are the linear theory rms density fluctuations smoothed with a 'top-hat' filter of mass M and M_0 at redshifts z and z_0 , respectively, and $\delta_c(z)$ is the critical thresholds on the linear overdensity for spherical collapse at redshift z . Integrating this function over the range $0 < M < M_0$ gives unity: all the mass of M_0 was in smaller subclumps at an earlier epoch $z > z_0$. From Eq. (3.1) we can compute a fragmentation probability that, via rejection methods, can be used to construct a binary merger tree. Implementing a successful Monte Carlo procedure, however, requires the use of two different numerical approximations (Somerville & Kolatt, 1999). First of all, since in a Λ CDM cosmology the number of haloes

diverges as the mass goes to zero, it is necessary to introduce a cut-off mass, M_{res} , that marks the transition from resolved progenitors (having $M > M_{\text{res}}$) to the accreted mass that accounts for the cumulative contribution of all mass accreted from unresolved haloes. Secondly, the time-step δz has to be small enough to guarantee a small mean number of fragments N_p in the range $M_{\text{res}} < M < M_0/2$, to avoid multiple fragmentation.

Once the appropriate choices for δz and M_{res} are made, the binary tree is constructed by using a Monte Carlo procedure similar to that of Cole et al. (2000), described in VHM. We have taken $M_{\text{res}} = 10^{-3}M_0$ at $z = 0$ decreasing with redshift as $(1+z)^{3.5}$. Finally, for each Monte Carlo realization we have used 820 time-steps logarithmically spaced between $z = 0$ and $z = 20$. As shown by VHM, with this parameter choice our merger tree algorithm not only conserves the mass, but also reproduces the EPS conditional mass function at all redshifts.

In the second step of the procedure, we implement a set of analytic prescriptions and follow the accretion history of BHs within their host haloes to model the AGN activity. The VHM model assumes that the seed BHs formed with masses of $150M_{\odot}$ (note that, as shown by VHM, the final results are not very sensitive to this choice) following the collapse of the very rare Pop III stars, in minihaloes forming at $z = 20$ from the density peaks above a 3.5σ threshold. In the assumed Λ CDM cosmology this corresponds to minihaloes with mass $\sim 1.6 \times 10^7 M_{\odot}$.

Due to the lack of an exhaustive study of the ultimate consequences of a galaxy merger in its whole parameter space, we are forced to make some simplifying assumptions to follow the merging events. Following Cox (2004), we can assume that all halo mergers, except the ones with mass ratio smaller than 0.1, can destabilize the gas at the centre of the more massive halo, and consequently induce star formation and BH mass accretion. Notice that this threshold is lower than the value of $P > 0.25$ adopted by WL03, but it is not low enough to reproduce the observed faint AGN number counts, as we will describe later. So, a higher value of the mass ratio would worsen our results, while a lower one would be in disagreement with the results of Cox (2004), which show that a typical merger with a mass ratio of 0.05 does not induce starbursts. Moreover, according to Taffoni et al. (2003), when $P < 0.1$ the dynamical friction timescale is larger than the Hubble time, hence preventing the merging of satellite galaxies and, arguably, making the accretion efficiency onto the central BH very low.

Two main features differentiate the VHM model from the WL03 one. First, the VHM model is naturally biased, as the BH seeds are associated with

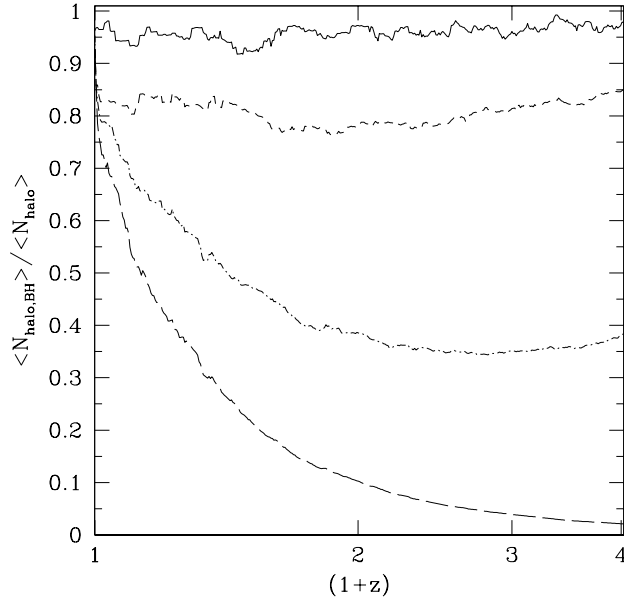


Figure 3.1: Fraction of haloes hosting at least a nuclear massive BH vs. redshift. The long-dashed curve shows the occupation fraction computed by weighting over all branches of the merger trees. The occupation fraction increases with increasing halo mass: $M_{\text{halo}} > 10^{10}M_{\odot}$ (dot-dashed curve), $M_{\text{halo}} > 10^{11}M_{\odot}$ (short-dashed curve) and $M_{\text{halo}} > 10^{12}M_{\odot}$ (solid curve).

high-density peaks in the fluctuations field. Second, VHM take into account the dynamical evolution of BHs, including strong gravitational interactions such as the gravitational rocket effect (Merritt et al., 2004; Volonteri & Perna, 2005). Such dynamical interactions can possibly eject BHs at high velocities from the centre of haloes. The net effect is to contribute to selecting massive haloes (i.e. those with a large escape velocity) as BH hosts. In all scenarios we consider (see below), we have included a treatment of the ‘gravitational rocket’ effect following Favata et al. (2004) and Merritt et al. (2004) (upper limit to the recoil velocity). More details can be found in Volonteri & Perna (2005). Fig. 3.1 shows the occupation fraction, i.e. the fraction of haloes hosting nuclear BHs for haloes of different masses. The occupation fraction of large haloes ($M_{\text{halo}} > 10^{12}M_{\odot}$) is of order unity at all times, while smaller haloes have a large probability of being deprived of their central BH.

Following a major merger, the BH at the centre of the massive progenitor can grow in mass in two ways: (i) after a dynamical friction time when a bound BH binary system forms at the centre of the halo, hardens via three body interactions (Quinlan, 1996; Milosavljević & Merritt, 2001) and then rapidly coalesces through the emission of gravitational waves (Peters, 1964);

(ii) after a dynamical free-fall time when a significant fraction of the gas falls to the centre of the merged system (Springel et al., 2005b; Di Matteo et al., 2005) and is accreted on the BH at an appropriate rate. Yet, as shown by VHM, the first mechanism contributes little to the BH mass accretion and will be neglected in this work. To implement the second mechanism we need to specify the prescription for the mass accretion and its rate.

We use the following definitions to parameterize the bolometric luminosity emitted by accretion onto BHs, as a function of the *accretion efficiency*, ε , and the *Eddington factor*, f_{Edd} :

$$\begin{aligned} L_{\text{bol}}(t) &= \frac{\varepsilon}{1-\varepsilon} \dot{M}_{\text{BH}}(t) c^2 \\ &= f_{\text{Edd}}(t) L_{\text{Edd}}(t) = f_{\text{Edd}}(t) \frac{M_{\text{BH}}(t)}{t_{\text{Edd}}} c^2, \\ \implies d \ln M_{\text{BH}}(t) &= \frac{dt}{t_{\text{ef}}(t)}, \end{aligned} \quad (3.2)$$

where L_{Edd} is the Eddington luminosity, $t_{\text{Edd}} = \sigma_T c / (4\pi m_p G) \sim 0.45 \text{ Gyr}$ and $t_{\text{ef}}(t) = \frac{\varepsilon}{1-\varepsilon} \frac{t_{\text{Edd}}}{f_{\text{Edd}}(t)}$ is the e-folding time ($t_{\text{ef}} \equiv t_{\text{Salpeter}}$ if $f_{\text{Edd}} = 1$). No strong observational constraints are available for ε and f_{Edd} , the parameters that regulate the BHs powering the AGN and, more importantly, if and how they depend on redshift, BH masses, AGN luminosities and so on. However, some observations at $z \sim 0$ indicate that $0.04 < \varepsilon < 0.16$ and $0.1 < f_{\text{Edd}} < 1.7$ (Marconi et al., 2004). Furthermore, it has been suggested that f_{Edd} may depend on redshift (Shankar et al., 2004) and BH mass (Netzer & Trakhtenbrot, 2007).

We start exploring three different scenarios. The first two assume that BHs start accreting mass at the Eddington rate after about one dynamical free-fall timescale from the merger. Accretion lasts until a mass ΔM_{accr} has been added to the BH.

- In the first one, labeled E1 in all plots, the accreted mass is proportional to the mass of the available gas and hence to the total mass of the massive progenitor: $\Delta M_{\text{accr}} = \alpha M_{\text{halo}}$. Here, $\alpha = 7 \times 10^{-6}$ guarantees the normalization of the $M_{\text{BH}} - \sigma_c$ relation at $z = 0$, where σ_c is the velocity dispersion of the host galaxy (Tremaine et al., 2002), scaling with the circular velocity of the halo as suggested by Ferrarese (2002). As in VHM, we have inhibited gas accretion in all haloes with $v_c > 600 \text{ km s}^{-1}$. This scenario is similar in spirit to the WL03 model, and is meant to compare the clustering properties of quasars at low redshift to that of their higher redshift counterparts.
- The second scheme, labeled E2, assumes a scaling relation between the accreted mass and the circular velocity of the host halo, $\Delta M_{\text{accr}} \propto$

$k \cdot v_c^5$, which is normalized *a-posteriori* to reproduce the observed relation between M_{BH} and v_c at $z = 0$ (Ferrarese, 2002). As in M06, we assume a linear dependence of k on redshift, as $k(z) = 0.15(1+z) + 0.05$, in order to account for the decrease of the gas available to fuel BHs. Unlike model E1, here the relation between M_{BH} and M_{halo} evolves in redshift as in Wyithe & Loeb (2003): $M_{\text{BH}} \propto M_{\text{halo}}^{5/3} \cdot (1+z)^{5/2} \cdot (\Delta_c/\Omega_m(z))^{5/6}$, in which $\Delta_c(z) = 18\pi^2 + 82d - 39d^2$, $d \equiv \Omega_m(z) - 1$ and $\Omega_m(z)$ represents the mass density parameter. Differently from the E1 model, we account for inefficient cooling in large haloes by preventing accretion within haloes of masses $M_{\text{halo}} > 10^{13.5} M_\odot$, in place of the $v_c > 600 \text{ km s}^{-1}$ cut-off. It is worth noticing that this prescription has a physical motivation connected to both galaxy and AGN formation since it has the same effect of including the low luminosity radio mode AGN heating, as done in many semi-analytic models of galaxy formation to produce a massive galaxy population similar to the one observed (see e.g. Kang et al., 2006; Bower et al., 2006; Cattaneo et al., 2006; Croton et al., 2006).

- The last prescription for mass accretion, labeled B, assumes an early stage of super-critical accretion during which the central BH accretes mass at a rate that can be estimated by the Bondi-Hoyle formula (Bondi & Hoyle, 1944). This model applies to metal-free haloes, therefore we assume that by $z = 12$ the interstellar medium has been enriched, and we inhibit super-critical accretion rates. When the super-critical phase ends, accretion proceeds in subsequent episodes as in model E2. This possibility has been recently advocated by Volonteri & Rees (2005) to reconcile a hierarchical evolution with the existence of AGN at $z \sim 6$, hosting BHs with masses $\sim 10^9 M_\odot$.

The end product of our semi-analytic models is a set of merging and accretion histories for 220 parent haloes with masses in the range ($1.43 \times 10^{11} M_\odot, 10^{15} M_\odot$). When active, i.e. during the period of mass accretion, the AGN shines with a *B*-band luminosity of $(L_B/L_\odot) = M_{\text{BH}} \times 10^{3.46} M_\odot$, obtained under the assumptions that the rest mass is converted to radiation with a 10 per cent efficiency and that only a fraction $f_B = 0.08$ of the bolometric power is radiated in the blue band.

Model vs. observations

3.2.1 $M_{\text{BH}} - \sigma_c$ scaling relation

In this section we compare the $M_{\text{BH}} - \sigma_c$ scaling relation derived by Ferrarese & Ford (2005) at $z = 0$ to the one predicted by our semi-analytic models. The bulge velocity dispersion σ_c is derived from the $V_c - \sigma_c$ relation of Baes et al. (2003). Every open circle in Fig. 3.2 represents one BH in a halo of given σ_c , for our models E1, E2, and B, as indicated by the labels. We started at $z = 0$ with a discrete grid in halo masses (hence, with a discrete grid of σ_c) and performed several simulations for each mass. The filled black dots and the dashed lines in the Figure show the mean values of M_{BH} and the linear best fit to the model outputs, respectively. In each panel, the grey shaded area shows the best fit to the observational datasets of Ferrarese & Ford (2005), while the dark-grey line refers to the best-fit relation obtained by Wyithe (2006).

As shown in Figure 3.2, all our models agree well with the data. Model E1, which assumes $M_{\text{halo}} \propto v_c^3$, predicts a flatter relation with respect to the best-fit of Ferrarese & Ford (2005); however, we note that this prediction is in excellent agreement with the non-linear fit derived by Wyithe (2006). We also note that the scatter in the predicted scaling relation increases for low values of σ_c , i.e. for less massive host haloes, a trend common to almost all previous semi-analytic studies of BH growth in galaxy formation (see e.g. Cattaneo et al., 1999). We will come back to this point in Section 4.2.1. Finally, we stress that our semi-analytic recipes only fix the normalization of the $M_{\text{BH}} - \sigma_c$ relation, through the amount of mass accreted after each major merger. So the slope and the shape of such relation have to be regarded as real predictions of our models.

3.2.2 AGN optical luminosity function

The model AGN LF at different redshifts has been computed by evaluating the number density of active BHs in each luminosity bin in redshift intervals centred on an effective redshift z_{eff} . In practice we have counted the number of active BHs in the redshift and luminosity bins in all merger trees, each of them weighted by the number density of their parent haloes at $z = 0$, evaluated using the Sheth & Tormen (1999) formula. The result has been normalized using the number of time-steps in the redshift interval and the number of merger trees considered. Associate uncertainties have been

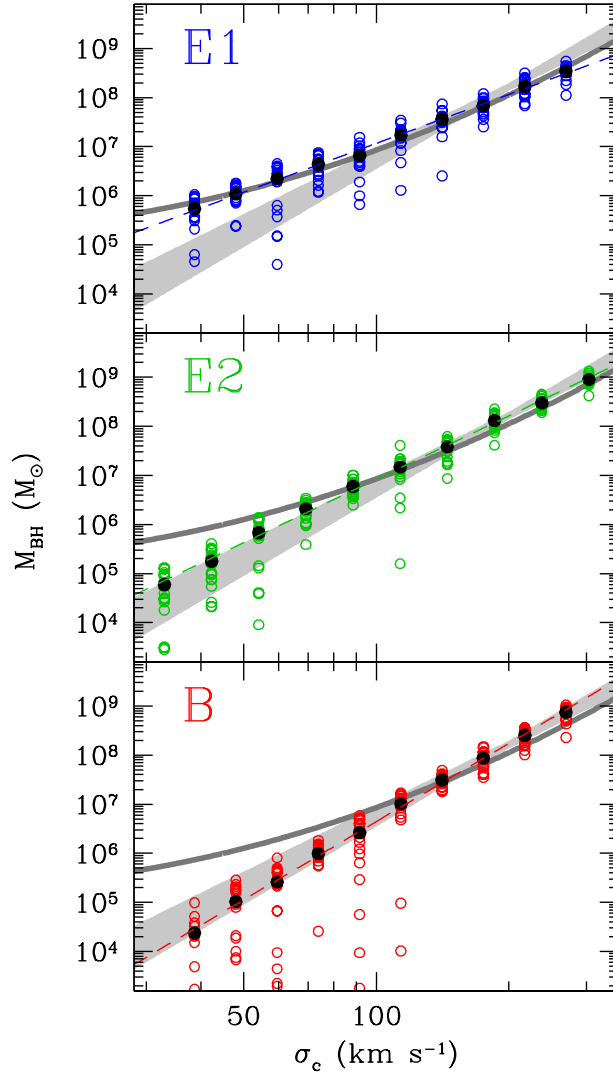


Figure 3.2: The $M_{\text{BH}} - \sigma$ scaling relation at $z = 0$: models vs. observations. The grey shaded area shows the best fit to the observational datasets of Ferrarese & Ford (2005). The dark-grey line refers to the best-fit relation obtained by Wytke (2006). Every open circle represents one BH in a halo of given σ_c , for our E1, E2, and B models, as indicated by the labels. We started at $z = 0$ with a discrete grid in halo masses (hence, with a discrete grid in σ_c) and performed several simulations for each mass. The filled black dots and the dashed lines show the mean values of M_{BH} and the linear best fit to the model outputs, respectively.

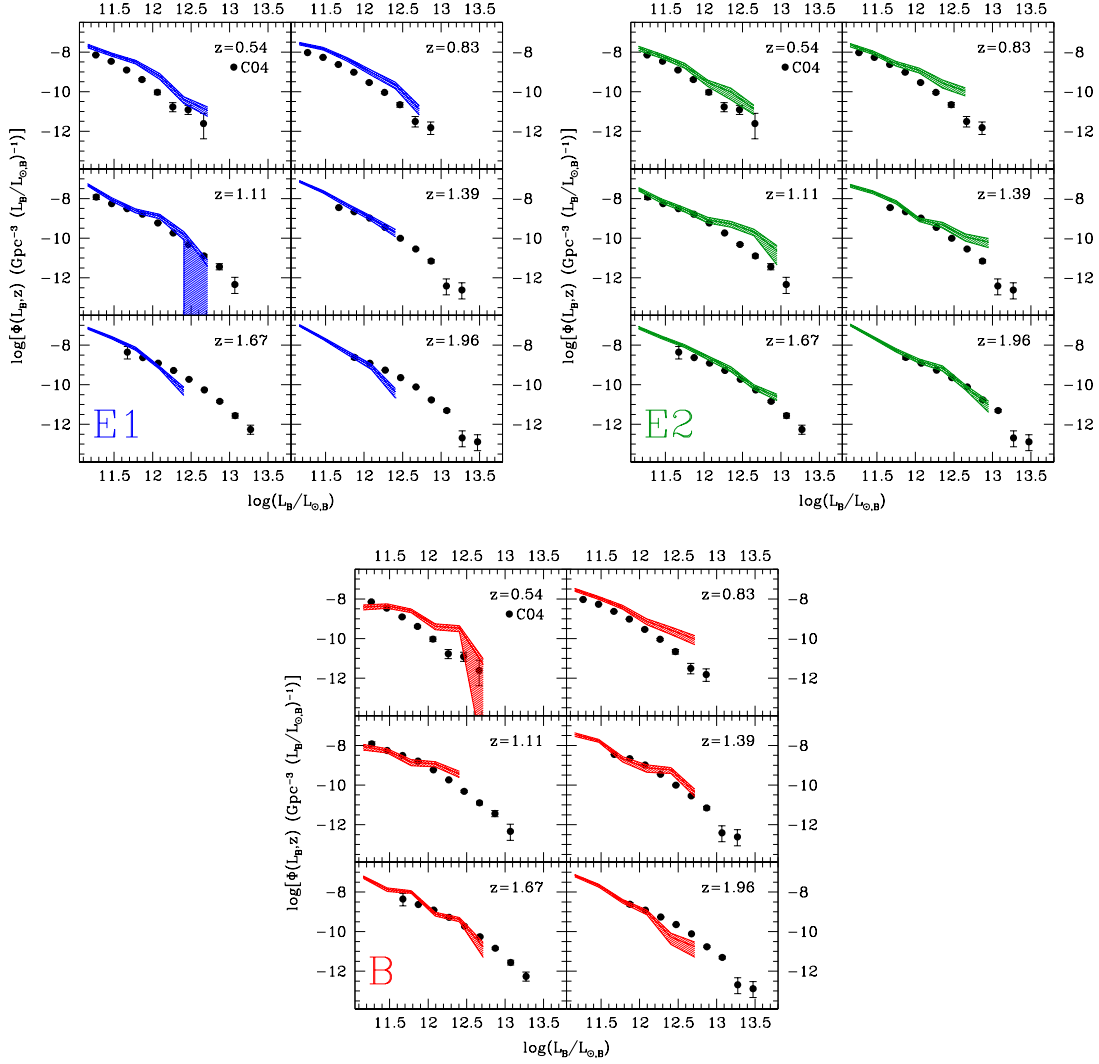


Figure 3.3: The AGN luminosity function in B -band at six different redshifts: models vs. observations. The filled dots show the 2dF/6dF AGN luminosity function measured by C04 together with their 1σ error bars. The dashed coloured areas refer to the E1, E2, and B model predictions as explicitly indicated by the labels.

computed by assuming Poisson statistics.

In Fig. 3.3 we compare our model optical LF with the observations. The 2dF/6dF LFs are plotted using black dots, as in Fig. 2.1. At low redshifts all models reproduce the faint end of the LF fairly well. However, they systematically overpredict the number of bright AGN: this indicates that having inhibited gas accretion in haloes with $v_c > 600 \text{ km s}^{-1}$ has little impact on our results. The disagreement is slightly less severe for the E2 model, in which we have imposed a similar mass threshold as the one of the WL03 model, in place of the $v_c > 600 \text{ km s}^{-1}$ cut-off.

3.2.3 AGN bolometric luminosity function

As we have explicitly demonstrated in the previous sections of this Thesis, at low redshifts, standard analytic and semi-analytic methods systematically overpredict the number density of bright objects. As already stressed, this could be caused by the fact that gas accretion is likely very inefficient within large haloes due to the high temperature of the baryons: this can inhibit accretion in haloes larger than $\sim 10^{13.5} M_\odot$, hence reducing the abundance of bright objects. Indeed, this prescription significantly improves the match to the bright end of the AGN LF, especially when implemented within the analytic framework. Yet, significant discrepancies still remain, especially at very low redshifts, that could be possibly eliminated by including two more factors that are missing from the models.

First, when comparing our model predictions to the observed *B*-band AGN LF, we have implicitly ignored the presence of a substantial population of (optically) obscured, luminous AGN, whose existence, instead, is suggested by *Chandra* results (see, e.g., Barger et al., 2001; Rosati et al., 2002). Indeed, in our modeling we have not included any correction for type-II quasars, which appear to contribute between ~ 30 per cent (La Franca et al., 2005), and ~ 80 per cent (Brown et al., 2006; Franceschini et al., 2005) to the quasar population at $0.5 < z < 2$. We can thus improve our investigation computing directly the bolometric AGN LFs predicted by our models E1, E2, and B and compare them to the one derived by H07. In this way, we can account for the AGN obsuration; besides, this comparison also represents a more severe test to the models than the one performed in the previous section, since the number of AGN used by H07 to model their bolometric LF is significantly larger than those considered by C04, and consequently the uncertainties are smaller and the luminosity range is much larger ($L_{\text{bol}} \sim 10^{41} - 10^{49} \text{ erg s}^{-1}$).

Second, as previously mentioned, many authors have shown that low-redshift AGN are probably accreting inefficiently, i.e. both at an accretion

rate much smaller than the Eddington rate and with a low radiative efficiency. Evidence for a BH powering mechanism less efficient at low redshift is also provided by the fact that local bright AGN seem to be hosted in early-type galaxies that show no sign of recent merging events like disturbed morphology or recent star formation episodes (see, e.g. Grogin et al., 2005; Grazian et al., 2004; Dunlop et al., 2003, and references therein). These considerations suggest that a successful model for describing the evolution of AGN luminosity should include a more sophisticated mechanism for the AGN activity in which the BH accretion rate and the AGN duty-cycle might depend on halo masses and merger parameters, as suggested by recent numerical experiments (Di Matteo et al., 2005). Consequently, we consider also a different model, labeled H, which accounts for the results of the recent hydrodynamic simulations of galaxy mergers in which AGN feedback is included (Hopkins et al., 2005) that show that the Eddington ratio is not constant but depends on AGN luminosity. As the main variable in the model is the BH mass rather than the AGN luminosity, Volonteri et al. (2006) model $f_{\text{Edd}}(t)$ as follows. First, the average time spent by AGN per logarithmic luminosity interval can be approximated as (Hopkins et al., 2005)

$$\frac{dt}{d \ln L_{\text{bol}}} = |\alpha| t_9 \left(\frac{L_{\text{bol}}(t)}{10^9 L_{\odot}} \right)^{\alpha}, \quad (3.3)$$

where $t_9 \equiv t_Q(L' > 10^9 L_{\odot})$ and $t_Q(L' > L)$ is the total AGN lifetime above a given luminosity L ; $t_9 \sim 10^9$ yr over the range $10^9 L_{\odot} < L_{\text{bol}} < L_{\text{peak}}$. In the range $10^{10} L_{\odot} \lesssim L_{\text{peak}} \lesssim 10^{14} L_{\odot}$, Hopkins et al. (2005) found that α is a function of only the AGN luminosity at the peak of its activity, L_{peak} , given by $\alpha = -0.95 + 0.32 \log(L_{\text{peak}}/10^{12} L_{\odot})$, with $\alpha = -0.2$ (the approximate slope of the Eddington-limited case) as an upper limit. Then, since the AGN luminosity can be written as $L = \varepsilon f_{\text{Edd}}(t) \dot{M}_{\text{Edd}} c^2$, where ε is the radiative efficiency, $\varepsilon = L/(f_{\text{Edd}}(t) \dot{M}_{\text{Edd}} c^2) = 0.1$ ¹, the following differential equation is used to describe the evolution of $f_{\text{Edd}}(t)$:

$$\frac{df_{\text{Edd}}(t)}{dt} \sim \frac{f_{\text{Edd}}^{1-\alpha}(t)}{|\alpha| t_Q} \left(\frac{\varepsilon \dot{M}_{\text{Edd}} c^2}{10^9 L_{\odot}} \right)^{-\alpha}. \quad (3.4)$$

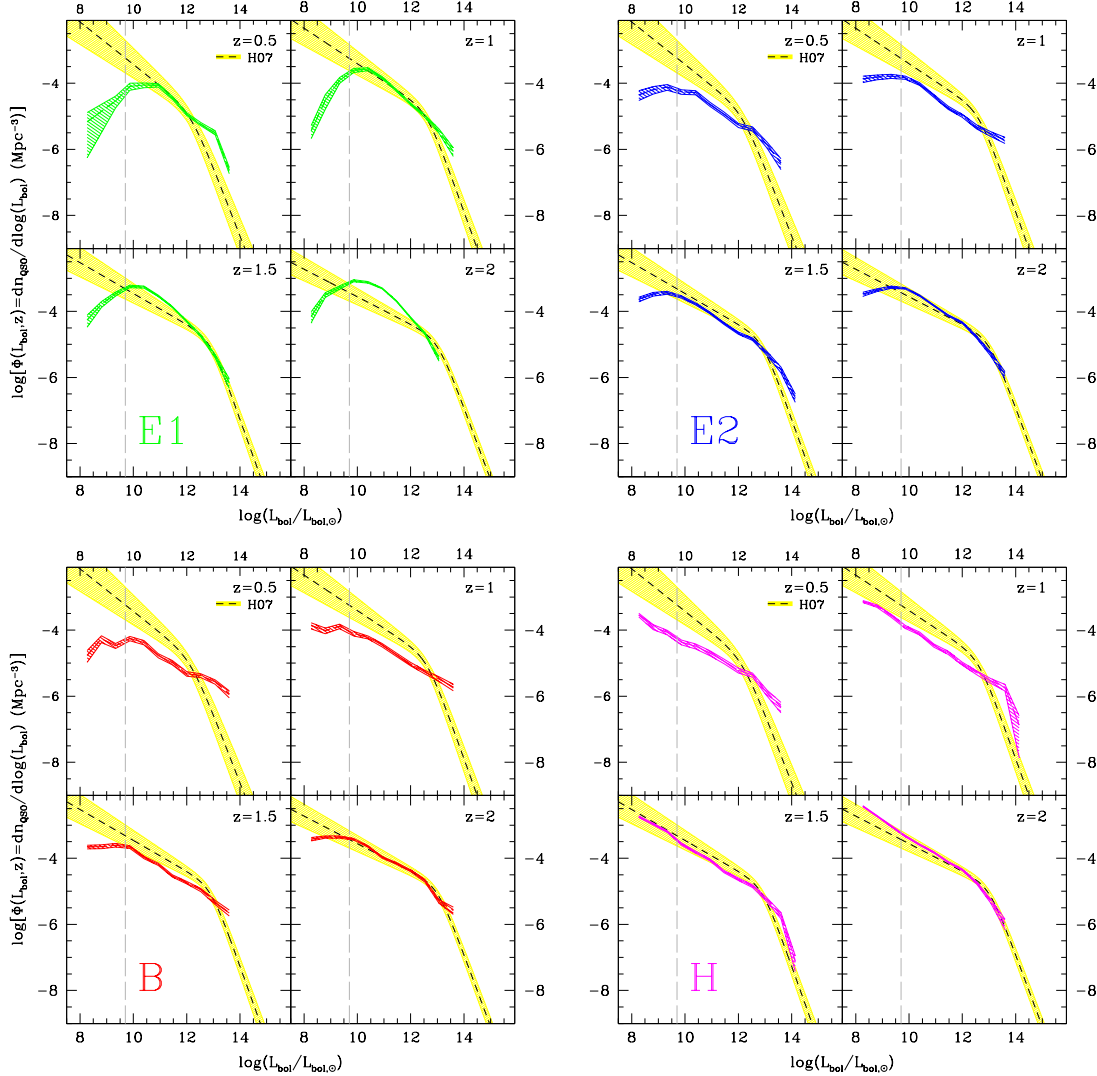
Model H assumes that the final mass of the black hole is determined by the circular velocity of the host halo, as in model E2.

The results are shown in Fig. 3.4, which is divided in four sets of plots, each one referring to a different model. In each set, composed by four panels, the shaded area represents the 1σ uncertainty strip around the model

¹The radiative efficiency has been self-consistently determined by tracking the evolution of BH spins throughout the calculations (Volonteri et al., 2005).

Table 3.1: Values of Ξ^{model} and the corresponding per cent probability $P(\Xi^{\text{zamodel}})$, indicated in parentheses, for each models and redshifts.

Model	$\Xi (P(\Xi))$				
	$z = 0.1$	$z = 0.5$	$z = 1$	$z = 1.5$	$z = 2$
E1	5.3 (0.2%)	2.2 (13.6%)	1.5 (34.9%)	1.1 (45.0%)	6.6 (2.5%)
E2	2.5 (2.4%)	3.3 (7.4%)	4.6 (4.9%)	2.8 (16.4%)	0.5 (80.8 %)
B	5.4 (0.3%)	5.2 (3.2%)	5.7 (4.0%)	3.1 (12.2%)	1.1 (50.8 %)
H	2.3 (2.5%)	3.7 (6.0%)	5.5 (4.3%)	1.9 (26.9%)	0.4 (90.8 %)


 Figure 3.4: The AGN bolometric LF at $0.5 \leq z \leq 2$: models vs. observations. The dashed black lines show the bolometric LF of H07, while the yellow shaded areas take account of the estimated errors of the fit. The dashed vertical lines show the minimum bolometric luminosity accessible to observations. Each set of plots, composed by four panels corresponding to different redshifts, refers to a different model, as indicated by the labels.

LF. The dashed curve shows the bolometric LF of H07 while the yellow shaded areas take account of the estimated errors of the fit. In all plots the vertical, dashed line shows the minimum bolometric luminosity accessible to observations, $L_{\text{obs}}^{\text{min}}$, which turns out to be remarkably constant in the interval of redshifts considered. Note also that with the bolometric correction of H07, the minimum bolometric luminosities of the C04 sample are much higher than $L_{\text{obs}}^{\text{min}}$ (see Fig. 2.1 and 3.3). Model predictions extend up to a maximum luminosity $L_{\text{model}}^{\text{max}} \sim 10^{14} L_{\odot}$ resulting from having set an upper limit to the mass of our DM haloes ($M^{\text{max}} \sim 10^{15} M_{\odot}$).

To quantify the consistency between models and data we have estimated the following χ^2 -like quantity:

$$\Xi^{\text{model}}(z) = \frac{1}{N_{\text{bin}}} \sum_{i=1}^{N_{\text{bin}}} \frac{[\log(n_{\text{model}}(\Delta L_i, z)) - \log(n_{\text{obs}}(\Delta L_i, z))]^2}{\sigma_{\text{model}}^2 + \sigma_{\text{obs}}^2}, \quad (3.5)$$

where $n_{\text{model}}(\Delta L_i, z)$ and $n_{\text{obs}}(\Delta L_i, z)$ represent the model and observed mean comoving number density of AGN in the luminosity interval ΔL_i at redshift z , σ_{model} and σ_{obs} are the 1σ logarithmic errors and the sum runs over the N_{bin} luminosity bins in the interval $L_{\text{obs}}^{\text{min}} - L_{\text{model}}^{\text{max}}$. We have verified that all our results are not sensitive to the choice of the bin size.

The values of $\Xi^{\text{model}}(z)$, evaluated at all redshifts, are shown in Table 4.2.1 for all models explored. To compare these values with theoretical expectations, we use Monte Carlo techniques to compute distribution of Ξ , $f(\Xi, z)$, expected when $n_{\text{model}}(\Delta L_i, z)$ is a Gaussian random variable, normally distributed around $n_{\text{obs}}(\Delta L_i, z)$ with variance $10^{(\sigma_{\text{model}}^2 + \sigma_{\text{obs}}^2)}$. This function is used to evaluate the cumulative probability of Ξ by integrating $f(\Xi, z)$:

$$P(\Xi^{\text{model}}, z) = \int_{>\Xi^{\text{model}}(z)} d\Xi f(\Xi, z), \quad (3.6)$$

which is defined in analogy to the χ^2 -probability and represents the probability that a function that genuinely describes the dataset would give a value larger or equal to Ξ^{model} . The values of $P(\Xi^{\text{model}}, z)$ are listed (in parentheses) in Table 4.2.1.

The results confirm those of the previous sections, in the sense that all models, apart from E1 that significantly overpredicts the abundance of AGN at $z = 2$, match the LFs in the range $1 \lesssim z \lesssim 2$ and in the luminosity range of Fig. 3.3 fairly well. The advantage of considering bolometric rather than B-band or hard X-ray LFs is apparent at lower redshifts where discrepancies between models and observations at the bright and faint ends of the luminosity functions are more significant here than previously. Indeed, all models overpredict the abundance of bright objects and underpredict the

abundance of the faint ones (at luminosities fainter than the one of the C04 sample), at $z = 0.5$ and $z = 1$.

In the bright end of the LF, the mismatch can be reduced by advocating some physical mechanism, like inefficient cooling, that hampers mass accretion in large haloes. Our simple model E2, in which mass accretion is inhibited in haloes with masses larger than $10^{13.5} M_{\odot}$, provides a better match to the data, especially at $z = 0.5$, although the effect is less apparent here than previously. The overabundance of bright AGN is also alleviated in model H since the variable Eddington ratio guarantees that a BH hosted in the largest haloes accretes most of the time at a sub-Eddington rate, resulting in a fainter AGN.

In all models, but E1, the LF faint end is biased low. The effect is systematic and, in the luminosity range accessible to observations, it does not depend on luminosity. Discrepancies grow larger when extrapolating the comparison below to objects fainter than $L_{\text{bol}}^{\text{min}}$, below which the LF predicted by most semi-analytic models turns-over while the model LF of H07 is fitted by a power-law. The power-law behaviour is, however, recovered by model H, that assumes a time-dependent Eddington ratio.

3.2.4 AGN hard X-ray luminosity function at $z \sim 0.1$

To understand whether the under-abundance of faint AGN predicted by most semi-analytic models is real or a mere artifact resulting from having extrapolated the power-law behaviour of the bolometric LF of H07 below $L_{\text{bol}}^{\text{min}}$ requires probing the AGN LF to lower luminosities, which is only possible in the nearby universe.

In this section we do not compare the model LFs with the bolometric one at $z \sim 0$. Instead, we apply the inverse bolometric conversion of H07 to compare model predictions with the LFs of the two most recent determinations of the AGN LF in the hard ($\geq 2\text{keV}$) X-ray band that, despite being very local, provides strong constraints to AGN models. The first one, provided by Shinozaki et al. (2006) [S06], consists of a complete, flux-limited sample of 49 sources from the HEAO-1 All-Sky catalogue, complemented with spectral information from ASCA, XMM-Newton and Beppo-SAX observations. All objects in the catalogue are optically classified as emission-line Seyfert galaxies at high galactic latitude ($b \geq 20^\circ$) with column density $N_H > 10^{21.5} \text{cm}^{-2}$ and $L_X = L[2 - 10\text{keV}] > 10^{42} \text{erg s}^{-1}$. The second AGN LF has been determined in a harder X-ray band [20 – 40keV] by Beckmann et al. (2006) [B06], using a sample of 38 objects, preferentially located at low galactic latitude, detected by the imager IBIS/ISGRI on-board INTEGRAL, with $L_X = L[20 - 40\text{keV}] >$

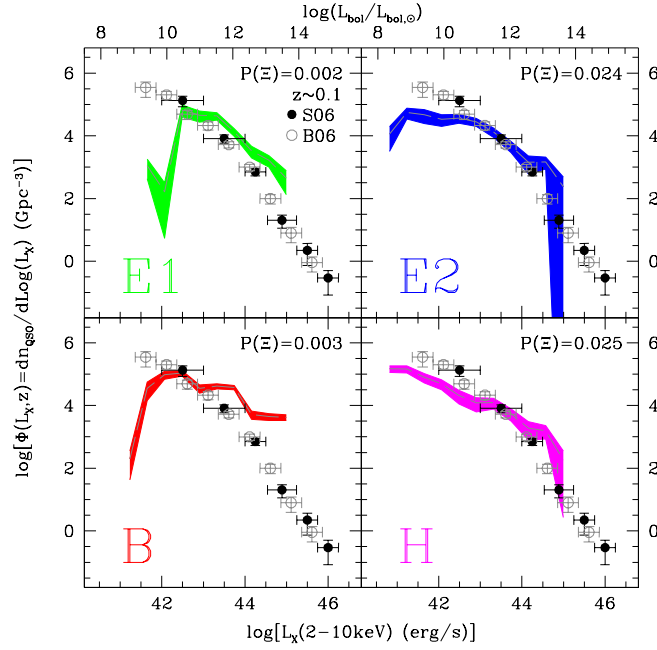


Figure 3.5: The AGN bolometric LF at $z = 0.1$: models vs. observations. S06 and B06 LFs are represented by filled and open dots, respectively. Vertical error bars represent 1σ uncertainties while horizontal bars indicate the size of the luminosity bins. Each plot refers to a different model, as indicated by the labels.

$10^{41} \text{ erg s}^{-1}$. The main reason for concentrating on these two datasets is as follows. First of all, these two datasets, especially the B06 one, include objects that were not considered in the H07 analysis. Second, selection in the hard X-ray allows to include obscured AGN which make bolometric corrections less severe in this band. Third, the two samples have rather similar composition as 90% of the objects are Seyfert galaxies. As a result, comparing model with S06 and B06 LFs allows to maximize the number of nearby, homogeneous objects, while reducing uncertainties in model bolometric corrections.

Model vs. data comparisons are shown in Fig. 3.5, where the S06 and B06 LFs are represented by filled and open dots, respectively. Vertical errorbars represent 1σ uncertainties, while horizontal bars indicate the size of the luminosity bins. The AGN luminosity in the B06 sample are measured in the $[20 - 40 \text{ keV}]$ band and transformed in the $[2 - 10 \text{ keV}]$ band according to $L_{[2-10 \text{ keV}]} / L_{[20-40 \text{ keV}]} = 2.3$ (Beckmann et al., 2006).

The shaded areas show the model LFs at $z = 0.1$ together with their 1σ uncertainties expressed in the $[2 - 10 \text{ keV}]$ band by using the bolometric

correction of H07:

$$\frac{L}{L_{[2-10\text{keV}]}} = c_1 \left(\frac{L}{10^{10}L_{\odot}} \right)^{k_1} + c_2 \left(\frac{L}{10^{10}L_{\odot}} \right)^{k_2}, \quad (3.7)$$

with $c_1 = 10.83$, $k_1 = 0.28$, $c_2 = 6.08$ and $k_2 = -0.02$. The bolometric luminosities are indicated on the X-axis in the upper part of the plot. In order to correct for the extinction in the X-ray bands, we have used the following equation, also provided by H07:

$$\frac{\Phi(L_{[2-10\text{keV}]})}{\Phi(L_{\text{bol}}[L_{[2-10\text{keV}]}])} = f_{46} \left(\frac{L_{\text{bol}}[L_{[2-10\text{keV}]}]}{10^{46} \text{erg s}^{-1}} \right)^{\beta}, \quad (3.8)$$

where $f_{46} = 1.243$, $\beta = 0.066$ and $L_{\text{bol}}[L_{[2-10\text{keV}]}]$ is the bolometric luminosity correspondent to $L_{[2-10\text{keV}]}$, as given by the bolometric corrections of Eq. (3.7).

The comparison between model and data confirm our previous extrapolation, since the observed number density of faint AGN with $L_X = 10^{42} - 10^{43} \text{erg/s}$ is significantly larger than that predicted by all models, as indicated by the sudden drop in the values of the $P(\Xi^{\text{model}})$ at $z = 0.1$. This is due to the fact that, for a given value of Ξ^{model} , the $f(\Xi)$ distribution at redshifts ≥ 0.5 is more positively skewed than at $z = 0.1$, as we have verified. Discrepancies are larger for models E1 and B, while models E2 and H provide a better match to the faint end of the local LF. The sharp downturn in the E1 and B models is a robust feature since the characteristic mass of haloes populating the faint luminosity bins ($\sim 10^{11.5} M_{\odot}$) is well above the mass resolution limit in our merger trees.

Note that the largest discrepancies are found in the faintest luminosity bin which can only be probed by the B06 sample. With this respect, it is worth noticing that Sazonov & Revnivtsev (2004) have used yet another dataset of hard X-ray selected AGN to estimate the AGN LF down to $L_{[3-20\text{keV}]} \sim 10^{41} \text{erg/s}$. Their LF is consistent with those of S06 and B06 down to the faintest objects. The sample of Sazonov & Revnivtsev (2004) consists of 95 AGN in the $[3 - 20\text{keV}]$ interval at high galactic latitude serendipitously detected in the RXTE slew survey. However, only 60% of these AGN are classified as Seyfert galaxies, many of which also belong to the S06 sample. Since in this work we prefer to deal with a homogeneous sample of local AGN, we have decided not to consider the Sazonov & Revnivtsev (2004) LF in our quantitative analysis.

3.2.5 AGN biasing function

As discussed in Section 1.1.6, further observational constraints to theoretical models are provided by the AGN spatial clustering, which is often

quantified by means of the angular or spatial two-point correlation function. Uncertainties in current modeling of the AGN clustering, however, make this constraint less effective than the LF. In spite of that, as for the analytic models introduced in the previous chapter, we also check the ability of our semi-analytic models in matching the AGN biasing function as a function of redshift. To do that, we compare model predictions to the observational determination of the biasing function estimated in the B-band by PMN, as in Section 2.3.2.

The model AGN biasing function can be computed by weighting the analytic biasing function of the DM haloes provided by Sheth et al. (2001), $b(M_{\text{halo}}, z)$, with the mass function of the haloes hosting AGN with luminosities larger than the thresholds of the observations, $\Psi(M, z)$ (similarly to the Eq. (2.8)):

$$b_{\text{eff}}(z) = \frac{\int_0^{+\infty} b(M_{\text{halo}}, z) \Psi(M_{\text{halo}}(L_B > L_{\text{min}, B}), z) dM_{\text{halo}}}{\int_0^{+\infty} \Psi(M_{\text{halo}}(L_B > L_{\text{min}, B}), z) dM_{\text{halo}}}, \quad (3.9)$$

The result is shown in Fig. 3.6, where the points represent the observed B-band AGN biasing function and the shaded areas show the 1σ uncertainty interval around model predictions. To convert our bolometric luminosities to B-band ones we used the bolometric correction of H07, i.e. Eq. (3.7) with $c_1 = 6.25$, $k_1 = -0.37$, $c_2 = 9$ and $k_2 = -0.012$, and Eq. (3.8) with $f_{46} = 0.26$, $\beta = 0.082$. As we have also verified, using the bolometric correction provided by Marconi et al. (2004), or the one provided by Eq. (2.1) adopted in the analytic WL02 and WL03 models, does not change significantly our results. As shown in Fig. 3.6, the large model uncertainties do not allow us to place strong constraint based on the AGN clustering. Indeed, all our models are in acceptable agreement with the data, suggesting, however, that possible disagreements may become significant at $z > 2$.

As pointed out by Wyithe & Loeb (2005a), the evolution of clustering is slightly faster when the BH mass scales with the halo mass (model E1) rather than the circular velocity (model E2), although the difference is of very little significance given the large scatter in the model predictions. Fig. 3.7 represents the mean halo occupation number, $N_{\text{AGN}}(M_{\text{halo}})$, of the E1 and E2 models, i.e. the average number of active BHs hosted in haloes with mass between M_{halo} and $M_{\text{halo}} + dM_{\text{halo}}$:

$$N_{\text{AGN}}(M_{\text{halo}}) = \frac{\Psi(M_{\text{halo}})}{dN/dM_{\text{halo}}}, \quad (3.10)$$

where $\Psi(M_{\text{halo}})$ is the mass function of haloes hosting active quasars in the halo merger trees and dN/dM_{halo} is the Sheth & Tormen (1999) halo

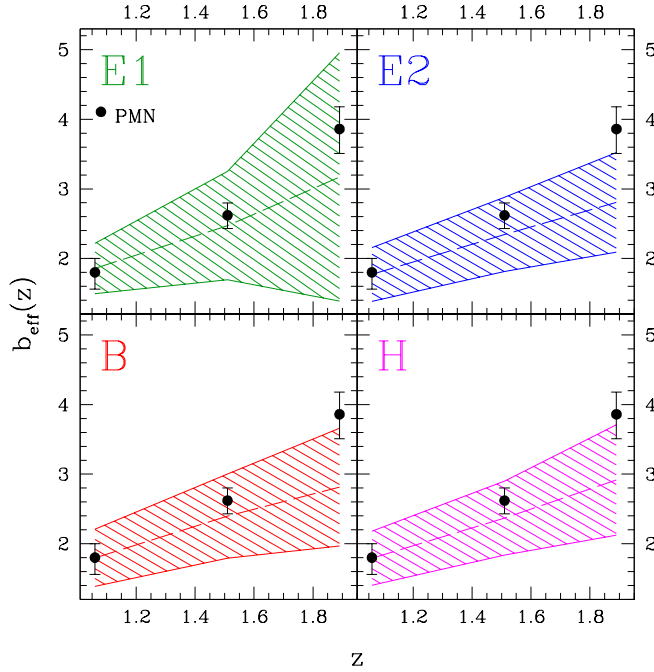


Figure 3.6: The AGN bias function at $z < 2$: models vs. observations. The solid black points show the bias estimated by PMN. The four dashed lines, with their shaded areas, show our model predictions with their 1σ uncertainties.

mass function. Model uncertainties have been evaluated from Poisson errors associated to $\Psi(M_{\text{halo}})$. At $z = 1.89$ model E1 exhibits a steeper dependence on halo mass compared to the E2 model, meaning that AGN are preferentially found in massive haloes with a high degree of spatial clustering. This result derives from the fact that the accretion scheme of model E1 is more efficient at very high redshift ($z > 6$) than that of model E2, due to the different scaling of ΔM_{accr} with redshift. Fig. 3.8 exemplifies this effect. On one hand, ΔM_{accr} is a steeper function of redshift in model E2, implying that massive BHs accrete more mass in every accretion episode, thus leading to a longer duty-cycle, and a larger occupation number, in general. On the other hand, at redshift $z = 1.89$, only quasars above $L_{B,\text{min}}$ are selected. In model E2 the 2σ -peak haloes contain BHs massive enough to be above threshold, while for model E1 a slightly more massive halo is needed. Consequently this enhances the bias, though the effect is very little at $z < 2$.

This behaviour agrees with that found by Adelberger & Steidel (2005): at $z > 2$ BH masses correlate with the halo mass instead of with velocity dispersion, or circular velocity. We can speculate that there might be a transition in the interaction between BHs and their hosts, which switches on at $z \simeq 2$: at higher redshifts the BH mass scales with the halo mass, at

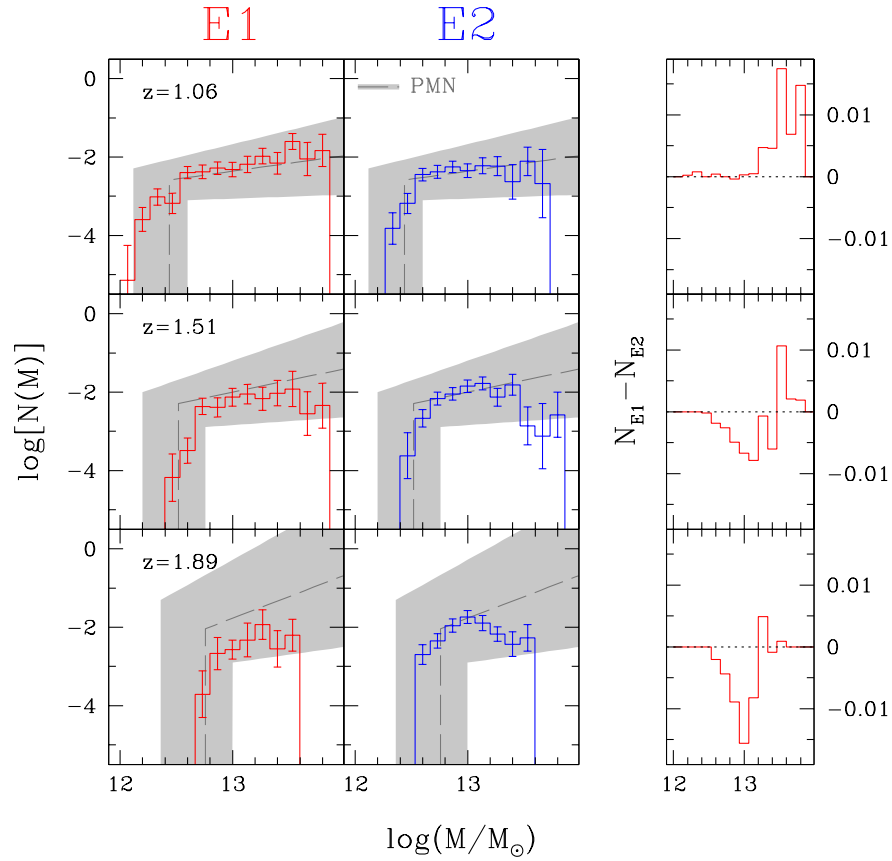


Figure 3.7: The mean halo occupation number of AGN at three effective redshifts $z = 1.06$, $z = 1.51$ and $z = 1.89$ (from top to bottom). Histograms represent model predictions, while the dashed lines, with their shaded areas, show the mean halo occupation number proposed by PMN and consistent with 2dF/6dF AGN data. Left panels: model E1. Central panels: model E2. Right panels: difference between the halo occupation number predicted by the models E1 and E2.

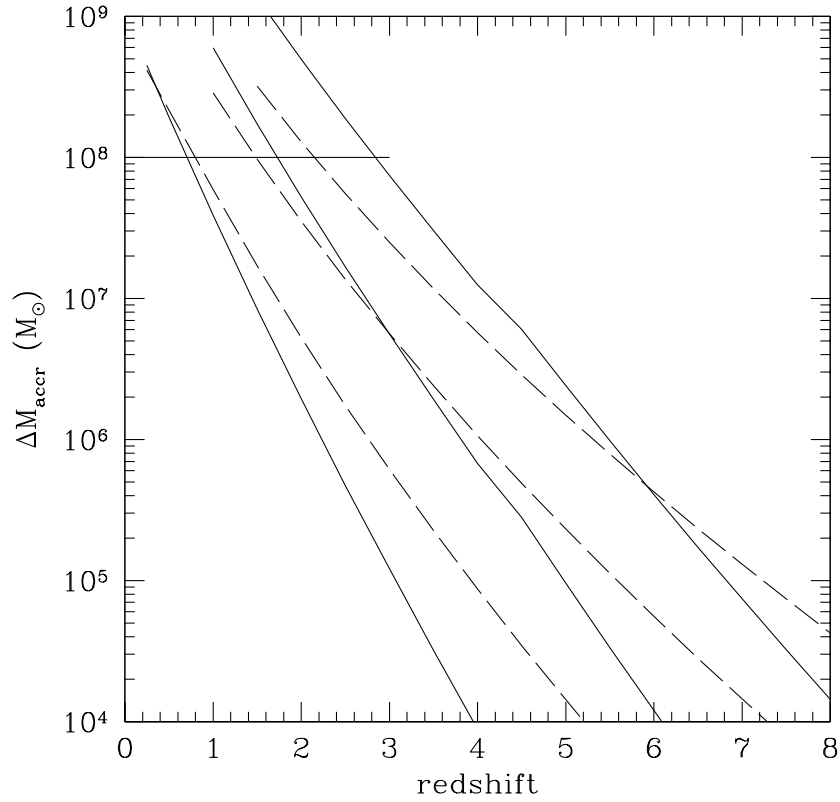


Figure 3.8: Accreted mass as a function of redshift for different halo masses. From top to bottom, curves are for 2.5σ , 2σ and 1.5σ peak haloes. Dashed curves: model E1. Solid curves: model E2. The horizontal line shows the BH mass corresponding to $L_{B,\text{min}}$ at $z = 1.89$ of PMN, assuming Eddington accretion rate.

lower redshifts with its velocity. As shown in Fig. 3.8, the accreted mass in a given episode is larger in model E1 than in model E2 for haloes representing density peaks below 2σ at $z > 3$. Model E1, therefore, implies an earlier growth for BHs. On the contrary, model B, in which massive BHs accrete mass with very high efficiency at high redshifts preferentially populate smaller haloes. Massive BHs in more massive haloes have already grown to masses close to the $M_{\text{BH}} - \sigma$ threshold. At $z = 1.06$ all models, especially E1, predicts a number of AGN in haloes which is systematically larger than the one inferred from PMN, especially in high-mass haloes. This discrepancy, which is marginally significant, considering the errors estimated by PMN, reflects the fact that semi-analytic models overestimate the optical LF of bright quasars at low redshifts. On the other hand, at high redshifts our models predict a halo occupation number that is systematically smaller than the PMN one, which again reflects the fact that our model LFs slightly underestimate the observed one at high redshifts. This effect is particularly evident for model E1, which predicts no AGN with $L > 10^{12} L_{\odot, B}$ at $z > 1.25$.

SECTION 3.3

Discussion

In this chapter we have tested the validity of the assumption that the evolution of AGN is simply related to the cosmological merging history of DM haloes. To do that, we have compared the predictions of hierarchical semi-analytic models to the most recent determination of the AGN LF and their biasing at $z < 2$.

Our main results can be summarized as follows.

(i) We confirm the success of simple semi-analytic models in reproducing both the $M_{\text{BH}} - \sigma_c$ relation at $z = 0$, the AGN bolometric LF at $1 \lesssim z \lesssim 2$, i.e. around the peak of activity, and the AGN clustering, quantified by the biasing function, at $z < 2$.

(ii) As pointed out by several previous analyses, problems occur at low redshifts, where hierarchical models systematically overestimate the number density of bright AGN and underestimate the faint ones.

(iii) Comparing bolometric LFs rather than the optical or hard X-rays ones allows to spot significant discrepancies already at moderate redshifts $z \sim 1$, i.e. earlier than what was found in previous analyses.

(iv) The predicted number density of bright AGN can be reduced not only

by advocating inefficient cooling within massive haloes, as in model E2, but also by accounting for feedback mechanisms, as we did in model H.

(v) The underestimate of faint AGN looks like a more serious problem that we have tried to tackle by assuming a time-dependent Eddington ratio, as suggested by the outcome of the hydrodynamical simulations by Hopkins et al. (2005). As shown by Volonteri et al. (2006), implementing this prescription within a semi-analytic framework, as we did in model H, proved to be successful in reproducing the redshift distribution of the faint X-ray counts (Volonteri et al., 2006). In this work, we extended the analysis of Volonteri et al. (2006) by comparing model predictions with the most recent determinations of the local AGN LF by S06 and B06 in the hard X-ray band, to include absorbed AGN and minimize the impact of bolometric corrections. This is a very demanding test for semi-analytic models, which constitutes the main focus of this chapter since, as we have pointed out, the mismatch in the number density of faint AGN grows larger when decreasing the redshift. We found that the two most successful models E2 and H are in acceptable agreement with the data at $z \gtrsim 0.5$, but struggle to match the correct number density of faint X-ray sources in the nearby universe.

Model H, based on the results of hydrodynamical simulations of Hopkins et al. (2005) within a pure merger driven scenario, seems unable to account for local faint AGN. If the accretion efficiency were much lower, the lifetime of faint AGN would increase proportionally and help alleviate the discrepancy. However, the Eddington factors derived from Hopkins et al. (2005) light curve are well below $f_{\text{Edd}} = 0.1$ only when a galaxy hosts a BH with an initial mass anomalously smaller than that predicted by the $M_{\text{BH}} - \sigma_c$ correlation. This is evident in Figure 3.9: our models assume that accretion processes bring the BHs onto the $M_{\text{BH}} - \sigma_c$ relation and the accretion efficiency is for most systems above $f_{\text{Edd}} = 0.1$. This can be understood using a very simple argument. Let us assume that (i) quiescent BHs sit on the $M_{\text{BH}} - \sigma_c$ relation, as observed in the nearby galaxy where the $M_{\text{BH}} - \sigma_c$ relation was indeed derived. This is therefore a safe assumption in the local Universe. (ii) Accretion is triggered only by major mergers, that is mergers between galaxies with a mass-ratio larger than at least 0.1. And, (iii) an accretion episode grows BHs until they reach the $M_{\text{BH}} - \sigma_c$ relation for the newly formed galaxy, due to feedback effect. Within these simple but sensible assumptions, the accretion efficiency is bound to be high, as can be easily estimated by Eq. 3.4. If we consider, for example, a major merger of a Milky-Way sized galaxy, the Eddington factor of the BHs remains $f_{\text{Edd}} < 0.1$ for only about 10^6 yr.

The inadequacy of the pure merger driven scenario becomes more evident

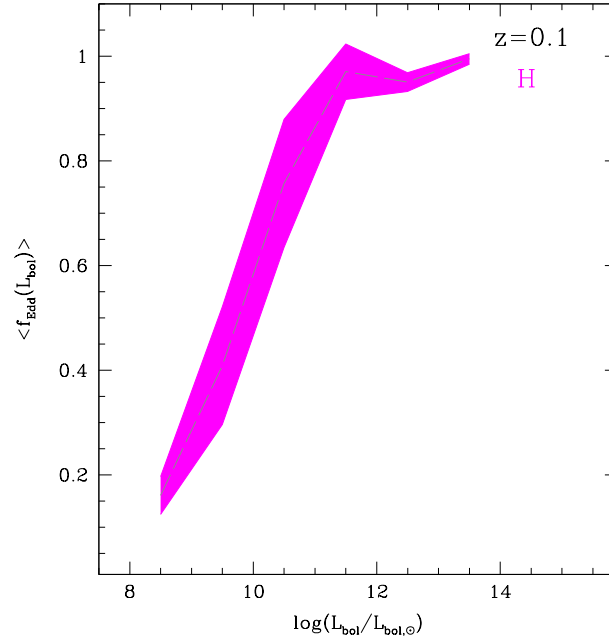


Figure 3.9: The mean Eddington ratio in function of the AGN luminosity, at $z = 0.1$, for the model H. The coloured area represents the $1\sigma_c$ uncertainties.

when considering the observational constraints on the Eddington factor of Seyfert galaxies, which constitute about 90% of the local AGN population. Woo & Urry (2002) analyze a sample of 234 AGN at $0.001 < z < 1$, composed, at $z \leq 0.1$ mainly by Seyfert galaxies. They find a large scatter (2 orders of magnitude) in the Eddington factor at both fixed luminosity and fixed BH mass. Woo & Urry (2002) do not find any trends of the Eddington factor with either luminosity, mass or redshift, which cannot be explained by selection effects.

It turns out that the S06 and B06 catalogues are largely composed by Seyfert galaxies that constitute respectively 94% and 88% of the total galaxy host populations. Only a small fraction of these local Seyfert galaxies have disturbed morphology, and thus did not experience any recent merging event. Indeed, only 4% of the sources in the S06 catalog are hosted in galaxies that show evidences of recent interactions. The AGN in the B06 catalogue are typically found at low galactic latitudes which hamper a systematic analysis of their host galaxy morphology. Yet, the similar galaxy composition of the two catalogues suggests that also B06 AGN preferentially populate quiescent environments. Based on this observational evidence, it may be suggested that galaxy mergers might not constitute the only trigger to AGN activity.

To decide whether this is indeed a viable hypothesis, it is worth reviewing

the observational evidences of local AGN samples. Bright, low-redshift quasars and ultra luminous infrared galaxies, that are generally regarded as hosting obscured AGN, are often found in merging systems (see, e.g. Sanders & Mirabel, 1996; Canalizo & Stockton, 2001; Capetti & Balmaverde, 2006, and references therein) which indicates a possible connection between mergers of gas-rich galaxy and AGN activity. On the contrary, as we have seen, fainter AGN typically reside in quiescent, non-interacting galaxies (e.g. Kauffmann et al., 2003; Grogin et al., 2005, and references therein). However, this alone does not guarantee that an alternative AGN triggering mechanism is at work, as this observational evidence can still fit into a merger-driven scenario. In fact, the brightest among these objects could be the relics of a previous bright quasar epoch in a spheroid-forming merger (see, e.g. Hopkins et al., 2006a, and references therein), while the fainter ones would consist of AGN hosted in “dead” elliptical galaxies fueled via accretion of hot spheroid gas and steady mass loss from stars (see, e.g. Ciotti & Ostriker, 2001; Sazonov et al., 2005; Croton et al., 2006), an accretion mode which cannot dominate the BH growth.

The merger-driven scenario, however, proved to be inadequate in accounting for the relatively high accretion rate AGN observed at low redshifts in undisturbed, late-type, star-forming galaxies with low mass ($\lesssim 10^7 M_\odot$) BHs (e.g. Kauffmann et al., 2003). Indeed alternative mechanisms, not included in our simple models, have been suggested to trigger the mass accretion in these objects. For instance, it has been proposed that a significant contribution to the faint AGN mass accretion could come from the material liberated by the tidal disruption of stars by the central BHs (Milosavljević et al., 2006), or by the mass of the stars captured by the BH disks and eventually dissolved (Miralda-Escudé & Kollmeier, 2005). Other studies have considered the stochastic accretion of molecular clouds in quiescent systems (see e.g. Hopkins & Hernquist, 2006; Croton et al., 2006). Moreover, it was suggested that also disk instability could trigger mass accretion, contributing to increase even more the number density of faint AGN (see e.g. Croton et al., 2006; Bower et al., 2006), or a better treatment of mergers between haloes with low mass ratio may also contribute to solve these problems (see e.g. Malbon et al., 2007; Croton et al., 2006). In the next chapter we will come back to these points with more details.

Finally, the redshift evolution predicted by semi-analytic schemes is slightly faster than the one of the analytic models, and matches observations out to $z \sim 2$. The high degree of clustering predicted by the VHM model does not derive from having placed the first seed BHs in correspondence of high- σ_c

overdensity peaks of the mass density field. The adopted threshold, $3.5\sigma_c$ at $z = 20$, in fact corresponds to having at least one seed massive BH in haloes with $M_{\text{halo}} \simeq 10^{11}M_{\odot}$ at $z = 0$, which host massive BHs with masses well below that sampled by the optical LF of quasars. Moreover, dynamical effects such as the gravitational rocket (Volonteri & Perna, 2005) can possibly eject BHs and thus lower the occupation fraction only in haloes with $M_{\text{halo}} < 10^{12}M_{\odot}$ that host BHs too faint to be included in the range probed by the optical LF. Placing seed BHs in correspondence of even higher peaks would certainly increase the biasing of the AGN without modifying their luminosity function at $z > 0.5$, provided that the major merger threshold is changed accordingly (VHM). In this case, however, it would be difficult to explain the presence of BHs in galaxies like the Milky Way or smaller, and, in general, AGN harboured in dwarf galaxies (Barth et al., 2005), which anyway are not sampled by the quasar LF at $z > 0.4$. The large values of bias in the semi-analytic models have a different explanation: it derives from the lack of a deterministic relation between the DM halo masses and the AGN luminosities at a given time. Indeed, a finite time is required to accrete a mass ΔM_{accr} to the central BH. During the accretion phase, the BH is smaller than predicted by the simple scaling relations with halo masses (i.e. $M_{\text{BH}} - \sigma_c$ or $M_{\text{BH}} - M_{\text{halo}}$). This means that, on average, the hosting halo of a quasar of a given luminosity is larger in the semi-analytic scheme than in the analytic models, the masses being the same only at the very end of the accretion episode. Consequently, the bias is enhanced in the semi-analytic model even if the LF looks similar.

CHAPTER 4

Hybrid simulations: dark matter + baryons + black holes



WE model the cosmological co-evolution of galaxies and their central BHs with an hybrid simulation developed on the outputs of the Millennium Simulation. This model, described in detail in Croton et al. (2006) and De Lucia & Blaizot (2007), introduces a radio mode feedback from AGN at the centre of X-ray emitting atmospheres in galaxy groups and clusters. We investigate how well such model can reproduce the physical properties of BHs, analyzing their scaling relations, fundamental plane and mass function, and comparing them with the most recent observational data available. Moreover, we extend the original model to follow the evolution of the BH mass accretion and its conversion into radiation, and compare the derived AGN bolometric luminosity function with the observed one. While we find for the most part a very good agreement between predicted and observed BH properties, the model underestimates the number density of luminous AGN at high redshifts, independently of the adopted Eddington factor and accretion efficiency. However, an agreement with the observations is possible within the framework of our model, provided it is assumed that the cold gas fraction accreted by BHs at high redshifts is larger than at low redshifts. The chapter is mainly based on “Modeling the cosmological co-evolution of supermassive black holes and galaxies: I. BH scaling relations and the AGN luminosity function”, Marulli et al. (2008).

In Chapter 2, we have demonstrated that simple analytic models in which AGN activity is only triggered by DM halo major mergers succeeded in quantitatively describing the observed evolution of the AGN number counts and luminosity at all but low redshifts, provided that some mechanism is advocated to inhibit accretion within massive haloes hosting bright AGN (Fig. 2.1). However, they fail in reproducing the observed AGN clustering at high redshifts (Fig. 2.2). As discussed in Chapter 3, slightly more sophisticated semi-analytic models in which the halo merger history and associated BHs are followed by Monte Carlo realizations of the merger

hierarchy, while the baryonic physics is neglected as well, can better reproduce the AGN clustering function at $z \gtrsim 1.5$ (Fig. 3.6). However, at low redshifts, the predicted number density of faint AGN is significantly below observations (Fig. 3.4), a clear indication that DM halo mergers cannot constitute the only trigger to accretion episodes in the local BH population, and that in order to properly describe the cosmological evolution of BHs and AGN, the main baryonic phenomena involving the gas contents of DM haloes cannot be neglected.

Hydrodynamic simulations which integrate both the equations of motions for the baryons and those for the DM, and *hybrid* simulations, which combine together an N-body treatment of the DM with semi-analytic modelling of the baryons are the main methods for studying the formation and evolution of galaxies in a cosmological scenario, while retaining the spatial information on the galaxy distribution. The fully numerical approach can treat the gas dynamics self-consistently. However, at the present time, these simulations are rather expensive in CPU time and this limits the resolution mass and the size of the simulated box, the latter resulting in poor sampling of rare objects. Viceversa, for the same CPU time, hybrid methods allow one to explore a wider set of physical assumptions, though in this case the gas physics can only be modelled through several simplifying hypothesis, such as the one that the gas starts cooling from a spherical distribution at the virial temperature of the halo or the dynamical friction formula to compute merging rates.

In this chapter we will study the cosmological co-evolution of galaxies and their central BHs using an hybrid simulation developed on the outputs of the Millennium Simulation and described in detail in Croton et al. (2006) and De Lucia & Blaizot (2007). In this scenario, *radio mode* feedback from AGN at the centre of galaxy groups and clusters is invoked to prevent significant gas cooling in large haloes, thus limiting the mass of the central galaxies and preventing them from forming stars at late times when their mass and morphology can still change through mergers. Thanks to this mechanism, Croton et al. (2006) demonstrated that such a model can simultaneously explain the low observed mass drop-out rate in cooling flows, the exponential cut-off in the bright-end of the galaxy luminosity function, and the bulge-dominated morphologies and stellar ages of the most massive galaxies in clusters.

Here we are interested in investigating how well this model can also reproduce the statistical properties of BHs and AGN. To do that, we extend the original model by adding new semi-analytical prescriptions to describe the BH mass accretion rate in the accretion episodes triggered by galaxy mergers,

which fuel the *quasar mode*, and their conversion into radiation. We then analyze the scaling relations, the fundamental plane and the MF of BHs, and compare them with the most recent observational data available. Finally, we compare the predicted AGN bolometric LF with the observed one, and propose some modifications to the original semi-analytic assumptions to better fit the data.

The chapter is organized as follows. In Section 4.1, we will briefly describe the main aspects of our hybrid simulation and illustrate the new equation introduced to describe the BH mass accretion in the *quasar mode* in more detail. In Section 4.2, we will compare the model predictions with the best observational data available for the BH and AGN populations. Finally, in Section 4.3 we will summarize our conclusions.

SECTION 4.1

Model description

Our hybrid simulation for the co-evolution of DM haloes, galaxies and their central BHs consists of three ingredients, that we describe separately in this section: a numerical simulation to obtain the merger history of the DM haloes, a set of analytic prescriptions to trace the evolution of galaxies within their host haloes and a set of recipes to follow the BH accretion history and the AGN phenomenon.

4.1.1 Numerical simulation

In this work we use the outputs of the Millennium Simulation, which followed the dynamical evolution of $2160^3 \simeq 10^{10}$ DM particles with mass $8.6 \times 10^8 h^{-1} M_\odot$ in a periodic box of $500 h^{-1} \text{Mpc}$ on a side, in a ΛCDM “concordance” cosmological framework (Springel et al., 2005a). The computational box is large enough to include rare objects such as quasars or rich galaxy clusters, the largest of which contain about 3 million simulation particles at $z=0$. At the same time, the mass resolution is high enough to resolve the DM halo of $0.1 L_*$ galaxies with ~ 100 particles. The short-range gravitational force law is softened on the comoving scale $5 h^{-1} \text{kpc}$ (Plummer-equivalent) which may be taken as the spatial resolution limit of the calculation. The cosmological parameters (the matter density parameter $\Omega_m = 0.25$, the baryon density parameter $\Omega_b = 0.045$, the Hubble parameter $h = H_0/100 \text{ km s}^{-1} \text{ Mpc}^{-1} = 0.73$, the cosmological constant contribution to the density parameter $\Omega_\Lambda = 0.75$,

the primordial spectral index $n = 1$, and the power spectrum normalization $\sigma_8 = 0.9$), are consistent with determinations from the combined analysis of the 2-degree Field Galaxy Redshift Survey (2dFGRS) (Colless et al., 2001) and first-year WMAP data (Spergel et al., 2003), as shown by Sánchez et al. (2006). We recall that the more recent analysis of the WMAP 3-year data (Spergel et al., 2007) suggests slightly different values (in particular smaller values for Ω_m , σ_8 and n). However, as demonstrated by Wang et al. (2007), due to the current modelling uncertainties, it is not possible to distinguish the two WMAP cosmologies on the basis of the observed galaxy properties, since the variations induced by acceptable modifications of the free parameters of the galaxy formation model are at least as large as those produced by the variation in the cosmological parameters.

The Millennium Simulation was carried out with a special version of the GADGET-2 code (Springel, 2005c), optimized for very low memory consumption, at the Computing Centre of the Max-Planck Society in Garching, Germany. We make use of hierarchical merging trees extracted from this simulation which encode the full formation history of DM haloes and subhaloes, previously identified with, respectively, a friends-of-friends (FOF) group-finder and an extended version of the SUBFIND algorithm (Springel et al., 2001b). These trees constitute the backbone of our hybrid simulation, which is implemented during the post-processing phase: this allows us to simulate the wide range of baryonic processes occurring during the formation and evolution of galaxies and their central BHs.

Fig. 4.1 shows the DM density field on various scales at $z = 0$ in the Millennium Simulation. The panel at the bottom of the figure reveals a tight network of cold DM clusters and filaments. On larger scales, there is little discernible structure and the distribution appears homogeneous and isotropic. Subsequent images zoom in by factors of four onto the region surrounding one of the many rich galaxy clusters. The final image reveals several hundred DM substructures, resolved as independent, gravitationally bound objects orbiting within the cluster halo.

4.1.2 Galaxy evolution

We use the galaxy formation model of Croton et al. (2006) as updated by De Lucia & Blaizot (2007). Although not in agreement with some properties of the red and blue galaxy populations (see, e.g., Weinmann et al., 2006; Kitzbichler & White, 2007), this model is able to reproduce the overall observed properties of galaxies, i.e. the relations between stellar mass, gas mass and metallicity, the luminosity, colour and morphology distributions

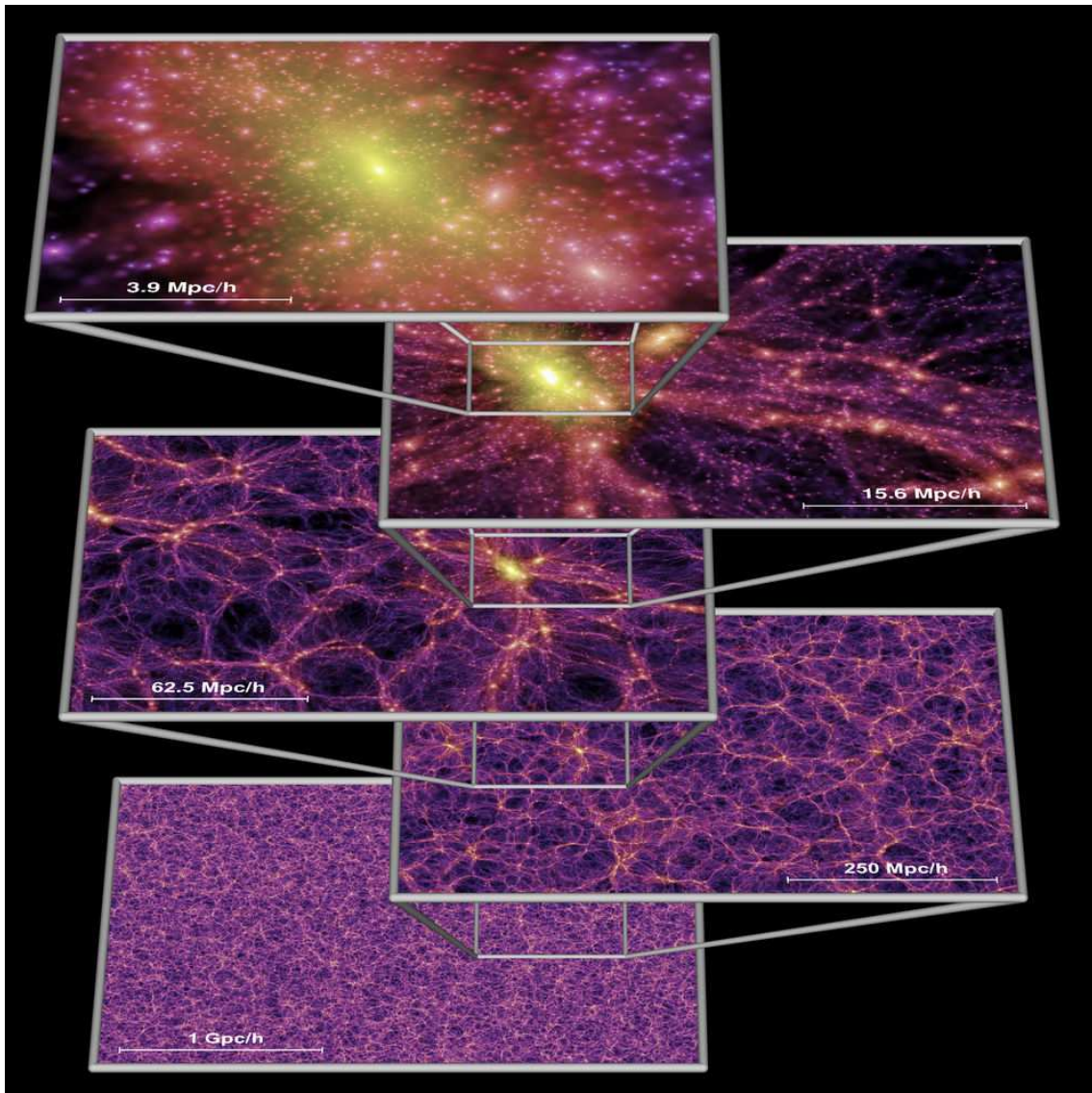


Figure 4.1: The DM density field on various scales predicted by the Millennium Simulation. Each individual image shows the projected DM density field in a slab of thickness $15h^{-1}Mpc$ (sliced from the periodic simulation volume at an angle chosen to avoid replicating structures in the lower two images), colour-coded by density and local DM velocity dispersion. The zoom sequence displays consecutive enlargements by factors of four, centred on one of the many galaxy cluster haloes present in the simulation (from Springel et al. (2005a)).

(Croton et al., 2006; De Lucia et al., 2006), the two-point galaxy correlation functions (Springel et al., 2005a), and the global galaxy LF and MF at high redshift (Kitzbichler & White, 2007). We refer to the original papers for a full description of the numerical implementation of the model. In the following, we briefly recall the treatment of the physical processes involved in the galaxy evolution, and describe the prescriptions for the BH growth and the AGN evolution.

Following the standard paradigm set out by White & Frenk (1991) and adapted to high-resolution N-body simulations by Springel et al. (2001b), we assume that as a DM halo collapses, a fraction $f_b = 0.17$ of its mass is in the form of baryons and collapses with it, consistent with the first-year WMAP result (Spergel et al., 2003). Initially, these baryons are in the form of a diffuse gas with primordial composition, but later they include gas in several phases as well as stars and heavy elements. Conventionally, with the simplifying assumption of an ideal gas which cools isobarically, the cooling time of the gas is computed as the ratio of its specific thermal energy to the cooling rate per unit volume,

$$t_{\text{cool}} = \frac{3}{2} \frac{\bar{\mu} m_p k T}{\rho_g(r) \Lambda(T, Z)}, \quad (4.1)$$

where $\bar{\mu} m_p$ is the mean particle mass, k is the Boltzmann constant, $\rho_g(r)$ is the hot gas density, and $\Lambda(T, Z)$ is the cooling function (Sutherland & Dopita, 1993; Maio et al., 2007). Eq. (4.1) is valid at temperature higher than $\sim 10^4$ K, where hydrogen and helium remain ionized and the number of particles remains approximately constant.

We assume the post-shock temperature of the infalling gas to be the virial temperature of the halo, $T = 35.9 (V_{\text{vir}}/\text{km s}^{-1})^2$ K, where V_{vir} is the halo virial velocity. Moreover, we assume that the hot gas within a static atmosphere has a simple “isothermal” distribution,

$$\rho_g(r) = \frac{m_{\text{hot}}}{4\pi R_{\text{vir}} r^2}, \quad (4.2)$$

where m_{hot} is the total hot gas mass associated with the halo and is assumed to extend to its virial radius R_{vir} .

In order to estimate an instantaneous cooling rate onto the central object of a halo, given its current hot gas content, we define the cooling radius, r_{cool} , as the radius at which the local cooling time (assuming the structure of Eq. 4.2) is equal to the halo dynamical time, $R_{\text{vir}}/V_{\text{vir}} = 0.1 H(z)^{-1}$ (Springel et al., 2001a; De Lucia et al., 2004; Croton et al., 2006); here $H(z)$ represents the redshift evolution of the Hubble constant. The cooling rate can then be

determined through the following continuity equation,

$$\dot{m}_{\text{cool}} = 4\pi\rho_g(r_{\text{cool}})r_{\text{cool}}^2\dot{r}_{\text{cool}}. \quad (4.3)$$

More details about our cooling prescriptions can be found in Croton et al. (2006).

The photo-ionization heating of the intergalactic medium suppresses the concentration of baryons in shallow potentials (Efstathiou, 1992), and can be responsible of the inefficient accretion and cooling in low-mass haloes. Following Gnedin (2000), we model the effect of such photo-ionization heating by defining a characteristic mass scale, M_F , below which the gas fraction f_b is reduced relatively to the universal value:

$$f_b^{\text{halo}}(z, M_{\text{vir}}) = \frac{f_b^{\text{cosmic}}}{[1 + 0.26M_F(z)/M_{\text{vir}}]^3}. \quad (4.4)$$

We adopt the $M_F(z)$ parameterization of Kravtsov et al. (2004), which results in a filtering mass M_F of $4 \times 10^9 M_\odot$ at the reionization epoch, and $3 \times 10^{10} M_\odot$ by the present day (but see Hoeft et al., 2006).

In the semi-analytic framework we use in this work, the star formation is assumed to occur at a rate given by:

$$\dot{m}_* = \alpha_{\text{SF}}(m_{\text{cold}} - m_{\text{crit}})/t_{\text{dyn,disk}}, \quad (4.5)$$

where m_{cold} is the cold gas mass, $t_{\text{dyn,disk}}$ is the dynamical time of the galaxy, defined as the ratio between the disk radius and the virial velocity, m_{crit} corresponds to a critical value for the gas surface density (Kauffmann, 1996; Kennicutt, 1998; Mo et al., 1998), and $\alpha_{\text{SF}} = 0.03$ controls the efficiency of the transformation of cold gas into stars. Massive stars explode as supernovae shortly after star formation events and are assumed to reheat a gas mass proportional to the mass of stars:

$$\Delta m_{\text{reheated}} = \varepsilon_{\text{disk}}\Delta m_*, \quad (4.6)$$

where we set the free parameter $\varepsilon_{\text{disk}} = 3.5$ based on the observational data. The energy released by an event which forms a mass Δm_* in stars is assumed to be:

$$\Delta E_{\text{SN}} = 0.5\varepsilon_{\text{halo}}\Delta m_*V_{\text{SN}}^2, \quad (4.7)$$

where $0.5V_{\text{SN}}^2$ is the mean supernova energy injected per unit mass of newly formed stars, and $\varepsilon_{\text{halo}}$ represents the efficiency with which this energy is able to convert cold interstellar medium into hot, diffuse halo gas. The amount of gas that leaves the DM halo in a “super-wind” is determined by computing

whether excess SN energy is available to drive the flow after reheating of material to the halo virial temperature.

We model the disk instabilities using the analytic stability criterion of Mo et al. (1998); the stellar disk of a galaxy becomes unstable when the following inequality is met:

$$\frac{V_c}{(Gm_{\text{disk}}/r_{\text{disk}})^{1/2}} \leq 1. \quad (4.8)$$

At each time-step we evaluate the left-hand side of Eq. (4.8) for each galaxy, and if it is smaller than unity we transfer enough stellar mass from disk to bulge (at fixed r_D) to restore stability.

In the Millennium Run, substructures are followed down to masses of $1.7 \times 10^{10} h^{-1} M_\odot$, so that we can properly follow the motion of galaxies inside their hosting DM haloes until tidal truncation and stripping disrupt their subhaloes at this resolution limit. At this point, we estimate a survival time for the galaxies using their current orbit and the dynamical friction formula of Binney & Tremaine (1987) multiplied by a factor of 2, as in De Lucia & Blaizot (2007). After this time, the galaxy is assumed to merge onto the central galaxy of its own halo. Galaxy mergers induce starburst which we describe using the “collisional starburst” prescription introduced by Somerville et al. (2001). In this model, a fraction e_{burst} of the combined cold gas from the two merging galaxies is turned into stars as follows:

$$e_{\text{burst}} = \beta_{\text{burst}} (m_{\text{sat}}/m_{\text{central}})^{\alpha_{\text{burst}}}, \quad (4.9)$$

where the two parameters are taken as $\alpha_{\text{burst}} = 0.7$ and $\beta_{\text{burst}} = 0.56$, appropriate for merger mass ratios ranging from 1:10 to 1:1 (Cox, 2004).

4.1.3 BH mass accretion and AGN

The “radio mode”

When a static hot halo has formed around a galaxy, we assume that a fraction of the hot gas continuously accretes onto the central BH, causing a low-energy “radio” activity in the galaxy centre. Following Croton et al. (2006), the BH mass accretion rate during these phases is postulated to scale as follows:

$$\dot{M}_{\text{BH,R}} = \kappa_{\text{AGN}} \left(\frac{M_{\text{BH}}}{10^8 M_\odot} \right) \left(\frac{f_{\text{hot}}}{0.1} \right) \left(\frac{V_{\text{vir}}}{200 \text{ km s}^{-1}} \right)^3, \quad (4.10)$$

where M_{BH} is the BH mass, f_{hot} is the fraction of the total halo mass in the form of hot gas, and κ_{AGN} is a free parameter set equal to $7.5 \times 10^{-6} M_\odot \text{ yr}^{-1}$ in order to reproduce the turnover at the bright end of the galaxy LF. Since f_{hot} is approximately constant for $V_{\text{vir}} \gtrsim 150 \text{ km s}^{-1}$, the dependence of $\dot{m}_{\text{BH,R}}$ on this

quantity has a little effect. Note that the accretion rate given by Eq. (4.10) is typically orders-of-magnitude below the Eddington limit. In fact, the total mass growth of BHs in the radio relative to the quasar mode discussed below is negligible.

It is also assumed that the *radio mode* feedback injects energy efficiently into the surrounding medium, which can reduce or even stop the cooling flow in the halo centres. The mechanical heating generated by this kind of BH mass accretion and described as $L_{\text{BH}} = \epsilon \dot{M}_{\text{BH}} c^2$, where $\epsilon = 0.1$ is the *accretion efficiency* and c is the speed of light, induces a modified infall rate of the following kind:

$$\dot{m}'_{\text{cool}} = \dot{m}_{\text{cool}} - \frac{L_{\text{BH}}}{0.5V_{\text{vir}}^2}. \quad (4.11)$$

For consistency we never allow \dot{m}'_{cool} to fall below zero. In this scenario, the effectiveness of radio AGN in suppressing cooling flows is greatest at late times and for large values of the BH mass, which is required to successfully reproduce the luminosities, colours and clustering of low-redshift bright galaxies.

The “quasar mode”

In our model BHs accrete mass after a galaxy merger both through coalescence with another BH and by accreting cold gas, the latter being the dominant accretion mechanism. For simplicity, the BH coalescence is modelled as a direct sum of the progenitor masses, thus ignoring gravitational wave losses. Following Kauffmann & Haehnelt (2000), we assume that the gas mass accreted during a merger is proportional to the total cold gas mass present, but with an efficiency which is lower for smaller mass systems and for unequal mergers:

$$\Delta M_{\text{BH,Q}} = \frac{f'_{\text{BH}} m_{\text{cold}}}{1 + (280 \text{ km s}^{-1} / V_{\text{vir}})^2}, \quad (4.12)$$

where

$$f'_{\text{BH}} = f_{\text{BH}} (m_{\text{sat}} / m_{\text{central}}), \quad (4.13)$$

and $f_{\text{BH}} \approx 0.03$ is chosen to reproduce the observed local $M_{\text{BH}} - M_{\text{bulge}}$ relation. Thus, any merger-induced perturbation to the gas disk (which might come from a bar instability or a merger-induced starburst) can in principle drive gas onto the central BH. However, the fractional contribution of minor mergers is typically quite small, so that accretion driven by major mergers is the dominant mode of BH growth in our scenario. This kind of accretion, which we call *quasar mode*, is also closely associated with starbursts, which occur

concurrently. We do not model feedback from the quasar activity in the current model, but it can be approximately represented by an enhanced effective feedback efficiency for the supernovae associated with the intense starburst.

AGN luminosity

The output of the model summarized hitherto, called *DeLucia2006a catalogue* (De Lucia & Blaizot, 2007), is publicly available at <http://www.mpa-garching.mpg.de/millennium> (Lemson & Virgo Consortium, 2006). In this default model, for simplicity, the BH mass accretion triggered by each merger is implemented as an instantaneous event and the BH seed masses are set equal to zero.

In order to study the evolution of AGN inside this cosmological framework, we improve the original model of De Lucia & Blaizot (2007) by adding new semi-analytical prescriptions to describe the BH mass accretion rate during each merger event in the *quasar mode*, and its conversion into radiation. In this implementation, BHs do not accrete mass instantaneously. Instead, the accretion is coupled to the light curve model adopted. If a galaxy undergoes a merger while the central BH is still accreting mass from a previous merger, the cold gas still to be accreted is added to the new gas reservoir, and the accretion re-starts under the new physical conditions. In Sect. 4.2.1 we show that the BH scaling relations are weakly affected by this change.

To parameterize the bolometric luminosity emitted by accretion onto BHs, as a function of the *accretion efficiency*, ϵ , and the *Eddington factor*, we use the same definitions of Sect. 3.1 (Eq.(3.2)). For simplicity, we do not follow in this model the evolution of the BH spins (see, e.g. Volonteri et al., 2007, and references therein) and we take a constant mean value for the accretion efficiency of $\epsilon = \langle \epsilon \rangle = 0.1$ at all redshifts.

For f_{Edd} , which determines the lightcurves associated with individual quasar events, we consider instead three different prescriptions:

- *I*: $f_{\text{Edd}} = 1$, the simplest possible assumption. Here the quasar is either “on” at its maximum Eddington luminosity, or “off”.
- *II*: f_{Edd} is assumed to decrease at low z as suggested by Cattaneo & Bernardi (2003) and Shankar et al. (2004) to match the BH MF derived from a deconvolution of the AGN LF and the local BH MF. Here, we adopt the fit derived by Shankar et al. (2004), Eq.(1.3), with $f_{\text{Edd},0} = 0.3$.

- *III*: as mentioned in Sect. 3.2.3, based on the analysis of self-consistent hydrodynamical simulations of galaxy mergers, Hopkins et al. (2005) noticed that the light curves of active BHs are complex, showing periods of rapid accretion after “first passage” of the merging galaxies, followed by a long-lasting quiescent phase, then a transition to a highly luminous, peaked quasar phase, finally a fading away when quasar feedback expels gas from the remnant’s centre in a self-regulated mechanism after the BH reaches a critical mass. In spite of this complexity, as a first order approximation, the typical evolution of an active BH can be simply described as a two-stage process of a rapid, Eddington-limited growth up to a peak BH mass, preceded and followed by a much longer quiescent phase with lower Eddington ratios. In this latter phase, the average time spent by AGN per logarithmic luminosity interval can be approximated with the Eq.(3.3). Differently from our semi-analytic model H (introduced in Sect. 3.2.3), here we interpret the Hopkins model as describing primarily the decline phase of the quasar activity, after the BH has grown at the Eddington rate to a peak mass $M_{\text{BH,peak}} = M_{\text{BH}}(t_{\text{in}}) + \mathcal{F} \cdot \Delta M_{\text{BH,Q}} \cdot (1 - \epsilon)$, where $M_{\text{BH}}(t_{\text{in}})$ is the initial BH mass and $\Delta M_{\text{BH,Q}}$ is the fraction of cold gas mass accreted. Here \mathcal{F} is an additional free parameter, in the range $0 \leq \mathcal{F} \leq 1$. For $\mathcal{F} = 1$ the BH emits at the Eddington rate. In the opposite limit ($\mathcal{F} = 0$) the AGN reaches instantaneously a peak luminosity, and the whole light curve is described by Eq. (3.3). We found that $\mathcal{F} = 0.7$ is the value that best matches the AGN LF. We note that this interpretation of the Hopkins model is plausible but not unique, as part of the time described by Eq. (3.3) could also be associated with the rising part of the lightcurve.

From Eq. (3.3) and with the following definition

$$\tilde{f}_{\text{Edd}}(t) := \frac{L_{\text{bol}}(t)}{L_{\text{peak}}} = f_{\text{Edd}}(t) \frac{L_{\text{Edd}}(t)}{L_{\text{peak}}}, \quad (4.14)$$

we can derive:

$$\frac{d\tilde{f}_{\text{Edd}}(t)}{dt} = -\frac{\tilde{f}_{\text{Edd}}^{1-\alpha}(t)}{\alpha t_9} \left(\frac{L_{\text{peak}}}{10^9 L_{\odot}} \right)^{-\alpha}, \quad (4.15)$$

$$\implies \tilde{f}_{\text{Edd}}(t) = \left[\tilde{f}_{\text{Edd},0}^{\alpha} + \left(\frac{L_{\text{peak}}}{10^9 L_{\odot}} \right)^{-\alpha} \frac{t}{t_9} \right]^{1/\alpha}. \quad (4.16)$$

Here we neglected the absolute value of α present in Eq. (3.3), for the purpose of having $\tilde{f}_{\text{Edd}}(t)$ a decreasing function of time. Finally, from Eqs. (3.4), (4.14) and (4.16), we have:

$$M_{\text{BH}}(t) = M_{\text{BH,peak}} + \frac{A}{BC} \left[(1 + Ct)^B - 1 \right], \quad (4.17)$$

Parameter	Description	Value
f_b	Cosmic baryon fraction	0.17
f_{BH}	Merger cold gas BH accretion fraction	0.03
k_{AGN}	Quiescent hot gas BH accretion rate ($M_\odot \text{yr}^{-1}$)	7.5×10^{-6}
α_{SF}	Star formation efficiency	0.03
ϵ_{disk}	SN feedback disk reheating efficiency	3.5
ϵ_{halo}	SN feedback halo ejection efficiency	0.35

Table 4.1: A summary of our main model parameters, as described in the text.

where $A = \frac{1-\epsilon}{\epsilon} \frac{M_{\text{BH,peak}}}{t_{\text{Edd}}}$, $B = \frac{1}{\alpha} + 1$, $C = \left(\frac{L_{\text{peak}}}{10^9 L_\odot}\right)^{-\alpha} \frac{1}{t_g}$. To derive Eq. (4.17) we set $\tilde{f}_{\text{Edd},0} = 1$ for continuity. We also impose $f_{\text{Edd}} = 10^{-3}$ as lower limit for the Eddington factor.

Figure 4.2 shows the evolution of $f_{\text{Edd}}(t)$ (top panel), $M_{\text{BH}}(t)$ (central panel) and $L_{\text{bol}}(t)$ (bottom panel) for an illustrative case of a BH of $M_{\text{BH}} = 10^7 M_\odot$ accreting a mass $M_{\text{accr}} = 5 \times 10^8 M_\odot$, starting at $z = 3$, in the three prescriptions considered. The three green curves refer to lightcurve model III, in which we set $\mathcal{F} = 0.5$ (short dashed), $= 0.7$ (dot-long dashed) and $= 0.9$ (short dashed-long dashed).

Due to the present uncertainties concerning the origin of the BH seeds and their mass distribution, we assume $M_{\text{BH,seed}} = 10^3 M_\odot$ for all seed BHs, irrespective of their halo host properties and their origin. Our results are robust with respect to this hypothesis since, as we have verified, they are basically unaffected by varying $M_{\text{BH,seed}}$ in the range $[10^2 - 10^5] M_\odot$ at $z \lesssim 3$. More significant differences occur at higher redshifts, which we will investigate in detail in future work.

The main parameters of our model, listed in Table 4.1, are the same as the ones used by Croton et al. (2006), with the exception of, as in De Lucia & Blaizot (2007), the values for the quiescent hot gas BH accretion rate, k_{AGN} (defined in Section 4.1.3) and the star formation efficiency α_{SF} of Eq. (4.5).

SECTION 4.2

Model vs. Observations

4.2.1 BH scaling relations

In this section we compare the most recently observed BH scaling relations at $z = 0$ with the predictions of the original model of De Lucia & Blaizot (2007),

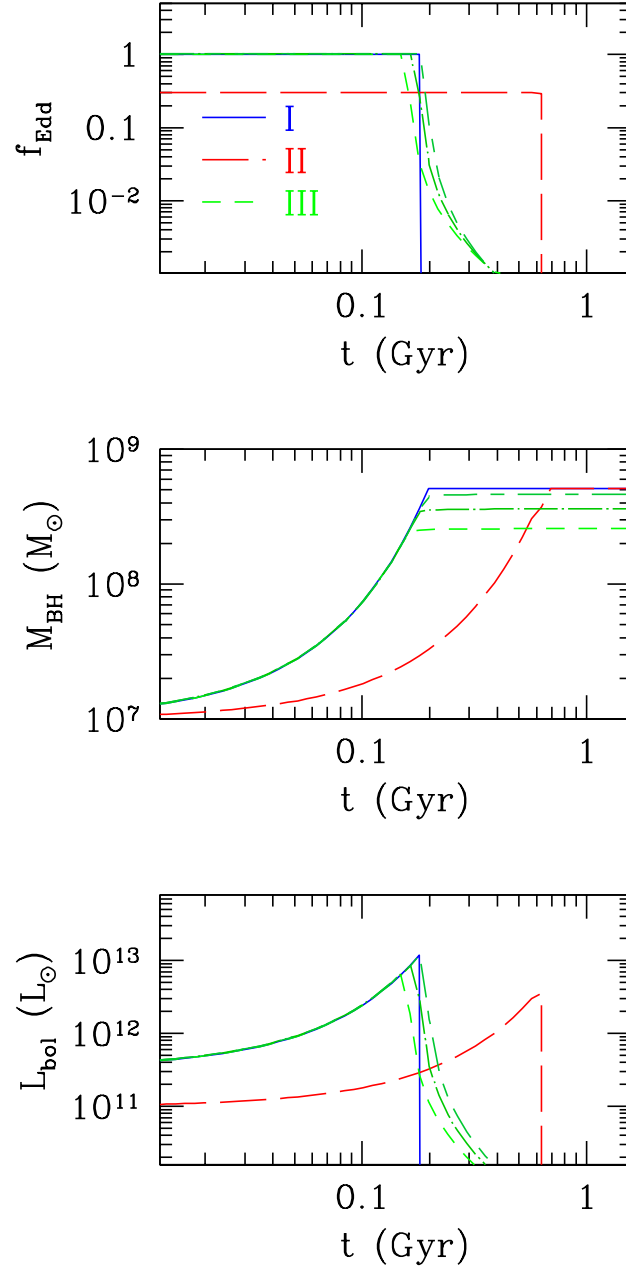


Figure 4.2: The time evolution of f_{Edd} (top panel), M_{BH} (central panel) and L_{bol} (bottom panel) for our three lightcurve models (*I* (blue solid lines), *II* (red short-dashed lines) and *III* (green lines)), for an illustrative case of a BH of mass $M_{\text{BH}} = 10^7 M_{\odot}$ accreting a mass $\Delta M_{\text{BH,Q}} = 5 \times 10^8 M_{\odot}$, starting at $z = 3$. The three green curves, showing our model *III*, have been obtained by setting $\mathcal{F} = 0.5$ (short dashed), 0.7 (dotted-long dashed) and 0.9 (short dashed-long dashed).

Relation	Normalization (α)	Slope (β)	Scatter	Scatter _{corrected}
$\log(M_{\text{BH}}) - M_{\text{K}}$	-4.37(0.24)	-0.52(0.01)	0.68	0.53
$\log(M_{\text{BH}}) - M_{\text{B}}$	-0.61(0.17)	-0.43(0.01)	0.62	0.53
$\log(M_{\text{BH}}) - \log(\sigma_{\text{c}})$	-0.26(0.16)	3.82(0.08)	0.42	0.28
$\log(M_{\text{BH}}) - \log(M_{\text{bulge}})$	-2.39(0.19)	0.96(0.02)	0.58	0.50
$\log(M_{\text{BH}}) - \log(V_{\text{c}})$	-1.61(0.18)	4.05(0.09)	0.45	
$\log(M_{\text{BH}}) - \log(M_{\text{DM}})$	-8.61(0.42)	1.35(0.04)	0.50	

Table 4.2: Parameters of the linear fits to the scaling relations shown in Figure 4.3. A correlation of the form $y = \alpha + \beta \cdot x$ has been assumed for all relations. The uncertainties in the normalizations and in the slopes are shown in parentheses. For details about the computation of the Scatter and the Scatter_{corrected} see Sect. 4.2.1.

Relation	α	β	γ	Scatter
$\log(M_{\text{BH}}) - M_{\text{K}}$	17.29(0.10)	1.25(0.01)	0.04(0.01)	0.51
$\log(M_{\text{BH}}) - M_{\text{B}}$	9.81(0.03)	0.63(0.01)	0.03(0.01)	0.47
$\log(M_{\text{BH}}) - \log(M_{\text{bulge}})$	14.16(0.07)	-2.21(0.01)	0.15(0.01)	0.44

Table 4.3: Parameters of the fits to the scaling relations shown in Figure 4.4. A correlation of the form $y = \alpha + \beta \cdot x + \gamma \cdot x^2$ has been assumed for all three relations. The uncertainties in the parameters are shown in parentheses. For details about the computation of the Scatter see Sect. 4.2.1.

i.e. the predictions we obtain when assuming instantaneous mass accretion. We explore the effect of specifying the mass accretion rate at the end of this section.

One-parameter relations

In Figure 4.3, we show the correlation between the masses of the model BHs with six properties of their hosts, the K- and B-band bulge magnitude (M_{B} and M_{K}), the bulge mass and velocity dispersion (M_{bulge} and σ_{c}), the circular velocity of the galaxy and the virial mass of the DM halo (V_{c} and M_{DM}). The blue dots represent the outputs of the model, while grey and yellow shaded areas show linear best fits to the model predictions and to the observational datasets, respectively.

The dots in the plot refer to the population of BHs hosted in the central galaxies of FOF groups, or subhaloes. We do not include those in satellite galaxies since in this case the host properties cannot be determined accurately. The data we have considered are: the $M_{\text{BH}} - M_{\text{B}}$ and $M_{\text{BH}} - M_{\text{K}}$ relations of Marconi & Hunt (2003) (top panels) the $M_{\text{BH}} - \sigma_{\text{c}}$ relation of Ferrarese & Ford (2005) (central left) the $M_{\text{BH}} - M_{\text{bulge}}$ relation of Häring

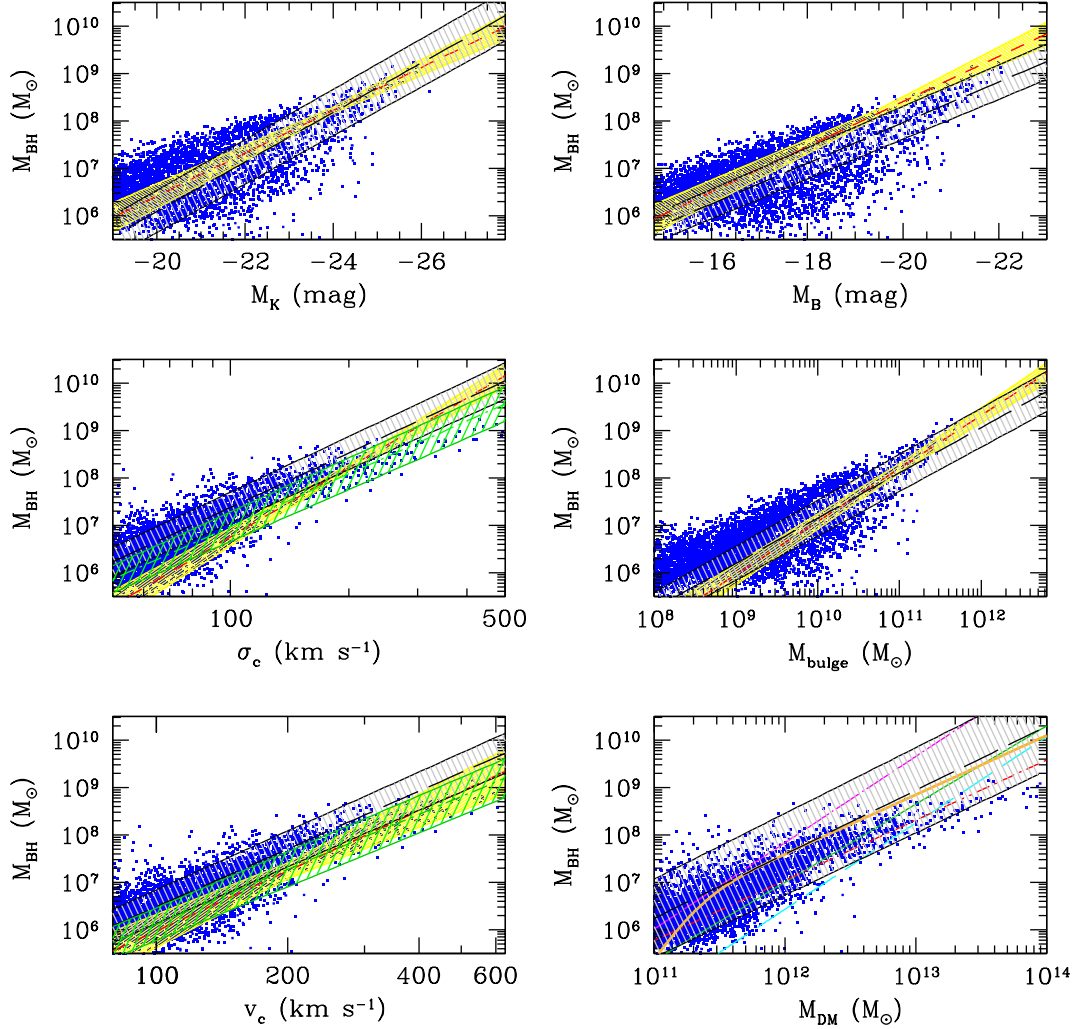


Figure 4.3: Starting from the upper left panel down to the bottom right one, scaling relations between the masses of the central BHs in the simulated galaxies with six different properties of their hosts: the K- and B-band bulge magnitude (top left and right panels, respectively), the bulge velocity dispersion and mass (central left and right panels, respectively), the circular velocity of the galaxy (bottom left panel) and the virial mass of the DM halo (bottom right panel). Blue dots represent the outputs of the *DeLucia2006a catalogue*, grey and yellow shaded areas show the best fit to the model predictions and to the observational datasets, respectively. Starting from the upper left panel down to the lower right, the yellow shaded areas refer to the best-fit relations obtained by Marconi & Hunt (2003) (the upper two panels of the plot), Ferrarese & Ford (2005), Häring & Rix (2004), Baes et al. (2003) and, in the lower-right panel, the curves show the Eqs. 4 (cyan), 6 (green) and 7 (magenta) of Ferrarese (2002), the results of Baes et al. (2003) (red) and of Shankar et al. (2006) (orange).

& Rix (2004) (central right) and the $M_{\text{BH}} - V_c$ relation of Baes et al. (2003) (bottom left). No direct observational estimate is available for the $M_{\text{BH}} - M_{\text{DM}}$ relation shown in the bottom right panel. The curves shown in this panel have been derived using different assumptions for the $M_{\text{DM}} - V_c$ relation. In particular, the cyan, green and magenta lines correspond to Eqs. (4), (6) and (7) of Ferrarese (2002), while the red and orange curves are taken from Baes et al. (2003) and Shankar et al. (2006).

Model predictions for V_c and σ_c have been obtained by adopting two different assumptions: i) $V_c = V_{\text{max}}$, where V_{max} is the maximum rotational velocity of the subhalo hosting the galaxy at its centre, and ii) $V_c = 1.8 V_{\text{vir}}$ as derived by Seljak (2002). As in Sect. 3.2, the bulge velocity dispersion σ_c is derived from the $V_c - \sigma_c$ relation of Baes et al. (2003). In the bottom panels, the grey areas correspond to a circular velocity obtained through hypothesis i) while the green ones, in better agreement with the data, assume hypothesis ii).

The linear fit to the model data has been obtained using the bisector modification to the ordinary least squares minimization approach, proposed by Akritas & Bershady (1996), for which the best-fit results correspond to the bisection of those obtained from minimizations in the vertical and horizontal directions. The estimator is robust and has the advantage of taking into account the possible intrinsic scatter in the relation. The values of the best fit slope and the normalization are listed in Table 4.2 along with the scatter around the best fitting line. The uncertainties of the best fit parameters, also reported in the table, have been obtained by imposing $\chi_{\text{d.o.f.}}^2 = 1$.

As can be seen in Figure 4.3, the best fits to the model agree well with that to the data, within the scatter. We note that, in all relations plotted, the scatter in the model is larger than that of the real data and also larger than the internal scatter observed in similar relations obtained from the recent hydrodynamical simulations of galaxy mergers (see e.g. Hopkins et al., 2007a). However, we notice that a large fraction of our model BHs are found in low-mass systems for which the scatter in the scaling relation is large. On the contrary, in the real datasets (and hydro-simulations) the majority of BHs belong to massive galaxies for which, according to our model, the scatter in the scaling relation is significantly smaller. To investigate whether the difference in the intrinsic scatter is real or is induced by a different sampling of the BH population, for each BH scaling relation we have discretized the range of the observed host galaxy properties in finite bins and generated 500 sub-samples by randomly extracting $N_{\text{obs}}(\Delta_X)$ model BHs from the parent catalogue, where $N_{\text{obs}}(\Delta_X)$ is the number of BHs in the real dataset in each bin Δ_X . We have

repeated the same fitting procedure in the 500 sub-samples and found that the scatter is significantly reduced in this exercise, as indicated in the last column of Table 4.2, that lists the average scatter in the sub-catalogues. Therefore, the mismatch in the scatter results from sampling different BH populations: small objects in the model, massive objects in the observations. Moreover, for the $M_{\text{BH}} - \sigma_c$ relation the scatter is very close to 0.21, which is the value measured by Hopkins et al. (2007a) both in the observed and simulated data.

Non-linear fits

The agreement between model and data is satisfactory. However, we need to keep in mind that the model predictions for V_c and σ_c and the observed relation between $\log(M_{\text{BH}})$ and $\log(M_{\text{DM}})$ have been obtained assuming further theoretical hypotheses. Consequently, the more constraining and reliable relations are the ones between the BH masses and the bulge magnitudes and masses. Focusing on these relations and thanks to the huge number of model BHs, we have been able to investigate whether a non-linear fit provides a better match to the data. We find that the best fit is a quadratic function, $y = \alpha + \beta \cdot x + \gamma \cdot x^2$. Figure 4.4 shows this fit (heavy green lines), together with the medians, the first and third quartiles (black points with error bars) of the model output, computed in a discrete number of bins. The internal scatter is significantly smaller than in the linear fit case. The values of the best fit parameters are reported in Table 4.3. This kind of trend, i.e. a higher median BH-to-bulge mass ratio with a large internal scatter for low massive and faint bulges, is common to almost all previous semi-analytic studies of BH growth in galaxy formation (see e.g. Cattaneo et al., 1999).

While we predict, on average, too low BH masses for a fixed M_B with respect to the observations (still consistent within the errors) the model predictions are in very good agreement with the data for the $\log(M_{\text{BH}}) - M_K$ and $\log(M_{\text{BH}}) - \log(M_{\text{bulge}})$ relations. Interestingly, the 3-parameters fit of the latter relation is in excellent agreement with the one found by Wyithe (2006) (magenta solid line in lower panel of Figure 4.4).

BH fundamental plane relation

In Figure 4.5 we compare the BH fundamental plane relation of our model at different redshifts with that obtained by Hopkins et al. (2007a) using both observational data and the outputs of hydrodynamical simulations of galaxy mergers:

$$\log(M_{\text{BH}}/M_{\odot}) = 7.93 + 0.72 \log(M_{11}^*) + 1.4 \log(\sigma_{200}),$$

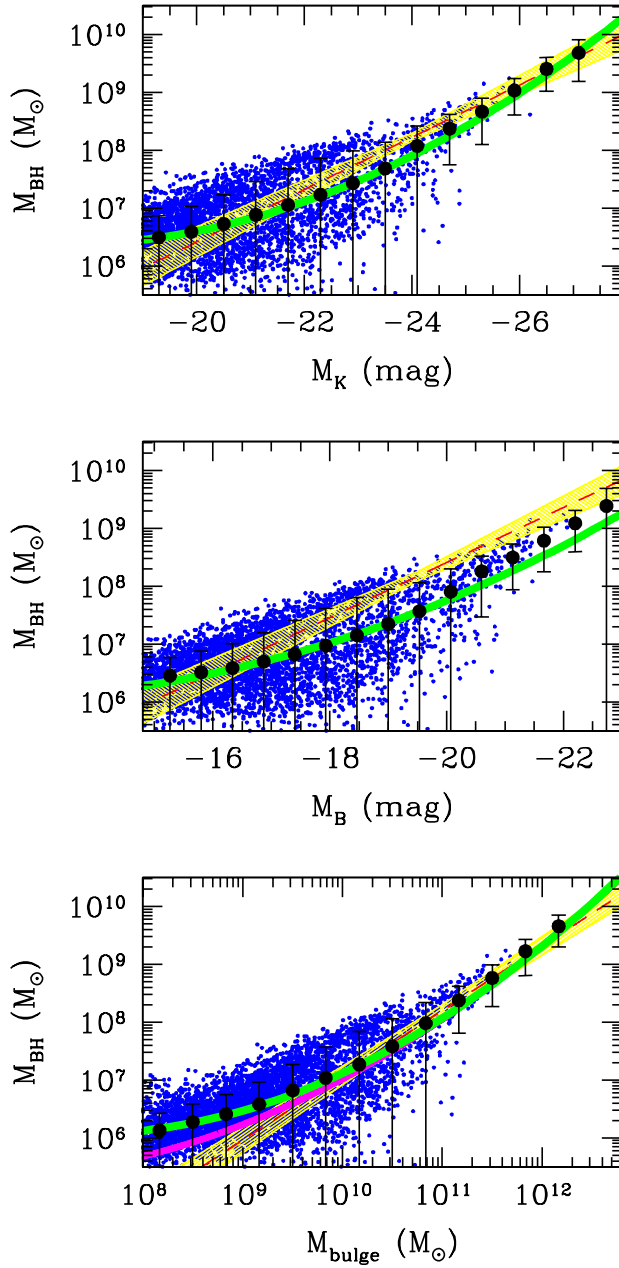


Figure 4.4: The tree model scaling relations best constrained by observations. Here the black dots (with error bars) represent the medians (and the corresponding first and third quartiles) of the model outputs, computed in a discrete number of bins. The green lines show the best three-parameters fits to the model outputs (blue points). The magenta line in the lower panel refers to the best-fit relation obtained by Wyithe (2006).

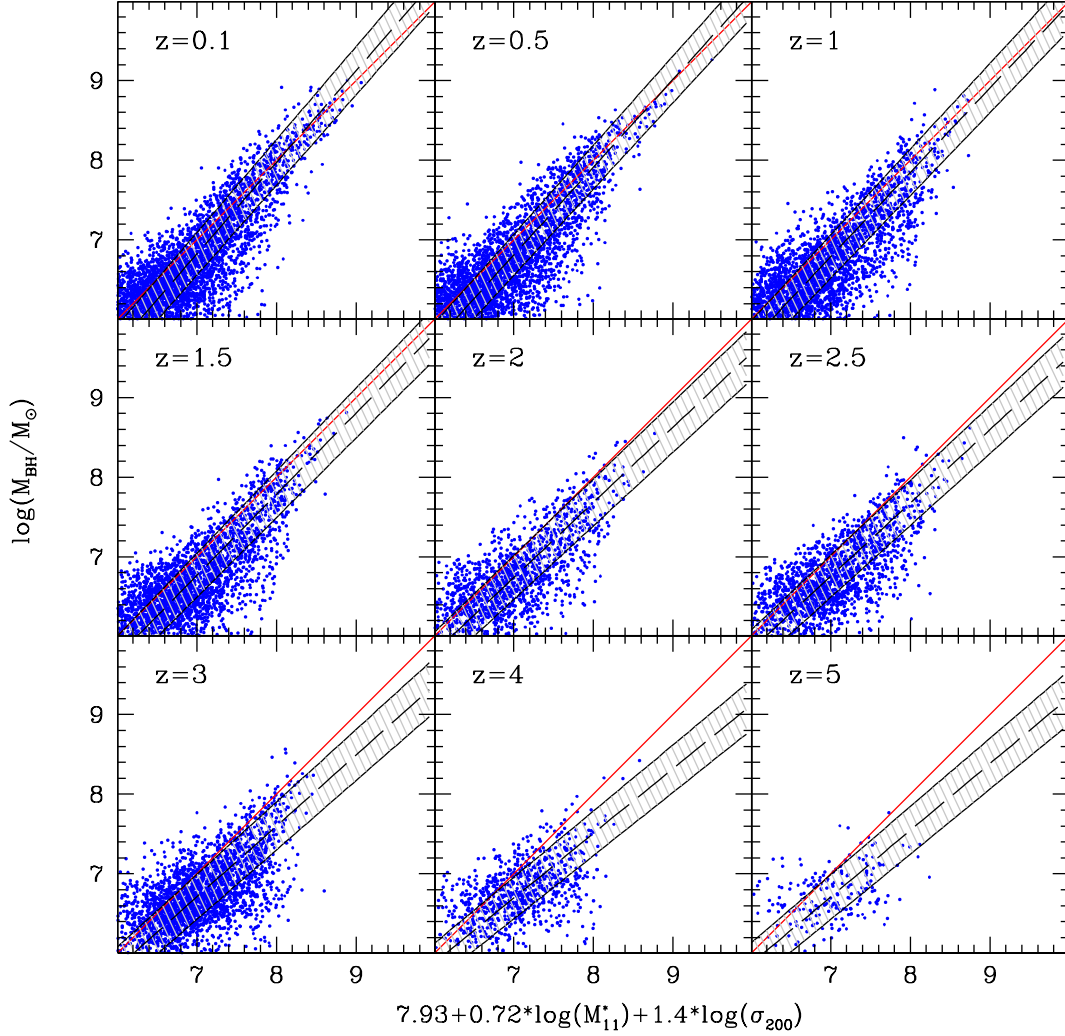


Figure 4.5: The BH fundamental plane in the redshift range $0.1 \leq z \leq 5$. The blue dots are the model outputs, while the grey shaded areas show the best-fits to them. The red lines, corresponding to the bisectors of the plots, are the predictions of Hopkins et al. (2007a). The galaxy stellar mass, M_{11}^* , is given in units of $10^{11} M_{\odot}$, while the bulge velocity dispersion, σ_{200} , is in units of 200 km s^{-1} .

where M_{11}^* is the galaxy stellar mass in units of $10^{11}M_{\odot}$, and σ_{200} is the bulge velocity dispersion in units of 200 km s^{-1} . The red lines, bisectors of the plots, show the fundamental plane relation proposed by Hopkins et al. (2007a). Model prediction are represented by blue dots, the black line is the best fit to the model and the shaded area its 1σ scatter. At low redshifts the agreement is very good. This is not surprising since at $z \sim 0$ our model agrees with the $M_{\text{BH}} - M_{\text{bulge}}$ and $M_{\text{BH}} - \sigma_c$ scaling relations that represent fundamental plane projections. A discrepancy appears at high redshifts. However, at $z > 3$ the fit involves only few objects and therefore may not be very significant, especially when we account for the non-zero intrinsic scatter in the fundamental plane proposed by Hopkins et al. (2007a). A remarkable success of our model is that it predicts very little evolution of the fundamental plane relation, at least out to $z = 3$, in agreement with Hopkins et al. (2007a). The intrinsic scatter, which does not evolve with time either, is 3 times larger than in Hopkins et al. (2007a) (we found a value around 0.6 at all redshifts, while the one reported by Hopkins et al. (2007a) is about 0.2). As discussed previously, the mismatch is reduced when using a number of model BHs consistent with the observed one. We also note that since the ratio between the coefficients multiplying the $\log(M_{11}^*)$ and $\log(\sigma_{200})$ terms in the BH fundamental plane is very close to 0.5, both our model and the hydrodynamical simulations of Hopkins et al. (2007a) are in agreement with the relationship between the masses of the BHs and the kinetic energy of random motions in their host galaxies found by Feoli & Mele (2005, 2007).

Dependence on the accretion history

All scaling relations predicted by our model assume that BHs accrete mass instantaneously after merging events. What happens if we relax this assumption and specify the mass accretion rate instead? Figure 4.6 shows the impact of adopting different accretion recipes on the $M_{\text{BH}} - M_{\text{bulge}}$ relation. As usual, filled dots represent model predictions, grey shaded areas show the linear fit to the *DeLucia2006a* model scaling relation and the other hatched areas indicate the linear fit to the model predictions obtained with our different recipes, as indicated by the labels¹. Clearly, these predictions depend little on the assumed mass accretion histories for each individual quasar event (the fit parameters have fluctuations of no more than about 1%). This is a consequence of the fact that the BH scaling relations depend mainly on the total mass accreted, and very little on the time spent in the accretion process. We have verified that all other scaling relations, including also the

¹The meaning of the black dots and shaded areas in the bottom left panel of Fig. 5 is discussed in section 4.2.3.

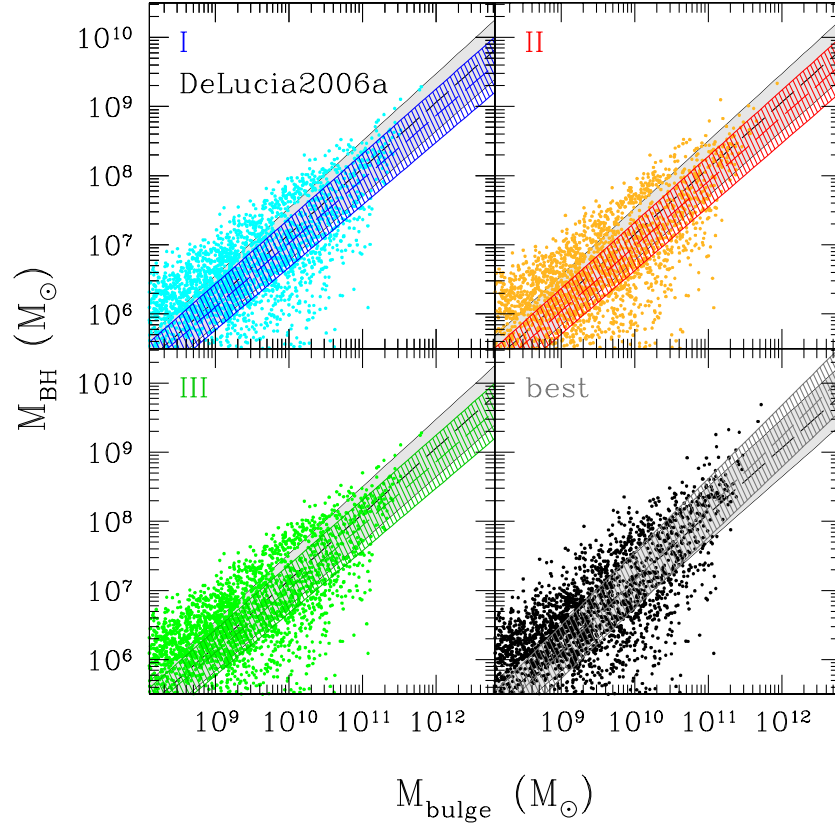


Figure 4.6: The $\log(M_{\text{BH}}) - \log(M_{\text{bulge}})$ scaling relation for our different prescriptions for the BH mass accretion. The filled dots represent model predictions, the grey shaded areas show the linear fit to the *DeLucia2006a* model scaling relation and the other hatched areas indicate the linear fit to the *I*, *II* and *III* lightcurve models, as indicated by the labels. The black dots and grey shaded areas, in the lower right panel, show the prediction obtained with the parameterization given by the Eqs. (4.18), as explained in section 4.2.3.

fundamental plane relation, does not change significantly by adopting any of the mass accretion prescriptions described in section 4.1.3.

4.2.2

 BH mass function

In Figure 4.7, we compare the BH MF predicted by our model for the prescriptions *I* (blue line), *II* (red) and *III* (green) with those observed by Shankar et al. (2004) (grey area) and by Shankar (private communication) (yellow area) at $z \sim 0$ (see section 1.1.3 for details). We note that the model BH MF is in good agreement with the observed ones, within the mass range accessible to observations except in the interval $\sim 10^7 - 10^9 M_{\odot}$, in which the number density of model BHs is smaller than the observed one.

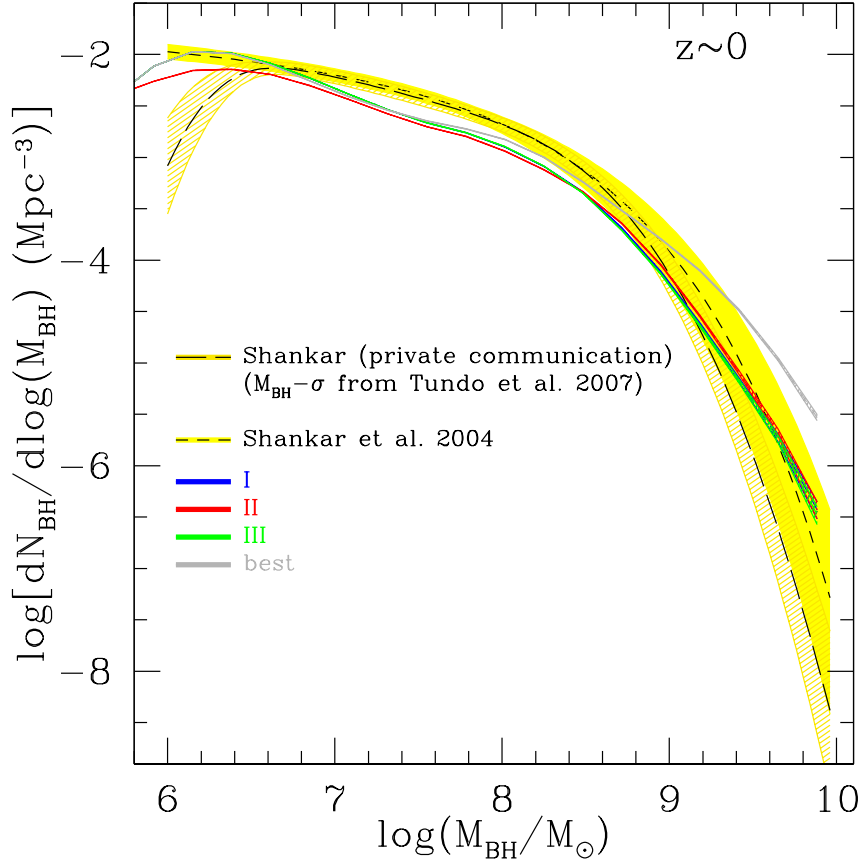


Figure 4.7: Comparison of the BH MF predicted by lightcurve models *I*, *II* and *III* with the one observationally derived by Shankar et al. (2004), and with the new one obtained by Shankar (private communication) using the $M_{\text{BH}} - \sigma$ relation by Tundo et al. (2007). The grey areas show the prediction obtained with the parameterization given by the Eqs. (4.18), as explained in section 4.2.3.

The reason of the small mismatch between the observed and the model BH MFs will be investigated in future work in which we study the redshift evolution of the BH MF and its dependency on the properties of the host galaxy. Finally, we note that, as shown in Figure 4.7, the model predictions for the BH MF are robust with respect to the prescription adopted for the mass accretion history of the individual quasar episodes.

4.2.3 AGN bolometric luminosity function

Here we compare our predictions with the bolometric LF obtained by H07 and described in section 1.1.4. Uncertainties in these corrections contribute to the scatter in the observed LF, i.e. to the width of the yellow areas in Figure 4.8 that show the AGN bolometric LF of H07 at different redshifts. The

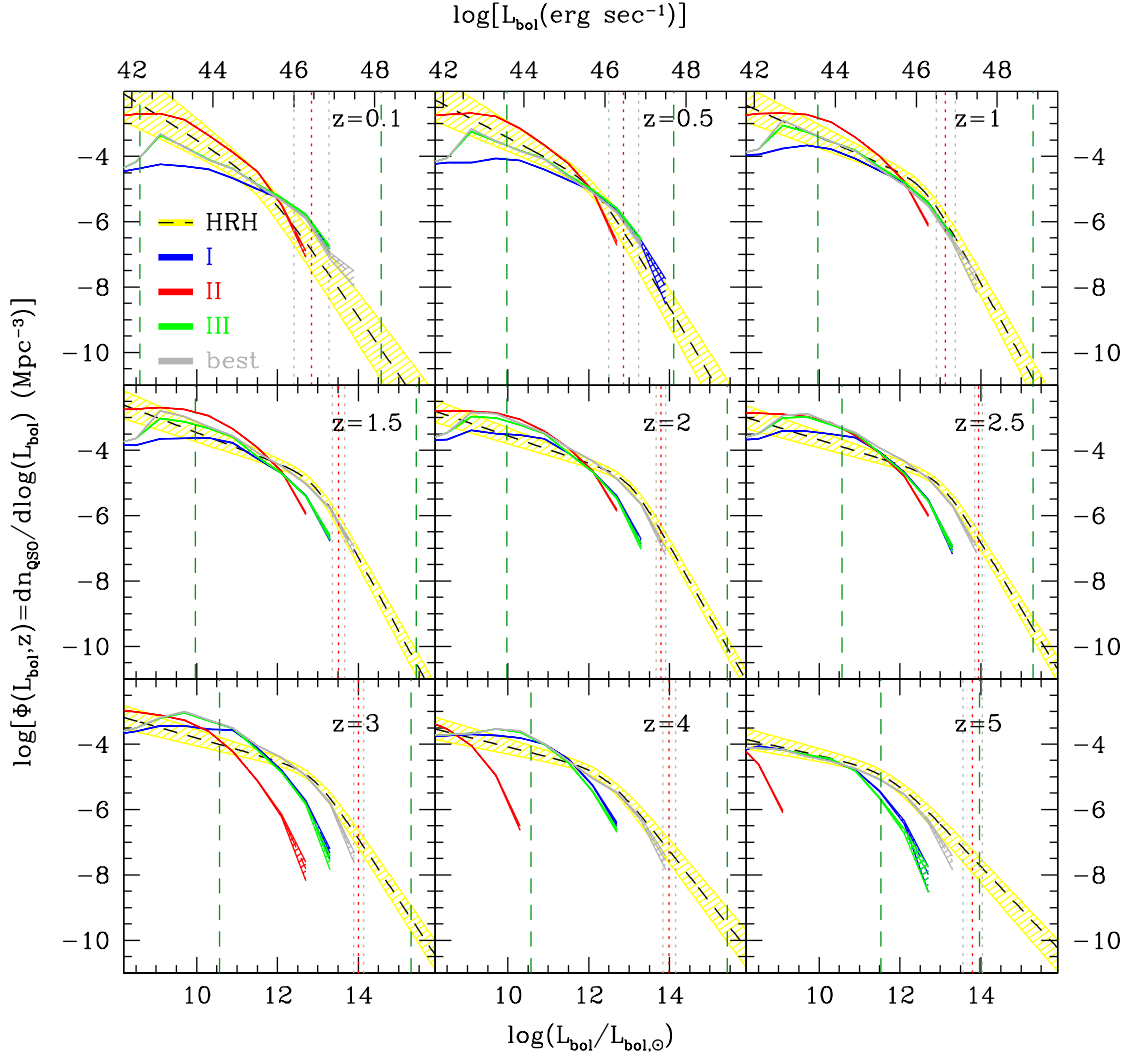


Figure 4.8: The bolometric LFs predicted by our lightcurve models *I* (blue bands), *II* (red bands) and *III* (green bands), in the redshift range $0.1 \leq z \leq 5$, are here compared with the best-fits to observational data obtained by H07 (yellow bands). The grey areas show the predictions obtained with the parameterization given by the Eqs. (4.18), as explained in Section 4.2.3. Uncertainties in the model LFs are computed by assuming Poisson statistics. The dashed vertical green lines mark the range of the bolometric luminosities accessible to observations. The dotted red vertical lines show the luminosities beyond which the LF of H07 predicts a number of AGN in the whole volume of our simulation smaller than 10. The vertical grey dotted lines around the red ones have been calculated considering the error in the best-fit of H07.

model predictions are also represented by areas with different colours, with a width corresponding to 1σ Poisson error bars. The vertical, green dashed lines bracket the bolometric luminosity range accessible to observations. The vertical, red dotted lines show the luminosities beyond which the LF of H07 predicts less than 10 AGN in the volume of our simulation, i.e. the maximum luminosities at which our model BH sample is statistically meaningful; 1σ uncertainties on this maximum luminosity are represented by the two grey dotted lines.

From Figure 4.8 we see that, on average, type-*I* lightcurve underestimates the AGN number density at all epochs. However, while at high redshifts the model matches the faint-end of the LF and underpredicts the number density of the bright objects, the situation is completely reversed at $z \sim 0$, where the model correctly reproduces the number density of bright AGN but underestimates the faint ones. At low redshifts the problem can be alleviated by reducing the Eddington factor, as in our type-*II* lightcurve. However, in this case the discrepancy between model and data at high redshifts increases. Adopting the type-*III* lightcurve allows to match observations in the whole range of luminosities in the redshift range $0.5 \lesssim z \lesssim 1$, but overestimates the number of luminous AGN at $z \lesssim 0.5$ and underestimates them at $z \gtrsim 1$.

Therefore, we conclude that in our present semi-analytical framework we can reproduce the observed AGN LF at low and intermediate redshifts. However, at $z \gtrsim 1$, we under-predict the number density of bright AGN, regardless of the BH mass accretion rate and light curve model assumed for each quasar episode. To investigate if it is possible to modify our prescription for the mass accretion to fit the AGN LF at all redshifts, we tried different values of f_{Edd} and ε as a function of t and M_{BH} , within physically motivated ranges. Despite of the considerable freedom in choosing $f_{\text{Edd}}(t, M_{\text{BH}})$ we failed to find a model able to match simultaneously the observed BH scaling relations, the BH MF, and the AGN LF, especially at high redshifts. We also used different plausible values for the BH seed mass, and we still were not able to fit the high- z LF. We interpret this failure as an indication that our theoretical framework itself is inadequate to account fully successfully for the AGN phenomenon.

One possible way out is to modify the model assumptions for the efficiency of BH growth in the *quasar mode* following mergers at high z . A significant improvement of our results at high redshifts can for example be obtained by

substituting Eqs. (4.12) and (4.13) with

$$\begin{cases} f_{\text{BH}} = 0.01 \cdot \log\left(\frac{M_{\text{BH}}}{10^3 M_{\odot}} + 1\right) \cdot z & z > 1.5 \text{ and } M_{\text{BH}} > 10^6 M_{\odot} \\ \Delta M_{\text{BH,Q}} = 0.01 \cdot m_{\text{cold}} & z > 6 \end{cases} \quad (4.18)$$

while keeping prescription *III* for the quasar lightcurves. The predictions of this new model for the $\log(M_{\text{BH}}) - \log(M_{\text{bulge}})$ scaling relation is shown as black dots in the bottom-right plot of Fig. 4.6. Model predictions for the BH MF and AGN LF are shown in Figures 4.7 and 4.8, respectively.

In Figure 4.9 we compare the AGN LF predicted by this model with the one obtained adopting our best semi-analytic model, H (magenta areas), described in the previous chapter, which also assumes a time-dependent Eddington ratio. Symbols are as in Fig. 1.8. As shown, the two models agree quite well in the redshift range $1 \lesssim z \lesssim 3$. At lower redshifts, the hybrid simulation described here better matches the AGN number density at $L_{\text{bol}} \lesssim 10^{46} \text{ergs}^{-1}$. At $z \gtrsim 3$, the predictions of the two models differ significantly, but only in the faint end of the LF, that is not yet accessible to observations.

An accretion efficiency that increases with the redshift has been already advocated by Cattaneo et al. (2005) and in the *dynamical model* of Croton (2006). Similar results have also been obtained in Lapi et al. (2006), where enhanced gas clumping factors and mild super-Eddington accretion at $z \geq 3$ were adopted to match the high-luminosity tail of the AGN LF at high redshifts. A physical justification to this assumption is provided by Mo et al. (1998), since their model predicts that galactic disks were more centrally concentrated in the past, making it more efficient the BH feeding at high redshift. It is worth stressing that Eq. (4.18) might not provide the best fit to the data as we did not explore the parameter space systematically. However, it suggests that a good match to the observed scaling relations, BH MF and AGN LF can be obtained within our semi-analytic framework by modest changes of the BH growth at high redshifts. The solution provided by Eq. (4.18) is not unique either, since larger amounts of mass can be accreted also by invoking alternative mechanisms that trigger gas accretion episodes, for example by secular evolution through disk instabilities, or by alluding to a higher gas cooling efficiency (see e.g. Viola et al., 2008).

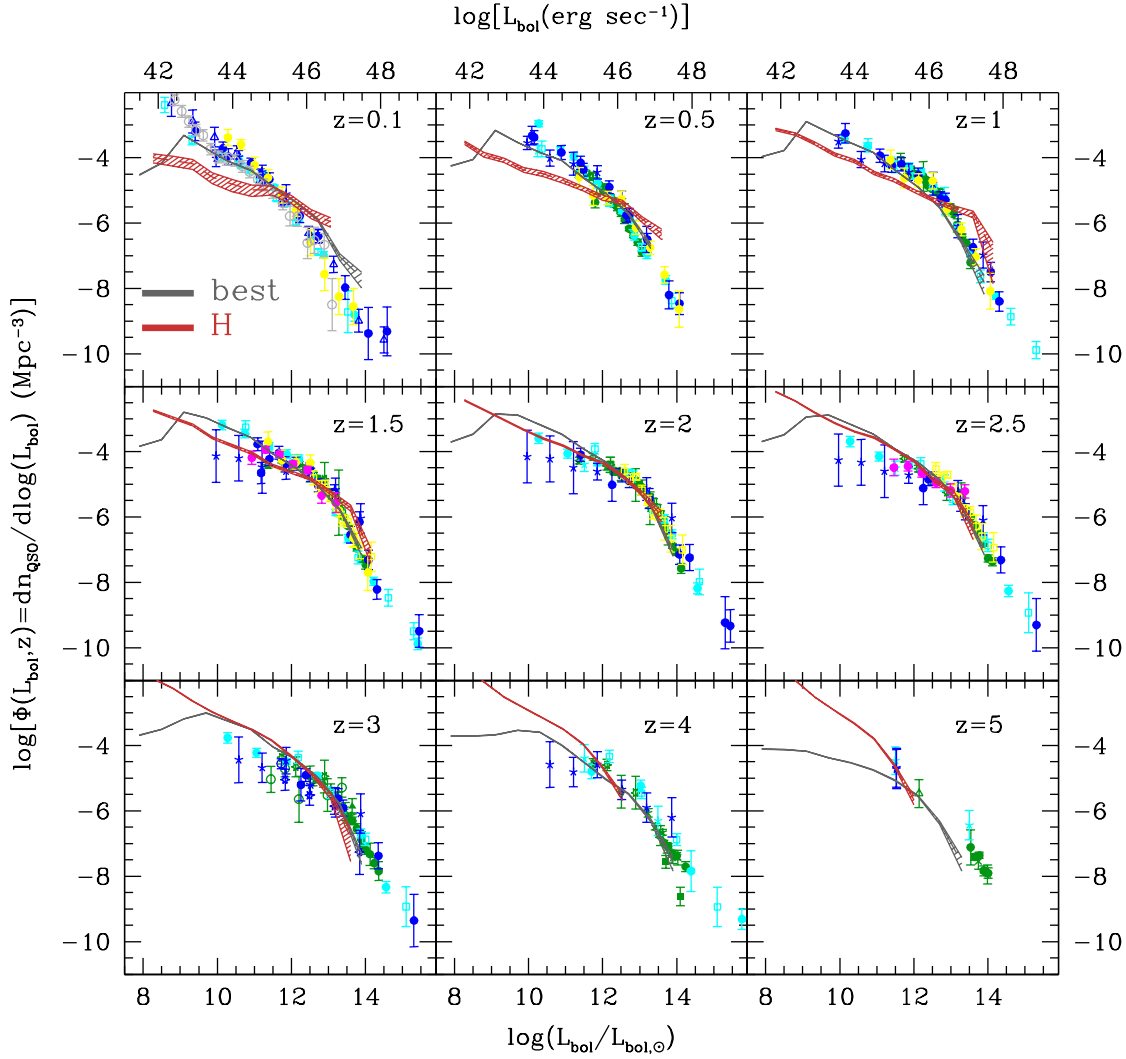


Figure 4.9: The bolometric LF predicted by our best model, as described in section 4.2.3 (red areas), compared with several observed binned LFs: Ueda et al. (2003) (filled blue circles), Silverman et al. (2005a) (blue stars), Barger et al. (2003a,b) (skeletal blue pentagons), Nandra et al. (2005) (open blue circles), Sazonov & Revnivtsev (2004) (open blue triangles), Hao et al. (2005) (open grey circles), Hasinger et al. (2005) (filled cyan circles), Silverman et al. (2005b) (skeletal cyan pentagons), Bongiorno et al. (2007) (filled magenta circles), Richards et al. (2005) (open green squares), Richards et al. (2006) (filled green circles), Wolf et al. (2003) (green stars), Hunt et al. (2004) (open green circles), Cristiani et al. (2004) (open green triangles), Kennefick et al. (1995) (filled green squares), Schmidt et al. (1995) (skeletal green pentagons), Fan et al. (2001b,a, 2003, 2004) (skeletal green squares), Matute et al. (2006) (filled red circles), Brown et al. (2006) (open red squares), Miyaji et al. (2000, 2001) (open cyan squares), Siana et al. (2007) (filled green triangles).

Discussion

In this chapter we have used and extended an hybrid simulation for the co-evolution of galaxies and their central BHs, developed on the outputs of the Millennium Simulation (Springel et al., 2005a), and described in detail in Croton et al. (2006) and De Lucia & Blaizot (2007). The aim of the model is to reproduce the observed properties of BHs, AGN and their galaxy hosts. The physical assumptions in the model with respect to BH growth can be divided into two sets. The first one concerns the mass accretion history of the central BHs in haloes, where we distinguish between *radio mode* and *quasar mode* (Croton et al., 2006). This set makes predictions for the relation between BH and galaxy host properties, which can be compared to the observed scaling relations between BH mass and different properties of their host galaxies. The second set of prescriptions specifies the detailed AGN activity and lightcurve of individual quasar episodes, and leads to predictions for the AGN LF as a function of redshift. We considered three different models for this detailed AGN activity, one of them motivated by the results of recent hydrodynamical simulations of galaxy mergers that include BH growth and feedback (Hopkins et al., 2005; Di Matteo et al., 2005; Springel et al., 2005b). The main results of our analysis are as follows:

(i) The hybrid simulation is approximately able to reproduce the observed BH scaling relations over the whole range of BH masses and galaxy properties probed by observations. The intrinsic scatter in the model is significantly larger than in the data, a mismatch that can in part be accounted for by adopting the observational selection criteria to obtain a mock BH catalogue with similar characteristics as the observed one.

(ii) We find evidence that a quadratic relationship provides a significantly better fit to some of the model scaling relationships than a linear one, as already noticed by Wyithe (2006).

(iii) Our model also matches the BH fundamental plane relation derived by Hopkins et al. (2007a), and successfully predicts very little evolution of this plane, at least out to $z \sim 3$.

(iv) The model BH MF is in good agreement with the observed one within the mass range accessible by observations, except on the range $\sim 10^7 - 10^9 M_\odot$, in which the number density predicted by the model is smaller than the observed one.

(v) Model predictions for the BH MF, scaling relations and fundamental

plane relation are basically unaffected when using different prescriptions for the AGN lightcurves of individual quasar events. This is because these predictions are only sensitive to the model assumptions for the absolute growth of the BHs in each merger event.

(vi) The AGN LF is systematically underestimated by assuming that BHs accrete mass with a constant Eddington factor $f_{\text{Edd}} = 1$. The detail of the discrepancy, however, change with redshift since at high z the model matches the faint-end of the LF but underpredicts the number density of the brightest objects, while the situation is reversed at $z \sim 0$, in agreement with the results of the semi-analytic models described in the previous chapter. Reducing the Eddington ratio, as in our lightcurve model *II*, alleviates the faint-end mismatch but amplifies the bright-end discrepancy at high redshifts. A significant improvement at low redshifts is obtained when the Eddington-limited growth of the BH is followed by a long quiescent phase with lower Eddington ratios, as suggested by Hopkins et al. (2005) and implemented in our lightcurve model *III*. In this case our model is able to match the observed AGN LF in the interval $0.1 \lesssim z \lesssim 1$, over the whole range of luminosities that are accessible to observations and where our predictions are statistically significant. However, our predicted number density of bright AGN is still biased low at $z \gtrsim 1$.

(vii) Our model is able to account for all observations considered in this work apart for the AGN LF at high redshifts. We were not able to eliminate this mismatch by simply modifying the accretion efficiency, ϵ , the Eddington factor, f_{Edd} , or the BH seed mass (when considered in physically plausible ranges). Clearly, we need to modify assumptions in the underlying semi-analytic framework for BH growth. A simple, *ad hoc* increase of the mass fraction accreted during the *quasar mode* at high redshift can indeed remedy the problem. However, this solution is not unique as several high-redshift modifications to the original model, like new mechanisms that trigger BH activity in addition to galaxy merging or more efficient gas cooling resulting in a larger reservoir of cold gas, can be advocated to bring the predictions in line with observations. However, it remains to be seen whether any of these alternatives is physically plausible.

(viii) Our model predictions at $z < 3$ are robust to changes in the assumed BH seed mass, but are sensitive to it at larger redshift. We will further explore this issue in future work where we plan to study to what extent current observations can constrain the seed BH MF.

From our analysis we conclude that the AGN LF at high redshifts constitutes a strong constraint for hybrid simulations that describe the

co-evolution of galaxies, BHs and AGN. This suggests that significant improvements can be obtained in two ways. From the theoretical side, we need to develop a physically motivated mechanism capable of increasing the number density of bright AGN at $z \gtrsim 1$ without modifying the model predictions at low redshifts. From the observational point of view, we need to improve the AGN LF estimates at high redshift, both by enlarging current high- z AGN samples and by reducing the current uncertainties originating from bolometric and incompleteness corrections, in particular for the population of Compton Thick AGN. In addition, other observational tests should be performed, like the ability of our model to match the observed AGN clustering, as quantified by the angular and spatial two-point correlations function. In particular, Lidz et al. (2006) pointed out that the luminosity dependence of quasar clustering can discriminate between different lightcurve models, a question we will address in the future.

Conclusions



IN this Thesis, we have investigated the cosmological co-evolution of BHs, AGN and their hosting DM halos and galaxies, within the standard Λ CDM scenario. We have analyzed both analytic, semi-analytic and hybrid techniques and used the most recent observational data available to constrain the assumptions underlying our models.

We have demonstrated that only minor modifications to the original WL02 and WL03 models are required to match the observed AGN LF at redshifts as small as ~ 0.5 , while more profound changes seem to be required for a successful modeling of the very local AGN population. We have also shown that both models predict a moderate degree of AGN clustering at low redshift, consistently with the observations. However, at $z \sim 2$ the AGN biasing appears to be significantly smaller than that observed in the 2QZ/6QZ AGN survey. The only way for reproducing the observed degree of clustering is to increase the normalization of the $M_{\text{BH}} - v_c$ relation, which, however, would overpredict the AGN number density in the local Universe.

We have confirmed the success of standard semi-analytic models in reproducing both the $M_{\text{BH}} - \sigma_c$ relation at $z = 0$, the AGN bolometric LF at $1 \lesssim z \lesssim 2$, i.e. around the peak of AGN activity, and the AGN clustering, quantified by the biasing function, at $z < 2$. However, as also pointed out by similar analyses, problems occur at low redshifts, where hierarchical models systematically overestimate the number density of bright AGN and underestimate the faint ones. The predicted number density of bright AGN can be reduced by advocating inefficient cooling within massive haloes or by accounting for feedback mechanisms. The underestimate of faint AGN looks like a more serious problem that we have tried to tackle by assuming a time-dependent Eddington ratio, as suggested by the outcome of recent hydrodynamical simulations.

The hybrid simulation considered in this Thesis is able to reproduce the observed BH scaling relations over the whole range of BH masses and galaxy properties probed by observations. This model also matches the

BH fundamental plane relation derived by Hopkins et al. (2007a), and successfully predicts very little evolution of this plane, at least out to $z \sim 3$. The AGN LF is systematically underestimated by assuming that BHs accrete mass with a constant Eddington factor $f_{\text{Edd}} = 1$. Reducing the Eddington ratio alleviates the faint-end mismatch but amplifies the bright-end discrepancy at high redshifts. A significant improvement at low redshifts is obtained when the Eddington-limited growth of the BH is followed by a long quiescent phase with lower Eddington ratios. However, the predicted number density of bright AGN is still biased low at $z \gtrsim 1$. We were not able to eliminate this mismatch by simply modifying the accretion efficiency, the Eddington factor, or the BH seed mass (when considered in physically plausible ranges). A simple, *ad hoc* increase of the mass fraction accreted during the *quasar mode* at high redshift can indeed remedy the problem.

All the above results support the following scenario:

- The cosmological co-evolution of BHs, AGN and galaxies can be well described within the Λ CDM model.
- At redshifts $z \gtrsim 1$, the evolution history of DM halo fully determines the overall properties of the BH and AGN populations. The AGN emission is triggered mainly by DM halo major mergers and, on average, AGN shine at their Eddington luminosity.
- At redshifts $z \lesssim 1$, BH growth decouples from halo growth. Galaxy major mergers cannot constitute the only trigger to accretion episodes in this phase.
- When a static hot halo has formed around a galaxy, a fraction of the hot gas continuously accretes onto the central BH, causing a low-energy “radio” activity at the galactic centre, which prevents significant gas cooling and thus limiting the mass of the central galaxies and quenching the star formation at late time.
- The cold gas fraction accreted by BHs at high redshifts seems to be larger than at low redshifts.

In the next future, we will further improve the hybrid simulation described in Chapter 4, including a better treatment of the *radio mode* feedback and of the gas cooling. We will investigate in detail the properties of the BH seeds and of the radio-loud and radio-quiet AGN. Besides, we will compare our model predictions with i) the BH MF as a function of redshift and host galaxy properties, ii) the AGN number counts, iii) the AGN clustering as a function

of luminosity and redshift and iv) the BH scaling relation as a function of the environment.



Bibliography

- Abbas U., Sheth R. K., 2005, MNRAS, 364, 1327
- Adelberger K. L., Steidel C. C., 2005, ApJ, 627, L1
- Akritas M. G., Bershady M. A., 1996, ApJ, 470, 706
- Aller M. C., Richstone D., 2002, AJ, 124, 3035
- Aller M. C., Richstone D. O., 2007, ApJ, 665, 120
- Babbedge T. S. R., et al., 2006, MNRAS, 370, 1159
- Baes M., Buyle P., Hau G. K. T., Dejonghe H., 2003, MNRAS, 341, L44
- Barger A. J., Cowie L. L., Mushotzky R. F., Richards E. A., 2001, AJ, 121, 662
- Barger A. J., et al., 2003a, AJ, 126, 632
- Barger A. J., et al., 2003b, ApJ, 584, L61
- Barkana R., Loeb A., 2001, PhysRep, 349, 125
- Barth A. J., Greene J. E., Ho L. C., 2005, ApJ, 619, L151
- Barway S., Kembhavi A., 2007, ApJ, 662, L67
- Bauer F. E., et al., 2004, AJ, 128, 2048
- Beckmann V., Soldi S., Shrader C. R., Gehrels N., Produit N., 2006, ApJ, 652, 126
- Benson A. J., Bower R. G., Frenk C. S., Lacey C. G., Baugh C. M., Cole S., 2003, ApJ, 599, 38
- Binney J., Tremaine S., 1987, Galactic dynamics. Princeton, NJ, Princeton University Press, 1987, 747 p.
- Bond J. R., Cole S., Efstathiou G., Kaiser N., 1991, ApJ, 379, 440
- Bondi H., Hoyle F., 1944, MNRAS, 104, 273

- Bongiorno A., et al., 2007, *A&A*, 472, 443
- Bower R. G., Benson A. J., Malbon R., Helly J. C., Frenk C. S., Baugh C. M., Cole S., Lacey C. G., 2006, *MNRAS*, 370, 645
- Boyle B. J., Shanks T., Croom S. M., Smith R. J., Miller L., Loaring N., Heymans C., 2000, *MNRAS*, 317, 1014
- Boyle B. J., Shanks T., Peterson B. A., 1988, *MNRAS*, 235, 935
- Brown M. J. I., et al., 2006, *ApJ*, 638, 88
- Canalizo G., Stockton A., 2001, *ApJ*, 555, 719
- Capetti A., Balmaverde B., 2006, *A&A*, 453, 27
- Cattaneo A., Bernardi M., 2003, *MNRAS*, 344, 45
- Cattaneo A., Blaizot J., Devriendt J., Guiderdoni B., 2005, *MNRAS*, 364, 407
- Cattaneo A., Dekel A., Devriendt J., Guiderdoni B., Blaizot J., 2006, *MNRAS*, 370, 1651
- Cattaneo A., Haehnelt M. G., Rees M. J., 1999, *MNRAS*, 308, 77
- Cavaliere A., Vittorini V., 2002, *ApJ*, 570, 114
- Cimatti A., Daddi E., Renzini A., 2006, *A&A*, 453, L29
- Ciotti L., Ostriker J. P., 2001, *ApJ*, 551, 131
- Cole S., Lacey C. G., Baugh C. M., Frenk C. S., 2000, *MNRAS*, 319, 168
- Colless M., et al., 2001, *MNRAS*, 328, 1039
- Comastri A., Setti G., Zamorani G., Hasinger G., 1995, *A&A*, 296, 1
- Cowie L. L., Binney J., 1977, *ApJ*, 215, 723
- Cowie L. L., Songaila A., Hu E. M., Cohen J. G., 1996, *AJ*, 112, 839
- Cox T. J., 2004, Ph.D. Thesis, University of California, Santa Cruz
- Cox T. J., et al., 2006, *ApJ*, 650, 791
- Cristiani S., et al., 2004, *ApJ*, 600, L119
- Croom S. M., et al., 2005, *MNRAS*, 356, 415
- Croom S. M., Smith R. J., Boyle B. J., Shanks T., Miller L., Outram P. J., Loaring N. S., 2004, *MNRAS*, 349, 1397

- Croton D. J., 2006, MNRAS, 369, 1808
- Croton D. J., et al., 2006, MNRAS, 365, 11
- de Francesco G., Capetti A., Marconi A., 2006, A&A, 460, 439
- De Lucia G., Blaizot J., 2007, MNRAS, 375, 2
- De Lucia G., Kauffmann G., White S. D. M., 2004, MNRAS, 349, 1101
- De Lucia G., Springel V., White S. D. M., Croton D., Kauffmann G., 2006, MNRAS, 366, 499
- Di Matteo T., Colberg J., Springel V., Hernquist L., Sijacki D., 2007, ArXiv e-prints, 705
- Di Matteo T., Springel V., Hernquist L., 2005, Nat, 433, 604
- Dunlop J. S., McLure R. J., Kukula M. J., Baum S. A., O'Dea C. P., Hughes D. H., 2003, MNRAS, 340, 1095
- Efstathiou G., 1992, MNRAS, 256, 43P
- Efstathiou G., Rees M. J., 1988, MNRAS, 230, 5P
- Elvis M., et al., 1994, ApJS, 95, 1
- Elvis M., Risaliti G., Zamorani G., 2002, ApJ, 565, L75
- Enoki M., Nagashima M., Gouda N., 2003, PASJ, 55, 133
- Fabian A. C., Iwasawa K., 1999, MNRAS, 303, L34
- Fabian A. C., Nulsen P. E. J., 1977, MNRAS, 180, 479
- Fabian A. C., Sanders J. S., Allen S. W., Crawford C. S., Iwasawa K., Johnstone R. M., Schmidt R. W., Taylor G. B., 2003, MNRAS, 344, L43
- Fan X., et al., 2001a, AJ, 122, 2833
- Fan X., et al., 2001b, AJ, 121, 54
- Fan X., et al., 2003, AJ, 125, 1649
- Fan X., et al., 2004, AJ, 128, 515
- Favata M., Hughes S. A., Holz D. E., 2004, ApJ, 607, L5
- Feoli A., Mele D., 2005, International Journal of Modern Physics D, 14, 1861
- Feoli A., Mele D., 2007, International Journal of Modern Physics D, 16, 1261

- Ferrarese L., 2002, *ApJ*, 578, 90
- Ferrarese L., Ford H., 2005, *Space Science Reviews*, 116, 523
- Ferrarese L., Merritt D., 2000, *ApJ*, 539, L9
- Fontanot F., Cristiani S., Monaco P., Nonino M., Vanzella E., Brandt W. N., Grazian A., Mao J., 2007, *A&A*, 461, 39
- Fontanot F., Monaco P., Cristiani S., Tozzi P., 2006, *MNRAS*, 373, 1173
- Franceschini A., et al., 2005, *AJ*, 129, 2074
- Gao L., Springel V., White S. D. M., 2005, *MNRAS*, 363, L66
- Gebhardt K., et al., 2000, *ApJ*, 539, L13
- Ghez A. M., Duchêne G., Matthews K., Hornstein S. D., Tanner A., Larkin J., Morris M., Becklin E. E., Salim S., Kremenek T., Thompson D., Soifer B. T., Neugebauer G., McLean I., 2003, *ApJ*, 586, L127
- Gilli R., et al., 2005, *A&A*, 430, 811
- Gilli R., Salvati M., Hasinger G., 2001, *A&A*, 366, 407
- Gnedin N. Y., 2000, *ApJ*, 542, 535
- Graham A. W., 2008, *ArXiv e-prints*, 801
- Graham A. W., Driver S. P., 2007a, *ApJ*, 655, 77
- Graham A. W., Driver S. P., Allen P. D., Liske J., 2007b, *MNRAS*, 378, 198
- Graham A. W., Erwin P., Caon N., Trujillo I., 2001, *ApJ*, 563, L11
- Granato G. L., et al., 2004, *ApJ*, 600, 580
- Grazian A., Cristiani S., D'Odorico V., Omizzolo A., Pizzella A., 2000, *AJ*, 119, 2540
- Grazian A., Negrello M., Moscardini L., Cristiani S., Haehnelt M. G., Matarrese S., Omizzolo A., Vanzella E., 2004, *AJ*, 127, 592
- Greene J. E., Ho L. C., 2006, *ApJ*, 641, L21
- Grogin N. A., et al., 2005, *ApJ*, 627, L97
- Haehnelt M. G., Rees M. J., 1993, *MNRAS*, 263, 168
- Haiman Z., Loeb A., 1998, *ApJ*, 503, 505

- Haiman Z., Menou K., 2000, *ApJ*, 531, 42
- Hamilton A. J. S., 1993, *ApJ*, 417, 19
- Hao L., et al., 2005, *AJ*, 129, 1795
- Häring N., Rix H.-W., 2004, *ApJ*, 604, L89
- Harker G., Cole S., Helly J., Frenk C., Jenkins A., 2006, *MNRAS*, pp 208–+
- Hartwick F. D. A., Schade D., 1990, *ARA&A*, 28, 437
- Hasinger G., Miyaji T., Schmidt M., 2005, *A&A*, 441, 417
- Hatziminaoglou E., Mathez G., Solanes J.-M., Manrique A., Salvador-Solé E., 2003, *MNRAS*, 343, 692
- Heckman T. M., Kauffmann G., Brinchmann J., Charlot S., Tremonti C., White S. D. M., 2004, *ApJ*, 613, 109
- Hernquist L., Mihos J. C., 1995, *ApJ*, 448, 41
- Hewett P. C., Foltz C. B., Chaffee F. H., 1993, *ApJ*, 406, L43
- Hickox R. C., Markevitch M., 2006, *ApJ*, 645, 95
- Hoefl M., Yepes G., Gottlöber S., Springel V., 2006, *MNRAS*, 371, 401
- Hopkins P. F., Hernquist L., 2006, *ApJS*, 166, 1
- Hopkins P. F., Hernquist L., Cox T. J., Robertson B., Di Matteo T., Springel V., 2006a, *ApJ*, 639, 700
- Hopkins P. F., Hernquist L., Cox T. J., Robertson B., Krause E., 2007a, *ApJ*, 669, 67
- Hopkins P. F., Hernquist L., Cox T. J., Robertson B., Krause E., 2007b, *ApJ*, 669, 45
- Hopkins P. F., Hernquist L., Martini P., Cox T. J., Robertson B., Di Matteo T., Springel V., 2005, *ApJ*, 625, L71
- Hopkins P. F., Lidz A., Hernquist L., Coil A. L., Myers A. D., Cox T. J., Spergel D. N., 2007d, *ApJ*, 662, 110
- Hopkins P. F., Richards G. T., Hernquist L., 2007e, *ApJ*, 654, 731
- Hopkins P. F., Robertson B., Krause E., Hernquist L., Cox T. J., 2006b, *ApJ*, 652, 107

- Hu J., 2008, ArXiv e-prints, 801
- Hunt M. P., Steidel C. C., Adelberger K. L., Shapley A. E., 2004, ApJ, 605, 625
- Kang X., Jing Y. P., Silk J., 2006, ApJ, 648, 820
- Kauffmann G., 1996, MNRAS, 281, 475
- Kauffmann G., Colberg J. M., Diaferio A., White S. D. M., 1999, MNRAS, 303, 188
- Kauffmann G., et al., 2003, MNRAS, 346, 1055
- Kauffmann G., Haehnelt M., 2000, MNRAS, 311, 576
- Kennefick J. D., Djorgovski S. G., de Carvalho R. R., 1995, AJ, 110, 2553
- Kennicutt Jr. R. C., 1998, ApJ, 498, 541
- Kitzbichler M. G., White S. D. M., 2007, MNRAS, 376, 2
- Koehler T., Grootte D., Reimers D., Wisotzki L., 1997, A&A, 325, 502
- Koo D. C., Kron R. G., 1988, ApJ, 325, 92
- Kormendy J., 2004, in *Coevolution of Black Holes and Galaxies The Stellar-Dynamical Search for Supermassive Black Holes in Galactic Nuclei*. pp 1–+
- Kormendy J., Richstone D., 1995, ARA&A, 33, 581
- Kravtsov A. V., Gnedin O. Y., Klypin A. A., 2004, ApJ, 609, 482
- La Franca F., et al., 2005, ApJ, 635, 864
- Lacey C., Cole S., 1993, MNRAS, 262, 627
- Lamastra A., Perola G. C., Matt G., 2006, A&A, 449, 551
- Landy S. D., Szalay A. S., 1993, ApJ, 412, 64
- Lapi A., Shankar F., Mao J., Granato G. L., Silva L., De Zotti G., Danese L., 2006, ApJ, 650, 42
- Lauer T. R., et al., 2007, ApJ, 662, 808
- Lemson G., Kauffmann G., 1999, MNRAS, 302, 111
- Lemson G., Virgo Consortium t., 2006, preprint, astro-ph/060801
- Li Y., et al., 2007, ApJ, 665, 187

- Lidz A., Hopkins P. F., Cox T. J., Hernquist L., Robertson B., 2006, *ApJ*, 641, 41
- Lynden-Bell D., 1969, *Nat*, 223, 690
- Madau P., Rees M. J., Volonteri M., Haardt F., Oh S. P., 2004, *ApJ*, 604, 484
- Magorrian J., et al., 1998, *AJ*, 115, 2285
- Maio U., Dolag K., Ciardi B., Tornatore L., 2007, *MNRAS*, 379, 963
- Malbon R. K., Baugh C. M., Frenk C. S., Lacey C. G., 2007, *MNRAS*, 382, 1394
- Mandelbaum R., McDonald P., Seljak U., Cen R., 2003, *MNRAS*, 344, 776
- Maoz E., 1998, *ApJ*, 494, L181+
- Marconi A., Hunt L. K., 2003, *ApJ*, 589, L21
- Marconi A., Risaliti G., Gilli R., Hunt L. K., Maiolino R., Salvati M., 2004, *MNRAS*, 351, 169
- Martini P., Weinberg D. H., 2001, *ApJ*, 547, 12
- Marulli F., Bonoli S., Branchini E., Moscardini L., Springel V., 2008, *MNRAS*, pp 257–+
- Marulli F., Branchini E., Moscardini L., Volonteri M., 2007, *MNRAS*, 375, 649
- Marulli F., Crociani D., Volonteri M., Branchini E., Moscardini L., 2006, *MNRAS*, 368, 1269
- Matute I., La Franca F., Pozzi F., Gruppioni C., Lari C., Zamorani G., 2006, *A&A*, 451, 443
- McLure R. J., Dunlop J. S., 2002, *MNRAS*, 331, 795
- McNamara B. R., Nulsen P. E. J., Wise M. W., Rafferty D. A., Carilli C., Sarazin C. L., Blanton E. L., 2005, *Nat*, 433, 45
- Merloni A., 2004a, *MNRAS*, 353, 1035
- Merloni A., Heinz S., di Matteo T., 2003, *MNRAS*, 345, 1057
- Merloni A., Rudnick G., Di Matteo T., 2004b, *MNRAS*, 354, L37
- Merritt D., Milosavljević M., Favata M., Hughes S. A., Holz D. E., 2004, *ApJ*, 607, L9
- Mihos J. C., Hernquist L., 1994, *ApJ*, 431, L9

- Miller L., Percival W. J., Croom S. M., Babić A., 2006, *A&A*, 459, 43
- Milosavljević M., Merritt D., 2001, *ApJ*, 563, 34
- Milosavljević M., Merritt D., Ho L. C., 2006, *ApJ*, 652, 120
- Miralda-Escudé J., Kollmeier J. A., 2005, *ApJ*, 619, 30
- Miyaji T., Hasinger G., Schmidt M., 2000, *A&A*, 353, 25
- Miyaji T., Hasinger G., Schmidt M., 2001, *A&A*, 369, 49
- Miyoshi M., Moran J., Herrnstein J., Greenhill L., Nakai N., Diamond P., Inoue M., 1995, *Nat*, 373, 127
- Mo H. J., Mao S., White S. D. M., 1998, *MNRAS*, 295, 319
- Mo H. J., White S. D. M., 1996, *MNRAS*, 282, 347
- Monaco P., Fontanot F., Taffoni G., 2007, *MNRAS*, 375, 1189
- Morandi A., Ettori S., 2007, *MNRAS*, 380, 1521
- Moretti A., Campana S., Lazzati D., Tagliaferri G., 2003, *ApJ*, 588, 696
- Nagar N. M., Falcke H., Wilson A. S., 2005, *A&A*, 435, 521
- Nandra K., Laird E. S., Steidel C. C., 2005, *MNRAS*, 360, L39
- Netzer H., Trakhtenbrot B., 2007, *ApJ*, 654, 754
- Novak G. S., Faber S. M., Dekel A., 2006, *ApJ*, 637, 96
- Olive K. A., Steigman G., Walker T. P., 2000, *PhysRep*, 333, 389
- Page M. J., Carrera F. J., 2000, *MNRAS*, 311, 433
- Peacock J. A., et al., 2001, *Nat*, 410, 169
- Peebles P. J. E., 1980, *The large-scale structure of the universe. Research supported by the National Science Foundation. Princeton, N.J., Princeton University Press, 1980. 435 p.*
- Pei Y. C., 1995, *ApJ*, 438, 623
- Pelupessy F. I., Di Matteo T., Ciardi B., 2007, *ApJ*, 665, 107
- Peng C. Y., Impey C. D., Rix H.-W., Kochanek C. S., Keeton C. R., Falco E. E., Lehár J., McLeod B. A., 2006, *ApJ*, 649, 616
- Percival W., Miller L., 1999, *MNRAS*, 309, 823

- Percival W. J., et al., 2002, *MNRAS*, 337, 1068
- Perlmutter S., et al., 1999, *ApJ*, 517, 565
- Peters P. C., 1964, *Physical Review*, 136, 1224
- Peterson J. R., Paerels F. B. S., Kaastra J. S., Arnaud M., Reiprich T. H., Fabian A. C., Mushotzky R. F., Jernigan J. G., Sakelliou I., 2001, *A&A*, 365, L104
- Porciani C., Magliocchetti M., Norberg P., 2004, *MNRAS*, 355, 1010
- Porciani C., Norberg P., 2006, *MNRAS*, 371, 1824, [PN06]
- Press W. H., Schechter P., 1974, *ApJ*, 187, 425
- Quinlan G. D., 1996, *New Astronomy*, 1, 35
- Rees M. J., 1984, *ARA&A*, 22, 471
- Richards G. T., et al., 2005, *MNRAS*, 360, 839
- Richards G. T., et al., 2006, *AJ*, 131, 2766
- Richstone D., et al., 1998, *Nat*, 395, A14+
- Riess A. G., et al., 1998, *AJ*, 116, 1009
- Rosati P., et al., 2002, *ApJ*, 566, 667
- Salpeter E. E., 1964, *ApJ*, 140, 796
- Sánchez A. G., Baugh C. M., Percival W. J., Peacock J. A., Padilla N. D., Cole S., Frenk C. S., Norberg P., 2006, *MNRAS*, 366, 189
- Sanders D. B., Mirabel I. F., 1996, *ARA&A*, 34, 749
- Sazonov S. Y., Ostriker J. P., Ciotti L., Sunyaev R. A., 2005, *MNRAS*, 358, 168
- Sazonov S. Y., Revnivtsev M. G., 2004, *A&A*, 423, 469
- Schmidt M., Green R. F., 1983, *ApJ*, 269, 352
- Schmidt M., Schneider D. P., Gunn J. E., 1995, *AJ*, 110, 68
- Schödel R., et al., 2002, *Nat*, 419, 694
- Seljak U., 2002, *MNRAS*, 334, 797
- Shankar F., Lapi A., Salucci P., De Zotti G., Danese L., 2006, *ApJ*, 643, 14
- Shankar F., Mathur S., 2007, *ApJ*, 660, 1051

- Shankar F., Salucci P., Granato G. L., De Zotti G., Danese L., 2004, *MNRAS*, 354, 1020
- Shen J., Abel T., Mo H., Sheth R., 2005, preprint, astro-ph/0511365
- Sheth R. K., Mo H. J., Tormen G., 2001, *MNRAS*, 323, 1
- Sheth R. K., Tormen G., 1999, *MNRAS*, 308, 119
- Shields G. A., Gebhardt K., Salviander S., Wills B. J., Xie B., Brotherton M. S., Yuan J., Dietrich M., 2003, *ApJ*, 583, 124
- Shields G. A., Menezes K. L., Massart C. A., Vanden Bout P., 2006, *ApJ*, 641, 683
- Shinozaki K., Miyaji T., Ishisaki Y., Ueda Y., Ogasaka Y., 2006, *AJ*, 131, 2843
- Siana B., et al., 2007, ArXiv e-prints, 711
- Silk J., Rees M. J., 1998, *A&A*, 331, L1
- Silverman J. D., et al., 2005a, *ApJ*, 618, 123
- Silverman J. D., et al., 2005b, *ApJ*, 624, 630
- Soltan A., 1982, *MNRAS*, 200, 115
- Somerville R. S., Kolatt T. S., 1999, *MNRAS*, 305, 1
- Somerville R. S., Primack J. R., Faber S. M., 2001, *MNRAS*, 320, 504
- Spergel D. N., et al., 2003, *ApJS*, 148, 175
- Spergel D. N., et al., 2007, *ApJS*, 170, 377
- Springel V., 2005c, *MNRAS*, 364, 1105
- Springel V., Di Matteo T., Hernquist L., 2005b, *MNRAS*, 361, 776
- Springel V., Di Matteo T., Hernquist L., 2005d, *ApJ*, 620, L79
- Springel V., et al., 2005a, *Nat*, 435, 629
- Springel V., White S. D. M., Tormen G., Kauffmann G., 2001b, *MNRAS*, 328, 726
- Springel V., Yoshida N., White S. D. M., 2001a, *New Astronomy*, 6, 79
- Steidel C. C., Hunt M. P., Shapley A. E., Adelberger K. L., Pettini M., Dickinson M., Giavalisco M., 2002, *ApJ*, 576, 653

- Sutherland R. S., Dopita M. A., 1993, *ApJS*, 88, 253
- Taffoni G., Mayer L., Colpi M., Governato F., 2003, *MNRAS*, 341, 434
- Tamura T., Kaastra J. S., Peterson J. R., Paerels F. B. S., Mittaz J. P. D., Trudolyubov S. P., Stewart G., Fabian A. C., Mushotzky R. F., Lumb D. H., Ikebe Y., 2001, *A&A*, 365, L87
- Tegmark M., et al., 2004, *PhRvD*, 69, 103501
- Toomre A., 1977, in Tinsley B. M., Larson R. B., eds, *Evolution of Galaxies and Stellar Populations Mergers and Some Consequences*. pp 401–+
- Toomre A., Toomre J., 1972, *ApJ*, 178, 623
- Tremaine S., et al., 2002, *ApJ*, 574, 740
- Tundo E., Bernardi M., Hyde J. B., Sheth R. K., Pizzella A., 2007, *ApJ*, 663, 53
- Ueda Y., Akiyama M., Ohta K., Miyaji T., 2003, *ApJ*, 598, 886
- Van Waerbeke L., Mellier Y., Pelló R., Pen U.-L., McCracken H. J., Jain B., 2002, *A&A*, 393, 369
- Viola M., Monaco P., Borgani S., Murante G., Tornatore L., 2008, *MNRAS*, 383, 777
- Volonteri M., Haardt F., Madau P., 2003a, *ApJ*, 582, 559
- Volonteri M., Madau P., Haardt F., 2003b, *ApJ*, 593, 661
- Volonteri M., Madau P., Quataert E., Rees M. J., 2005, *ApJ*, 620, 69
- Volonteri M., Perna R., 2005, *MNRAS*, 358, 913
- Volonteri M., Rees M. J., 2005, *ApJ*, 633, 624
- Volonteri M., Salvaterra R., Haardt F., 2006, *MNRAS*, 373, 121
- Volonteri M., Sikora M., Lasota J.-P., 2007, *ApJ*, 667, 704
- Walter F., Carilli C., Bertoldi F., Menten K., Cox P., Lo K. Y., Fan X., Strauss M. A., 2004, *ApJ*, 615, L17
- Wang J., De Lucia G., Kitzbichler M. G., White S. D. M., 2007, preprint, *astro-ph/0706.2551*, 706
- Wang L., Kauffmann G., 2008, *ArXiv e-prints*, 801

- Warren S. J., Hewett P. C., Osmer P. S., 1994, *ApJ*, 421, 412
- Weinmann S. M., van den Bosch F. C., Yang X., Mo H. J., Croton D. J., Moore B., 2006, *MNRAS*, 372, 1161
- White S. D. M., Frenk C. S., 1991, *ApJ*, 379, 52
- White S. D. M., Navarro J. F., Evrard A. E., Frenk C. S., 1993, *Nat*, 366, 429
- White S. D. M., Rees M. J., 1978, *MNRAS*, 183, 341
- Wolf C., Wisotzki L., Borch A., Dye S., Kleinheinrich M., Meisenheimer K., 2003, *A&A*, 408, 499
- Woo J.-H., Treu T., Malkan M. A., Blandford R. D., 2006, *ApJ*, 645, 900
- Woo J.-H., Urry C. M., 2002, *ApJ*, 579, 530
- Wyithe J. S. B., 2006, *MNRAS*, 365, 1082
- Wyithe J. S. B., Loeb A., 2002, *ApJ*, 581, 886
- Wyithe J. S. B., Loeb A., 2003, *ApJ*, 595, 614
- Wyithe J. S. B., Loeb A., 2005a, *ApJ*, 621, 95
- Wyithe J. S. B., Loeb A., 2005b, *ApJ*, 634, 910
- York D. G., et al., 2000, *AJ*, 120, 1579
- Yu Q., Tremaine S., 2002, *MNRAS*, 335, 965

Index

- Λ CDM model: Standard Cosmological Model, i.e. General Relativity + cold dark matter + cosmological constant, 36
- 2QZ: Two Degree Field QSO Redshift Survey, 25
- 6QZ: 6dF AGN Redshift Survey, 49
- AGN: Active Galactic Nuclei, 5
- B06: Beckmann et al. (2006), 68
- BH: supermassive black hole, 5
- C04: Croom et al. (2004), 49
- CDFN: Chandra Deep Field North, 29
- CDFS: Chandra Deep Field South, 29
- DM: dark matter, 5
- EPS: Extended Press-Schechter theory, 37
- FP: fundamental plane, 17
- H07: Hopkins et al. (2007e), 28
- LF: luminosity function, 7, 25
- MF: mass function, 19
- PMN: Porciani et al. (2004), 52
- S06: Shinozaki et al. (2006), 68
- SDSS: Sloan Digital Sky Survey, 22
- VHM: Volonteri, Haardt & Madau (2003), 56
- WL02: Wyithe & Loeb (2002), 43
- WL03: Wyithe & Loeb (2003), 43